



DISSERTATION

In Partial Fulfillment of the Requirements
for the Degree of Doctor of Philosophy
from TELECOM ParisTech

Specialization: Communications and Electronics

Jinhui Chen

On MIMO Systems with Limited Feedback: End-to-End Distortion, Analog Channel Feedback, and Layered Multiplexing

Defense scheduled on the 9th of July 2009 before a committee composed of:

Reporters	Prof. E. Telatar, EPFL Prof. M. Debbah, SUPÉLEC
Examiners	Prof. R. Knopp, EURECOM Associate Prof. P. Ciblat, TELECOM ParisTech Dr. M. Guillaud, FTW
Thesis supervisor	Prof. D. T. M. Slock, EURECOM



THESE

présentée pour obtenir le grade de

Docteur de TELECOM ParisTech

Spécialité: Communications et Electronique

Jinhui Chen

**Sur des Systèmes MIMO avec Retour Limité:
Distorsion Bout-à-Bout, Retour Analogique du
Canal , et Multiplexage par Couche**

Thèse prévue le 9 juillet 2009 devant le jury composé de :

Rapporteurs	Prof. E. Telatar, EPFL Prof. M. Debbah, SUPÉLEC
Examineurs	Prof. R. Knopp, EURECOM Maître de Conference HDR P. Ciblat, TELECOM ParisTech Dr. M. Guillaud, FTW
Directeur de thèse	Prof. D. T. M. Slock, EURECOM

Abstract

In this thesis, we investigate the following three fields on multi-input multi-output (MIMO) systems with limited feedback.

End-to-end distortion: The first part of the thesis presents the joint impact of antenna numbers, source-to-channel bandwidth ratio, spatial correlation and time diversity on the optimum expected end-to-end distortion in an outage-free MIMO system. In particular, based on the analytical expression for any signal-to-noise ratio (SNR), the closed-form expression of the asymptotic optimum expected end-to-end distortion at a high SNR is derived, comprised of the optimum distortion exponent and the optimum distortion factor. The simulation results illustrate that, at a practical high SNR, the analysis on the impacts of the optimum distortion exponent and the optimum distortion factor explains the behavior of the optimum expected end-to-end distortion. The results in this part could be the performance objectives for analog-source transmission systems as well as a guidance on system design.

Analog channel feedback: In the second part of this thesis, we propose to apply orthogonal space-time block codes (OSTBC) with linear analog channel feedback. Since MIMO channel information is a sort of analog source vector, relative to quantized channel feedback, linear analog feedback has the advantages such as outage-free, self channel adaptation and low complexity. It is proved that the linear analog transmission method with OSTBC can achieve the matched filter bound (MFB) on received SNR. In comparison with the linear analog transmission method with circulant space-time block coding (CSTBC), the method with OSTBC performs better with respect to received SNR and mean-squared error. In comparison with the random vector quantization methods with different modulation schemes, the simulation results show that with respect to average direction error, the linear analog transmission method with OSTBC performs over any RVQ method

with specific modulation scheme in the regimes of relatively high SNR and low SNR; with respect to average mean-squared error, it performs always better than the RVQ methods. We also evaluate the effect of applying the linear analog channel feedback with OSTBC to multiuser MIMO downlink beamforming. It is shown that the linear analog channel feedback with OSTBC can make the system approach the optimum performance within a short latency.

Layered multiplexing: In the third part of this thesis, with respect to the systems with short blocks, a new layered multiplexing strategy is proposed to adapt an uncertain channel by Walsh layer-time coding, successive interference canceller and HARQ signaling. As illustrated by simulation results, with respect to its high success rate, good performance on average latency and lower computational complexity, this strategy would be a good replacement to the widely-used adaptive QAM modulation strategy.

Acknowledgements

I would like first to extend my sincere thanks to my advisor Prof. Dirk T. M. Slock for letting me dictate the pace of my research, giving me freedom of a large extent on the choice of topics, his inspiring ideas, invaluable guidance and kind helps on all details, and for giving me invaluable insight into my research.

I would also like to extend my thanks to Dr. Uri Erez in Tel Aviv University for the inspiring discussions between us, and Prof. Giuseppe Caire in University of Southern California for kindly sending his breakthrough manuscript not-yet-published at that time.

I am grateful to my committee members, Prof. Emre Teletar, Prof. Mérouane Debbah, Prof. Raymond Knopp, Prof. Philippe Ciblat and Dr. Maxime Guillaud for their valuable inputs.

I would like to thank my friends at EURECOM and in Sophia. The list is too long to be put here. We had so much fun together and enjoyed our lives. Special thanks to Junbo and Randa for technical discussions and suggestions.

My sincere thanks to the secretaries at EURECOM for helping me dealing with all administrative things and the IT supporters for dealing with computers and networks. All of them are nice.

Finally, I would like to thank my family and family-in-law who have always encouraged me in my quest for higher education and especially my husband and best friend of many years Wu Jiaqi for encouraging me and listening to my occasional laments and for supporting my many decisions.

Contents

Abstract	i
Acknowledgements	iii
Contents	v
List of Figures	ix
Acronyms	xi
Notations	xiii
1 Introduction	1
1.1 MIMO systems with feedback	1
1.2 End-to-end distortion	2
1.3 MIMO channel estimate feedback	8
1.4 Multi-layer transmission	11
1.5 Thesis outline and contributions	14
2 End-to-End Distortion: Uncorrelated MIMO Channel	17
2.1 Introduction	17
2.2 System model	18
2.3 Mathematical preliminaries	19
2.4 Main results	21
2.4.1 Optimum expected distortion at any SNR	21
2.4.2 Asymptotic optimum expected distortion	23
2.5 Numerical analysis and discussion	27
2.6 Conclusion	32
2.A Proof of Lemma 1	33
2.B Proof of Lemma 2	34
2.C Proof of Lemma 3	35
2.D Proof of Lemma 4	36
2.E Proof of Lemma 5	38

3	End-to-End Distortion: Correlated MIMO Channel	41
3.1	Introduction	41
3.2	Mathematical preliminaries	42
3.3	Main results	44
3.3.1	Optimum expected distortion at any SNR	44
3.3.2	Asymptotic optimum expected distortion	45
3.4	Numerical analysis and discussion	54
3.5	Conclusion	55
4	End-to-End Distortion: With Time Interleaving	59
4.1	Introduction	59
4.2	System Model	62
4.3	Main Results	62
4.3.1	Optimum expected distortion at any SNR	62
4.3.2	Asymptotic optimum expected distortion	63
4.4	Interleaving Impact Analysis	63
4.5	Conclusion	67
5	Analog Channel Feedback	69
5.1	Introduction	69
5.2	Space-time coding in analog transmission	71
5.2.1	Channel model	71
5.2.2	MFB on receive SNR	71
5.2.3	OSTBC achieves SNR_{MFB}	72
5.2.4	OSTBC analog vs. RVQ digital	75
5.3	CSIT acquisition by analog channel feedback	81
5.3.1	Scheme description and channel model	81
5.3.2	Mean squared error evaluation	83
5.4	Multiuser MIMO downlink beamforming with analog channel feedback	90
5.4.1	Scheme description	90
5.4.2	Signal-to-interference ratio evaluation	91
5.5	Conclusion	93
6	Layered Multiplexing	95
6.1	Introduction	95
6.2	General description and channel model	96
6.3	Process description	98
6.3.1	Walsh layer-time coding	98
6.3.2	In the first transmission	99

6.3.3	In the m^{th} transmission when $2 \leq m \leq L_w$	100
6.3.4	When $L_w < m \leq M$	101
6.4	An example with simulation results	102
6.5	Conclusion and future works	105
6.A	Solving the equation array (6.16)	106
7	Conclusion and Future Work	109

List of Figures

1.1	Basic elements of a digital communication system	3
1.2	Distortion exponents for $N_t = N_r = 2$ case	5
1.3	Distortion exponents for $N_t = 2, N_r = 4$ case	5
1.4	Impact of distortion factor	7
1.5	The feedback model for our end-to-end distortion analysis . .	8
1.6	The feedback model for channel matrix or channel direction acquisition	9
1.7	Broadcast strategy for single user, i.e, multi-layer transmis- sion for channel adaption without any feedback	13
1.8	Rateless coding, i.e, multi-layer reliable transmission with ARQ signaling	13
2.1	Uncorrelated channel, one of (N_t, N_r) is fixed to 5, $\eta = 4$, high SCBR.	29
2.2	Uncorrelated channel, $N_t = 1, N_r = 2, \eta = 1.1$, high SCBR .	30
2.3	Uncorrelated channel, $N_t = 2, N_r = 2, \eta = 1.7$, moderate SCBR	30
2.4	Uncorrelated channel, $N_t = 2, N_r = 2, \eta = 1$, moderate SCBR	31
2.5	Uncorrelated channel, $N_t = 1, N_r = 2, \eta = 0.99$, low SCBR .	31
3.1	Uncorrelated and correlated channels, $N_t = 4, N_r = 2, \eta =$ 10 , high SCBR	55
3.2	Uncorrelated and correlated channels, $N_t = 2, N_r = 2, \eta =$ 1.7 , moderate SCBR	56
3.3	Uncorrelated and correlated channels, $N_t = 2, N_r = 2, \eta = 2$, moderate SCBR	56
3.4	Uncorrelated and correlated channels, $N_t = 2, N_r = 2, \eta =$ 0.6657 , low SCBR	57

4.1	Block diagram of the transmission model with perfect interleaving	61
4.2	With time interleaving, $N_t = 2$, $N_r = 1$, $\eta = 0.25$, low SCBR	64
4.3	With time interleaving, $N_t = 4$, $N_r = 2$, $\eta = 1$, high SCBR	65
4.4	SCBR state transition with time diversity branches. $N_t = 2$, $N_r = 3$, $\eta = 0.32$, and $\rho = 20\text{dB}$	66
5.1	Wrong decision ratios of QPSK, 16QAM and 64QAM modulation schemes	77
5.2	Average direction error comparison: OSTBC vs. RVQ	78
5.3	Average MSE comparison: OSTBC vs. RRVQ	80
5.4	Linear analog channel feedback scheme	81
5.5	MSE comparison: OSTBC vs. CSTBC	88
5.6	Average MSE comparison: OSTBC vs. CSTBC	89
5.7	Multiuser MIMO downlink channel with channel feedback	90
5.8	Average SIR comparison: OSTBC analog channel feedback with different latencies and upper bound	92
6.1	A multi-layer system with HARQ	96
6.2	Simulation results of the example	103

Acronyms

Here are the main acronyms used in this document. The meaning of an acronym is usually indicated once, when it first occurs in the text. The English acronyms are also used for the French summary.

AWGN	Additive White Gaussian Noise
ARQ	Automatic Repeat Request
CSTBC	Circular Space-Time Block coding/code
CQI	Channel Quality Indicator (CQI)
CSI	Channel State Information
CSIR	Channel State Information at Receiver
CSIT	Channel State Information at Transmitter
DMT	Diversity-gain-to-Multiplexing-gain Tradeoff
FDD	Frequency Division Duplex
HARQ	Hybrid Automatic Repeat Request
HDA	Hybrid Digital Analog
MAF	Matched Filter Bound
ML	Maximum Likelihood
MRC	Maximum Ratio Combining
MSE	Mean Square Error
MIMO	Multi-Input Multi-Output
MISO	Multi-Input Single-Output
OVSF	Orthogonal Variable Spreading Factor
QAM	Quadrature Amplitude Modulation
OFDM	Orthogonal Frequency Division Multiplexing
QPSK	Quadrature Phase-Shift Keying
OSTBC	Orthogonal Space-Time Block Coding/Code
RHS	Right Hand Side
RRVQ	Real Random Vector Quantization
RVQ	Random Vector Quantization

SCBR	Source-to-Channel Bandwidth Ratio
SIC	Successive Interference Cancellation
SIMO	Single-Input Multi-Output
SINR	Signal-to-Interference-Noise Ratio
SISO	Single-Input Single-Output
SSB	Single-Side Band
STBC	Space-Time Block Coding/Code
STC	Space-Time Coding/Code
TDD	Time Division Duplex
THP	Thomlinson-Harashimma Precoding
ZFBF	ZeroForcing BeamForming

Notations

\mathbb{E}_x	Expectation operator over the r.v. x
$ \mathbf{H} $	Determinant of the matrix \mathbf{H}
$ x $	Absolute value of x
$\lfloor x \rfloor$	Floor operation, rounds the elements of x to the nearest integers towards minus infinity
$\lceil x \rceil$	Ceil operation, rounds the elements of x to the nearest integers towards infinity
\mathbf{H}^*	Conjugate operation
\mathbf{H}^\dagger	Conjugate transpose operation
\mathbf{H}^T	Transpose operation
\mathbb{R}	Set of real numbers
\mathbb{R}^+	Set of positive real numbers
\mathbb{Z}	Set of integer numbers
\mathbb{Z}^+	Set of positive integer numbers
\mathbf{H}	matrix
\mathbf{h}	vector
h	scalar
\mathcal{CN}	Complex Normal Distribution
\mathcal{B}	Beta distribution
\mathcal{U}	Uniform distribution
η	Source-to-channel bandwidth ratio
W_s	Source bandwidth(Hz)
W_c	Channel bandwidth(Hz)
N_a	Number of antennas at the end A
N_b	Number of antennas at the end B
N_t	Number of transmit antennas
N_r	Number of receive antennas
N_{\min}	$N_{\min} = \min N_t, N_r$

N_{\max}	$N_{\max} = \max N_t, N_r$
L_b	Length of the block
L_s	Length of the source vector
$\Psi(a, c; x)$	Confluent hypergeometric function
$\Gamma(x)$	Gamma function
$B(m, n)$	Beta function
ρ	Signal-to-noise ratio
R	Rate
R_s	Source rate
R_c	Channel rate
P_o	Outage probability
D	Distortion
ED	Expected distortion
ED^*	Optimum expected distortion
ED_{asy}^*	Asymptotic optimum expected distortion
Δ	Distortion exponent
Δ^*	Distortion exponent in ED_{asy}^*
μ^*	Distortion factor in ED_{asy}^*
β_{bf}	Feedback delay factor
P_s	Source power

Chapter 1

Introduction

1.1 MIMO systems with feedback

In a wireless communication system, the propagation condition determines the performance of the system within limitations such as short-term or long-term power constraint, peak-to-average power ratio, and maximum latency. Although the channel model and the statistical information of propagation in some environments could be predicted [1–6], the instantaneous channel realization is uncertain. For a slow-fading channel, the transmitter-side knowledge on the instantaneous channel would help a system improve its performance [7–10].

In [11], from the viewpoint of information theory, Biglieri et al. gave an overview of the works on the role of channel side information on capacity. For an additive white Gaussian noise (AWGN) channel in the single-user setting, although the perfect channel state information at the transmitter (CSIT) in addition to the receiver gives only a little advantage in terms of ergodic capacity, the performance enhancement exhibited in terms of outage capacity (reliability) is dramatic [11–15] and encoding and decoding could be enormously simplified [16]. In the single user setting, for a multi-input multi-output (MIMO) Gaussian channel with a large number of transmit antennas, the optimal water-filling power control strategy requiring perfect CSIT brings a substantial four-fold increase in ergodic capacity at low signal-to-noise (SNR) [17], besides the improvement in the reliability. In the multi-

user setting, with perfect CSIT, the optimal power control for multiple access channel [18] and dirty paper coding for broadcast channel [19] can achieve the maximum sum rate.

In the case that the forward link is not reciprocal to the reverse link, to let the transmitter know about the forward link, conveying the channel knowledge via a feedback link is a simple and practical way. In practice, not only frequency division duplex (FDD) systems use feedback links, but also time division duplex (TDD) systems for calibration [20]. In accordance with the channel adaptive technique employed by the system, the information on the forward link to feedback is not necessarily the full channel state information (CSI). It could be some representation of the forward link condition (e.g., lossy channel state information, instantaneous channel capacity, channel direction, received power, interference level, success-failure state, etc.) which is referred to as *limited feedback*.

In this thesis, we shall introduce our works relevant to systems with limited channel feedback. They are about the end-to-end distortion in an outage-free MIMO system (e.g., with instantaneous channel capacity known at the transmitter and joint source-channel coding), channel estimate feedback approaches, and multi-layer transmission with automatic repeat request (ARQ). The background and the state-of-the-art of these three topics are presented as follows.

1.2 End-to-end distortion

It is well-known that the functional diagram and the basic elements of a digital communication system can be illustrated by Fig.1.1 [1]. The source input-output may be either an analog (continuous-amplitude) sequence or a digital (discrete-amplitude) sequence. Whichever is the source, there is always a tradeoff between the efficiency and the reliability. For transmitting a digital sequence, the tradeoff would be between the spectral efficiency (bits/s/Hz) [2] and the error probability. For transmitting an analog sequence, under the assumption of band-limited white Gaussian source, the tradeoff would be between the source-to-channel bandwidth ratio W_s/W_c (SCBR) [21] and the mean-squared error (MSE) [22, 23], i.e., end-to-end distortion.

A distinct point between digital-source transmission and analog-source transmission is: in digital-source transmission, if the spectral efficiency is below the upper bound subject to the channel state and the transmitter knows the instantaneous CSI perfectly, the error probability would go to

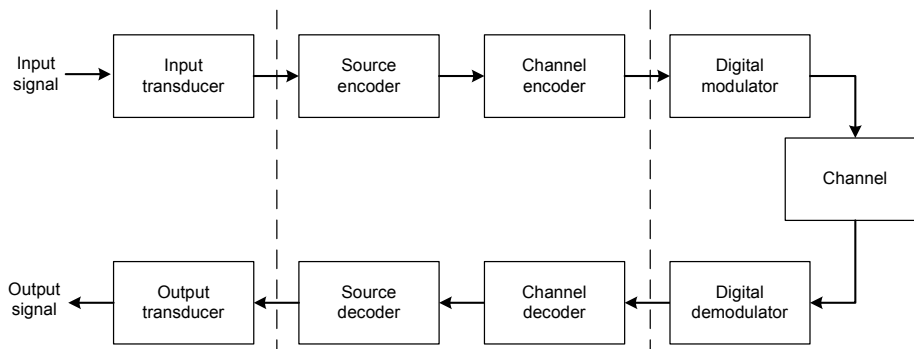


Figure 1.1: Basic elements of a digital communication system

zero; whereas, in analog-source transmission, whatever good are the channel condition and the system, the distortion is nonvanishing, because the entropy of a continuous-amplitude source is infinite and thus the exact recovery of an analog source requires infinite channel capacity [16, 22–24].

In [25], Zheng and Tse studied the optimal tradeoff between the *multiplexing gain* and the *diversity gain* (DMT) in the SNR-indicated adaptive-rate digital transmission with perfect CSIR. The transmission stage that they considered is between channel coding and channel decoding as illustrated by Fig.1.1. For an N_t -input N_r -output Rayleigh fading channel, the main result they obtained is

$$d^*(r) = (N_t - r)(N_r - r) \quad (1.1)$$

in the case that the block length $l \geq N_t + N_r - 1$, where r and d are defined as

$$r \triangleq \lim_{\rho \rightarrow \infty} \frac{R(\rho)}{\log_2 \rho} \quad \text{and} \quad d \triangleq - \lim_{\rho \rightarrow \infty} \frac{P_o(\rho)}{\log_2 \rho} \quad (1.2)$$

with ρ the average SNR, the rate $R(\rho)$ in bits per channel use (bpcu) and outage probability P_o . Therein, they assumed that the system supports that the data rate increases with average SNR, $R = r \log_2 \rho$, whereas the transmitter does not know the instantaneous channel rate, and thereby outage accidents happen.

Regarding end-to-end distortion, in [26, 27], Ziv and Zakai investigated the decay of MSE with SNR for analog-source transmission over a noisy single-input single-output (SISO) channel without any channel knowledge on the transmitter side. In [28, 29], Laneman et al. used *distortion exponent*

in the asymptotic expected distortion,

$$\Delta \triangleq - \lim_{\rho \rightarrow \infty} \frac{ED(\rho)}{\log_2 \rho}, \quad (1.3)$$

as a metric to compare channel diversity and source diversity for parallel channels, whose values are related to SCBR. Choudhury and Gibson presented the relations between the end-to-end distortion and the outage capacity for an AWGN channel [30]. Zoffoli et al. studied the characteristics of the distortions in MIMO systems with different strategies, with and without CSI [31, 32].

For tandem source-channel coding systems, assuming optimal block quantization and SNR-indicated adaptive-rate transmission as in [25], Holliday and Goldsmith investigated the expected end-to-end distortion for an uncorrelated slow-fading MIMO channel [33–35] based on the results of [25, 36, 37]. They gave the bound on the total expected distortion (MSE)

$$ED \leq 2^{-\frac{2r}{\eta} \log_2 \rho + O(1)} + 2^{-(N_r - r)(N_t - r) \log \rho + o(\log_2 \rho)} \quad (1.4)$$

where η is the SCBR. Considering the asymptotic high SNR regime, they proposed that r should satisfy

$$\Delta_{\text{sep}}^* = (N_r - r)(N_t - r) = \frac{2r}{\eta} + o(1) \quad (1.5)$$

where Δ_{sep}^* is the optimum distortion exponent for tandem source-channel coding systems. The explicit expression of Δ_{sep}^* is given by Theorem 2 in [38],

$$\Delta_{\text{sep}}^*(\eta) = \frac{2(jd^*(j-1)) - (j-1)d^*(j)}{2 + \eta(d^*(j-1) - d^*(j))}, \quad \eta \in \left[\frac{2(j-1)}{d^*(j-1)}, \frac{2j}{d^*(j)} \right) \quad (1.6)$$

for $j = 1, \dots, N_{\min}$. Note that $N_{\min} = \min\{N_t, N_r\}$.

In [38, 39], assuming an uncorrelated slow-fading channel, the transmitter perfectly knows the channel information and joint source-channel coding, Caire and Narayanan derived the *optimum distortion exponent*

$$\Delta^*(\eta) = \sum_{i=1}^{N_{\min}} \min \left\{ \frac{2}{\eta}, 2i - 1 + |N_t - N_r| \right\} \quad (1.7)$$

which is larger than Δ_{sep}^* as Fig.1.2 and Fig.1.3 shows. Concurrently, the same result as (1.7) was also provided by Gunduz and Erkip [40, 41].

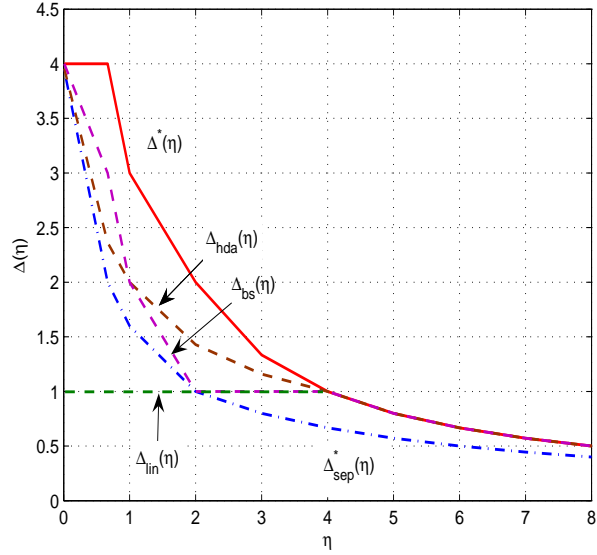


Figure 1.2: Distortion exponents for $N_t = N_r = 2$ case

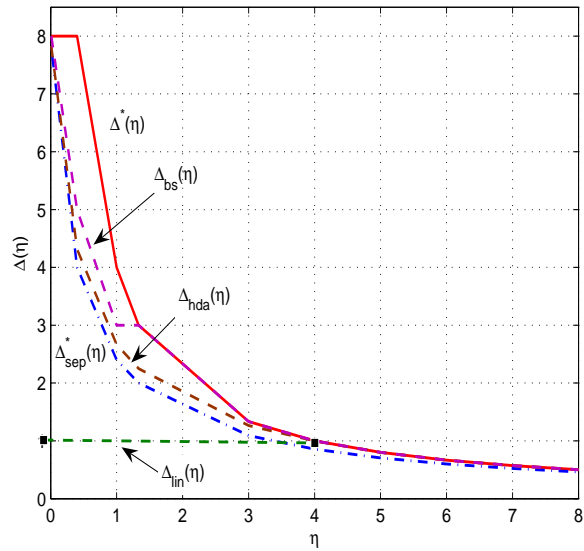


Figure 1.3: Distortion exponents for $N_t = 2, N_r = 4$ case

The derivation ways of Caire-Narayanan and Gunduz-Erkip are quite similar. Both are extensions of the outage probability analysis in [25] and based on the expression of MIMO channel mutual information in bpcu [42]

$$\mathcal{I} = \log_2 \left| \mathbf{I}_{N_r \times N_r} + \frac{\rho}{N_t} \mathbf{H}\mathbf{H}^\dagger \right|, \quad (1.8)$$

the rate-distortion function for a white Gaussian source [16]

$$D(R_s) = 2^{-2R_s}, \quad (1.9)$$

and Shannon's rate-capacity inequality for outage-free transmission [23]

$$R_s \leq R_c. \quad (1.10)$$

The optimum distortion exponent can be a performance objective for analog-source transmission systems. As seen in Fig.1.2 and Fig.1.3, the distortion exponent $\Delta_{\text{hda}}(\eta)$ of the hybrid digital analog (HDA) joint coding scheme for MIMO systems proposed by Narayanan and Caire [38, 43] achieves the distortion exponent upper bound when $\eta \geq 2N_{\min}$ (a stricter bandwidth compression case). Narayanan and Caire's HDA scheme is an extension to the MIMO case of Mittal and Phamdo's work [44]. The distortion exponent $\Delta_{\text{bs}}(\eta)$ of broadcast (superposition) scheme with varying power and rate allocation proposed by Bhattad et al. [45, 46] achieves the distortion exponent upper bound when $\eta \geq 2N_{\min}/(|N_t - N_r| + 1)$. A similar broadcast scheme in [41, 47] is a special case of [45, 46] when $N_{\min} = 1$. By simple linear analog schemes, when $\eta \leq 2N_{\min}$, the distortion exponent $\Delta_{\text{lin}}(\eta)$ is always one and achieves the optimum distortion exponent when $\eta = 2N_{\min}$. When $\eta > 2N_{\min}$, the linear analog approach is infeasible.

Note that, although the distortion exponent upper bound is derived under the assumption that CSIT is perfectly known [38, 39] or at least the transmitter knows the instantaneous channel capacity [40, 41], the three aforementioned optimum-exponent-achieved approaches (for specific ranges or points of SCBR) do not require any transmit side channel knowledge. Taking an insight into these approaches, we can see that all of them manage to avoid outage to assure the minimum reliability: in the HDA approach, it is done by the analog part; in the broadcast approach, it is done by supposing infinite layers bearing different rates. Nevertheless, there is something more than the distortion exponent in the expected end-to-end distortion.

Intuitively, at high SNR, the form of the *optimum asymptotic expected end-to-end distortion* could be

$$ED_{\text{asy}}^* = \mu^*(\rho)\rho^{-\Delta^*} \quad (1.11)$$

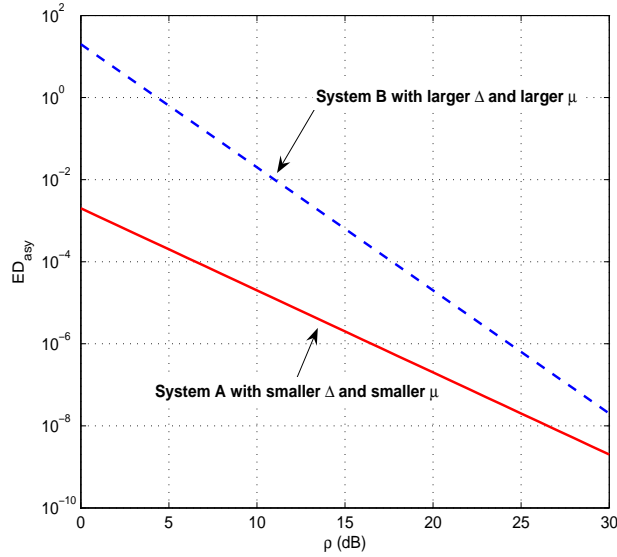


Figure 1.4: Impact of distortion factor

where the *optimum distortion factor* $\mu^*(\rho)$ should satisfy the equation

$$\lim_{\rho \rightarrow \infty} \frac{\log \mu^*(\rho)}{\log \rho} = 0. \quad (1.12)$$

For an analog-source transmission system, its performance at a high SNR could be measured via the asymptotic expected end-to-end distortion

$$ED_{\text{asy}} = \mu(\rho)\rho^{-\Delta} \quad (1.13)$$

where the distortion exponent Δ and the distortion factor $\mu(\rho)$ could be obtained analytically.

Apparently, we cannot say that a system must achieve the optimum asymptotic expected distortion ED_{asy}^* if what it achieves is only the optimum distortion exponent Δ^* . Also, we cannot say that, at a practical high SNR, the scheme with the larger distortion exponent must perform better than the other. As illustrated by Fig.1.4, in the regime of practical high SNR, the effect of the distortion factor must be taken into consideration. In other words, for practical cases, studying only the optimum distortion exponent is insufficient and giving the closed-form expression of ED_{asy}^* is more meaningful. Using ED_{asy}^* as an objective, via analyzing both Δ^* and

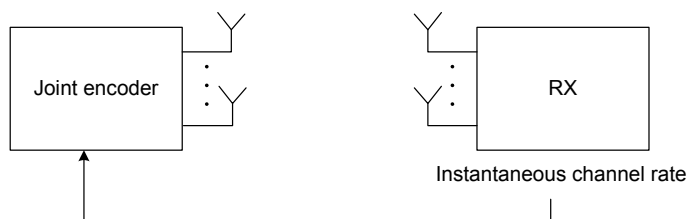


Figure 1.5: The feedback model for our end-to-end distortion analysis

μ^* , it is possible to design an analog-source transmission system performing better than the existing systems in the regime of practical SNR. For deriving ED_{asy}^* , if we could obtain the analytical expression of ED^* for any SNR, then it would be easy to find out the optimum distortion factor $\mu^*(\rho)$ and the optimum distortion exponent Δ^* .

1.3 MIMO channel estimate feedback

As the overview in [10], recently, precoding techniques requiring channel information at the transmitter are popular for improving the performance of MIMO system, e.g., Tomlinson-Harashima precoding (THP) [48–50], trellis precoding [51], transmit matched filter [52, 53], transmit zero-forcing [54, 55], transmit Wiener filter [56], linear precoders [57, 58], water-filling power control [13, 14, 18], dirty paper coding [59] and so on. In some precoding techniques, such as zero-forcing beamforming, only the directions of channel vectors are required to be known at the transmitter. If the forward link and the reverse link are not reciprocal, a feedback link (as shown in Fig.1.6) can let the transmitter know the channel estimate. Since the channel gain matrix or vector direction is a sort of continuous-amplitude source, the feedback procedure is in fact the procedure of analog-source transmission. The feedback approach could be in digital, analog, or hybrid digital analog (HDA). Then, our question would be again “to code, or not to code?” [60].

In digital feedback techniques, how to quantize the estimate of a MIMO channel is the key issue. In [61], D. J. Love et al. gave an overview of recent quantization techniques for limited feedback. Among them, the widely-discussed techniques are Lloyd vector quantization approach [62–64] based on Lloyd quantization algorithm [65], Grassmannian line packing [66], and random vector quantization (RVQ) [67, 68].

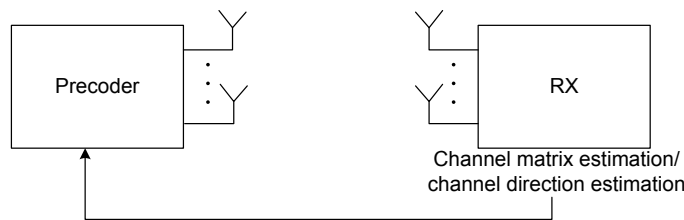


Figure 1.6: The feedback model for channel matrix or channel direction acquisition

In analog feedback techniques, feeding back the estimate of a MIMO channel is an issue of how to do analog transmission over a MIMO channel. For SISO channel, it is well known that for a white Gaussian source whose bandwidth is equal to the AWGN (real) channel bandwidth, the uncoded unquantized transmission is the optimal with respect to mean-squared error (MSE) [21, 69]. For a continuous-time AWGN channel, this optimality can be achieved by single-sideband (SSB) modulation [27, 70]. For a discrete-time AWGN channel, this optimality can be achieved by single-letter codes and MMSE receivers [71, 72]. In [72], considering downlink and uplink estimation errors, Samardzija and Mandayam proposed an analog scheme for CSI feedback in the case of independent Rayleigh fading AWGN SISO channel. Their criterion is to minimize the mean-squared error on the received channel estimate at the transmitter considering the downlink and uplink estimation errors, noise in the feedback phase, and channel distributions.

So far, many discussions on analog channel estimate feedback are focused on the scenario of vector channel for multiple users. That is, the base station has multiple antennas, each user has only one antenna, and the channel estimate feedback is from each user to the base-station. The discussion in the scenario of vector channel can be traced back to [73], where Visotsky and Madhow proposed to use analog feedback for the Rayleigh fading vector channel. In [74], Thomas et al. proposed to apply analog feedback in orthogonal frequency division multiplexing (OFDM) systems over a vector channel. In [75], Marzetta and Hochwald supposed a zero-forcing receiver for the direct analog CSI feedback. Feedbacks from different users are supposed to be distinguished by code-division or some other ways [74, 75].

If we compare linear analog channel feedback approaches to digital feedback approaches, the computational simpleness of linear analog approaches is obvious; whereas, digital feedback approaches cost much more process-

ing overhead. Furthermore, without external indicating signals such as the current SNR range, fixed-rate digital approaches cannot adapt to the channel, that is, they would perform worse at relatively low SNR due to outage accidents and reach an error floor at relatively high SNR due to the inevitable quantization error; whereas, linear analog approaches are to some extent self-adaptive to the instantaneous channel and free of outage and error floor. Also, it is hard to say that, in the analog-source transmission over a MISO/SIMO/MIMO channel subject to a strict delay limit, a rate-adaptive digital approach (with external indication) must perform better than a linear analog approach.

In [76,77], assuming that the vector channel direction feedback serves for multiuser MISO downlink zero-forcing beamforming, Caire et al. compared an analog feedback approach with an RVQ feedback approach with respect to respective rate gap upper bounds. They concluded that, with perfect channel state information at the receiver (CSIR), the RVQ digital feedback is far superior to analog when $\beta_{\text{fb}} > 1$. Note that the feedback latency is supposed to be $\beta_{\text{fb}} N_b$ channel uses with N_b the antenna number at the base station. As given in [76,77], the rate gap upper bounds of the analog feedback approach and the RVQ digital feedback approach with perfect CSIR are

$$\Delta R^{\text{AF}} \leq \log_2 \left(1 + \frac{1}{\beta_{\text{fb}}} \right) \quad (1.14)$$

$$\Delta R^{\text{DF}} \leq \log_2 \left(1 + \frac{\rho}{1 + (1 + \rho)^{\beta_{\text{fb}}}} \right). \quad (1.15)$$

Caire et al. drew their conclusion by comparing the right hand sides (RHS) of (1.14) and (1.15) [76,77]. But, is it fair to judge actual performance by upper bound? For instance, from (1.14), we can see that there is no impact from SNR on the upper bound, however, in fact, if the CSIR is perfect and the SNR in the feedback procedure is infinitely high, the acquired CSIT via the analog approach performs nearly perfect and thus the rate gap ΔR^{AF} approaches zero as the value of the rate gap ΔR^{DF} with the digital feedback approach (the RHS in (1.15)) at infinitely high SNR while of course ΔR^{AF} satisfies (1.14) as zero is smaller than any positive number.

From Fig.1.2 and Fig.1.3, we can see that digital feedback could achieve a larger distortion exponent than analog feedback and thus it would cause the the resulting performance curve of digital feedback decay or increase faster. However, even though a digital approach could achieve a larger distortion exponent, it may be with a much smaller distortion factor as Fig.1.4

shows.

In the case of quasi-static multi-input multi-output (MIMO) channels, space-time coding (STC) considerations with issues of diversity and spatial multiplexing arise also for analog transmission. Since the correctness of the received estimate within an allowable feedback latency deserves more concern, to find an STC to exploit the spatial diversity in linear analog transmission is of our particular interest.

1.4 Multi-layer transmission

Presently, two classes of multi-layer transmission are mainly discussed, *broadcast strategy* and *rateless coding*.

Broadcast strategy (for single user) is the multi-layer transmission for rate adaption without feedback [46, 78–81], which stems from successive refinement source coding [82, 83]. The framework of the broadcast strategy is as Fig.1.7 shows. Each source layer conveys the source at different rate corresponding to respective channel realizations. All layers are superimposed subject to certain power allocation scheme for transmission. If the number of layers is infinite, it ensures that no matter how the channel realization is, at least one layer can be successfully decoded, i.e., at least some information of the source can be transmitted successfully.

Rateless coding is the multi-layer transmission with ARQ feedback as Fig.1.8 shows. The layers are linearly combined at the transmitter and the system transmits as much of a codeword as necessary for decoding to be possible. Rateless codes for the erasure channel are known as fountain codes [84, 85], such as LT codes [86] and Raptor codes [87].

In [88–90], Erez et al. studied rateless coding for Gaussian channels with respect to transmission rate. For canceling inter-layer interference, they proposed to use random dithering to let all layered packets statistically independent to each other. Then, the system benefits from multiple transmissions through summing up the average received SINR (including the interference from lower layers) of each layer at each transmission by maximum ratio combining (MRC) and subsequent successive interference cancelation (SIC) and decoding. The receiver solution is similar to that in MIMO V-BLAST [91]. The corresponding layer-time codes and the power allocation scheme have been proposed [89, 90]. If the channel is very good,

all layer packets would be successfully decoded via just one block transmission; if it is bad, they would be successfully decoded after multiple block transmissions. In their schemes [89, 90], the decoder is supposed to rely on average block SINR, which has nothing to do with noise realizations but the noise variance. Namely, the block length should be long enough to let the noise during the transmission be ergodic and the block is supposed to be perfectly channel coded.

An alternative scenario is that the block length is limited and the noise experienced by one block transmission is not ergodic. In this case, the decoder would rely on the instantaneous SINR involving limited noise realizations rather than the average SINR. Thereby, the MRC receiver proposed in aforementioned schemes would not work in this scenario. So, how to benefit from layer-multiplexing with HARQ feedback in that case? It would be to design a multi-layer scheme as follows: if the channel is very good, all linear combined layers could be decoded via one block transmission; if the channel is not so good, inter-layer inference could be removed or alleviated by multiple block transmissions. Such a layer-multiplexing scheme is of our interest in this thesis.

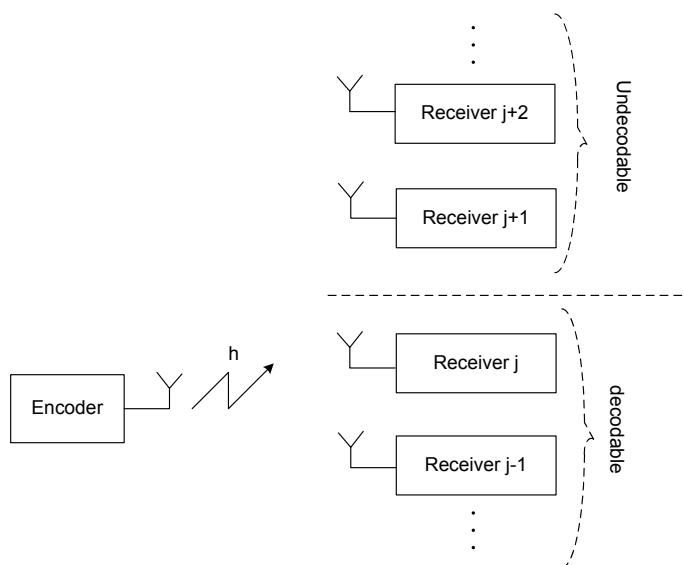


Figure 1.7: Broadcast strategy for single user, i.e, multi-layer transmission for channel adaption without any feedback

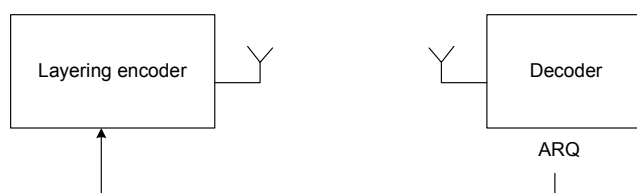


Figure 1.8: Rateless coding, i.e, multi-layer reliable transmission with ARQ signaling

1.5 Thesis outline and contributions

In this thesis, we make the following contributions. These contributions are divided into three fields: 1) Optimum end-to-end distortion analysis for outage-free MIMO systems; and 2) Analog channel feedback approach; and 3) Layer-multiplexing approach for delay-restricted cases.

1. In Chapter 2, we analyze the optimum expected end-to-end distortion in a system over an uncorrelated MIMO channel. We derive the analytical expression of the optimum expected end-to-end distortion for any SNR and its asymptotic value for high SNR, comprised of the optimum distortion exponent and the optimum distortion factor. The results were published in

- Jinhui Chen, Dirk T. M. Slock, “Bounds on Optimal End-to-End Distortion of MIMO Links”, *Proceedings of IEEE International Conference on Communications (ICC’08)*, Beijing, May 19-23, 2008.

and submitted as part of

- Jinhui Chen, Dirk T. M. Slock, “On Optimum End-to-End Distortion in MIMO Systems”, *EURASIP Journal on Wireless Communications and Networking*, under review

2. In Chapter 3, we extend our analysis on the optimum expected end-to-end distortion to the case of correlated MIMO channels. Besides the derivations on the analytical expression of the optimum expected end-to-end distortion for any SNR and its asymptotic value for high SNR, we also prove that, with the spatial correlation matrix approaching an identity matrix, the optimum asymptotic expected end-to-end distortion for correlated channel converges to that for uncorrelated channel. This work was submitted as the other part of

- Jinhui Chen, Dirk T. M. Slock, “On Optimum End-to-End Distortion of MIMO Systems”, *EURASIP Journal on Wireless Communications and Networking*, under review

and a part of this work was published in

- Jinhui Chen, Dirk T. M. Slock, “On Optimum End-to-End Distortion of Spatially Correlated MIMO Systems”, *Proceedings of*

IEEE Global Telecommunications Conferences (GLOBECOM 2008),
New Orleans, Nov.30 - Dec.4, 2008

3. In Chapter 4, we study the behavior of optimum expected end-to-end distortion in the long-frame block-fading case where the time diversity is exploited by interleaving. We show the impact of time diversity on the optimum expected distortion. This work was published in
 - Jinhui Chen, Dirk T. M. Slock, “Optimum end-to-end distortion of interleaved transmission via a Rayleigh MIMO channel”, *Proceedings of IEEE 19th International Symposium Personal, Indoor and Mobile Radio Communications (PIMRC 2008)*, Cannes, Septembre 15-18, 2008.
4. In Chapter 5, we introduce orthogonal space-time block coding (OSTBC) into linear analog channel feedback approaches for MIMO systems. We prove that the linear analog approach with OSTBC achieves the matched filter bound on received SNR and compare it with the random vector quantization (RVQ) approach and the linear analog approach with circulant STBC. Part of this work was published in
 - Jinhui Chen, Dirk T. M. Slock, “Orthogonal space-time block codes for analog channel feedback”, *Proceedings of IEEE International Symposium on Information Theory (ISIT 2008)*, Toronto, July 6-11, 2008.

The other work that we have done related to analog channel feedback, is the comparison of the channel estimate feedback with the received signal feedback in the linear feedback approach with spatial multiplexing. It was published in

- Jinhui Chen, Dirk T. M. Slock, “Comparison of Two Analog Feedback Schemes for Transmit Side MIMO Channel Estimation”, *Proceedings of IEEE 19th International Symposium Personal, Indoor and Mobile Radio Communications (PIMRC 2007)*, Athens, Septembre 3-7, 2007.

The result is that, in terms of mean squared error, the channel estimate feedback performs a little better than the received signal feedback in the supposed scenario. Since the derivation and the result are rather

straightforward, we shall not present it in this thesis.

5. In Chapter 6, considering short-block cases, we propose a simple practical layer-multiplexing scheme for reliable transmission with HARQ feedback. Part of this work was published in
 - Jinhui Chen, Dirk T. M. Slock, “A practical Walsh layering scheme for reliable transmission”, *Proceedings of IEEE Acoustics, Speech and Signal Processing (ICASSP 2009)*, Taipei, May 19-24, 2009.

Chapter 2

End-to-End Distortion: Uncorrelated MIMO Channel

2.1 Introduction

In this chapter, we investigate the optimum expected end-to-end distortion in an MIMO system over an uncorrelated slow-fading MIMO channel.

Shannon inequality shows the relationship between the end-to-end distortion (mean squared error) and the channel capacity [23]

$$W_s \log_2 \frac{P_s}{D} \leq R_c \quad (2.1)$$

where the source is assumed to be white Gaussian, W_s is the source bandwidth, P_s is the source power, D is the distortion (mean squared error) and R_c is the channel capacity.

This inequality implies the existence of the *optimum distortion exponent* in the optimum expected end-to-end distortion,

$$\Delta^* = - \lim_{SNR \rightarrow \infty} \frac{\log ED^*}{\log SNR}, \quad (2.2)$$

where ED^* denotes the optimum expected end-to-end distortion, $\mathbb{E}_{\mathbf{H}}^*[D]$.

The *optimum distortion exponent* in an outage-free system over an uncorrelated slow-fading MIMO channel has been derived [38, 40]:

$$\Delta_{\text{unc}}^* = \sum_{i=1}^{N_{\min}} \min \left\{ \frac{2}{\eta}, 2i - 1 + |N_t - N_r| \right\} \quad (2.3)$$

where N_t is the number of transmit antennas, N_r is the number of receive antennas, $N_{\min} = \min \{N_t, N_r\}$ and η is the *source-to-channel bandwidth ratio* (SCBR).

Nevertheless, as it has been stated in Chapter 1, the optimum distortion exponent does not suffice to reflect the behavior of optimum asymptotic expected end-to-end distortion. In this chapter, we will focus on deriving an analytical expression of the optimum expected end-to-end distortion and its asymptotic expression, exhibiting the joint impact of SCBR, antenna numbers and SNR.

The remainder of this chapter is organized as follows. The system model is given in Section 2.2. In Section 2.3, the mathematical preliminaries such as mathematical definitions, properties and lemmas are given as for derivations thereafter. The derivations of lemmas can be seen in Appendices at the end of this chapter. Section 2.4 is dedicated to the main results. Numerical results are presented in Section 2.5 with analysis. Finally, Section 2.6 concludes the contributions of this chapter.

2.2 System model

Assume $s(t)$, a continuous-time white Gaussian source of bandwidth W_s and source power P_s , is transmitted over a flat slow-fading MIMO channel of bandwidth W_c and the system is working on “short” frames due to strict time delay constraint, *i.e.*, time-interleaving is impossible to be done and no time diversity can be exploited. The transmitter is supposed to perfectly know the instantaneous channel capacity which can be fed back by the receiver as a real scalar. The recovered source at the receiver is denoted by $\hat{s}(t)$.

As in [38], a K -to- $(N_t \times T)$ joint source-channel encoder is supposed to be employed at the transmitter, which maps the sampled source block $\mathbf{s}' \in \mathbb{R}^K$ onto channel codewords $\mathbf{X} \in \mathbb{C}^{N_t \times T}$. The corresponding source-channel decoder is a mapping $\mathbb{C}^{N_r \times T} \rightarrow \mathbb{R}^K$ that maps the channel output $\mathbf{Y} = \{\mathbf{y}_1, \dots, \mathbf{y}_T\}$ into an approximation $\hat{\mathbf{s}}'$. Assuming that the continuous-time $s(t)$ is sampled by a Nyquist sampler, $2W_s$ samples per second, and

the bandlimited MIMO channel is used as a discrete-time channel at $2W_c$ channel uses per second [16, pp. 247-250], we have

$$\eta = \frac{W_s}{W_c} = \frac{K}{T}. \quad (2.4)$$

The model of the discrete flat slow-fading MIMO channel with N_t inputs and N_r is

$$\mathbf{y}_t = \mathbf{H}\mathbf{x}_t + \mathbf{n}_t, \quad t = 1, \dots, T \quad (2.5)$$

where $\mathbf{x}_t \in \mathbb{C}^{N_t}$ is the transmitted signal at time t , satisfying the long-term power constraint $\mathbb{E}[\mathbf{x}_t^H \mathbf{x}_t] = P_t$; $\mathbf{H} \in \mathbb{C}^{N_r \times N_t}$ is the channel matrix, assumed to be constant for all channel uses $t = 1, \dots, T$ and all its elements h_{ij} are i.i.d. $\mathcal{CN}(0, 1)$; $\mathbf{n} \in \mathbb{C}^{N_r}$ is the additive white noise all of whose elements $n_{t,i}$ are $\mathcal{CN}(0, \sigma_n^2)$. Note that P_t is the transmit power constraint and it is seen that the SNR per receive antenna $\rho = P_t/\sigma_n^2$.

2.3 Mathematical preliminaries

The mathematical definition and lemmas below will be used in the derivations and results thereafter.

We shall need the integral of an exponential function

$$\int_0^\infty e^{-px} x^{q-1} (1+ax)^{-\nu} dx = a^{-q} \Gamma(q) \Psi(q, q+1-\nu, p/a), \quad (2.6)$$

$$\operatorname{Re}\{q\} > 0, \quad \operatorname{Re}\{p\} > 0, \quad \operatorname{Re}\{a\} > 0.$$

as introduced in [92, pp. 365]. This involves the confluent hypergeometric function

$$\Psi(a, c; x) = \frac{1}{\Gamma(a)} \int_0^\infty e^{-xt} t^{a-1} (1+t)^{c-a-1} dt, \quad \operatorname{Re}\{a\} > 0 \quad (2.7)$$

which satisfies

$$x \frac{d^2 y}{dx^2} + (c-x) \frac{dy}{dx} - ay = 0. \quad (2.8)$$

Bateman has given a thorough analysis on $\Psi(a, c; x)$ [93, pp. 257-261]. In particular, he obtained the expressions on $\Psi(a, c; x)$ for small x as Table 2.1 shows.

We shall also need the following lemmas:

Lemma 1. Define an $m \times m$ full-rank matrix $\mathbf{W}(x)$ whose (i, j) th element is of the form $c_{ij}x^{\min\{a, i+j\}}$, $c_{ij} \neq 0$, $x, a \in \mathbb{R}^+$, $1 \leq i, j \leq m$. Then

$$\lim_{x \rightarrow 0} \frac{\log|\mathbf{W}(x)|}{\log x} = \sum_{i=1}^m \min\{a, 2i\}. \quad (2.9)$$

Proof. See Appendix 2.A. □

Lemma 2. Define an $m \times m$ Hankel matrix $\mathbf{W}(x)$ whose (i, j) th element is of the form $c_{i+j}x^{i+j}$, $c_{i+j} \neq 0$, $x \in \mathbb{R}^+$, $1 \leq i, j \leq m$. Then, each summand in the determinant of $\mathbf{W}(x)$ has the same degree $m(m+1)$ over x .

Proof. See Appendix 2.B. □

Lemma 3. Define an $m \times m$ Hankel matrix \mathbf{W} whose (i, j) th element is $\Gamma(a+i+j-1)$, $1 \leq i, j \leq m$, $a \in \mathbb{R}$. Then

$$|\mathbf{W}| = \prod_{k=1}^m \Gamma(k)\Gamma(a+k). \quad (2.10)$$

Proof. See Appendix 2.C. □

Lemma 4. Define an $m \times m$ Hankel matrix \mathbf{W} whose (i, j) th element is $\Gamma(a+i+j-1)\Gamma(b-i-j+1)$ where $1 \leq i, j \leq m$, $m \geq 2$ and $a, b \in \mathbb{R}$. Then

$$\begin{aligned} |\mathbf{W}| &= \Gamma(a+1)\Gamma(b-1)\Gamma^{m-1}(a+b) \\ &\times \prod_{k=2}^m \Gamma(k)\Gamma(a+k) \frac{\Gamma(b-2k+2)\Gamma(b-2k+1)}{\Gamma(a+b-k+1)\Gamma(b-k+1)}. \end{aligned} \quad (2.11)$$

Table 2.1: $\Psi(a, c; x)$ for small x , real c

c	Ψ
$c > 1$	$x^{1-c}\Gamma(c-1)/\Gamma(a) + o(x^{1-c})$
$c = 1$	$-[\Gamma(a)]^{-1} \log x + o(\log x)$
$c < 1$	$\Gamma(1-c)/\Gamma(a-c+1) + o(1)$

Proof. See Appendix 2.D. □

Lemma 5. *Define*

$$f(n) = \prod_{k=1}^m \frac{\Gamma(n - m - a + k)}{\Gamma(n - k + 1)}, \quad (2.12)$$

$$g(n) = n^{am} f(n), \quad (2.13)$$

subject to $a \in \mathbb{R}^+$, $m, n \in \mathbb{Z}^+$, $n \geq m$, and $n - m + 1 \geq a$. Then both $f(n)$ and $g(n)$ are monotonically decreasing.

Proof. See Appendix 2.E. □

2.4 Main results

In this section, assuming the channel is spatially and temporarily uncorrelated, we derive the analytical expression of the optimum expected end-to-end distortion for any SNR. Base on the analytic expression, we derive the optimum asymptotic expected distortion consisting of the optimum distortion exponent and the optimum distortion factor.

2.4.1 Optimum expected distortion at any SNR

Theorem 1 (Optimum Expected Distortion for Uncorrelated MIMO Channel). *The optimum expected end-to-end distortion in a MIMO system over an uncorrelated channel is*

$$ED_{\text{unc}}^*(\eta) = \frac{P_s |\mathbf{U}(\eta)|}{\prod_{k=1}^{N_{\min}} \Gamma(N_{\max} - k + 1) \Gamma(N_{\min} - k + 1)} \quad \text{for any } \rho \quad (2.14)$$

where $N_{\min} = \min\{N_t, N_r\}$, $N_{\max} = \max\{N_t, N_r\}$ and $\mathbf{U}(\eta)$ is an $N_{\min} \times N_{\min}$ Hankel matrix whose $(i, j)^{\text{th}}$ entry is

$$u_{ij}(\eta) = \left(\frac{\rho}{N_t}\right)^{-d_{ij}} \Gamma(d_{ij}) \Psi\left(d_{ij}, d_{ij} + 1 - \frac{2}{\eta}; \frac{N_t}{\rho}\right) \quad (2.15)$$

where $d_{ij} = i + j + |N_t - N_r| - 1$, $1 \leq i, j \leq N_{\min}$, and $\Psi(a, b; x)$ is the Ψ function (see [93, pp. 257-261]).

Proof. Under the assumption that the transmitter only knows the instantaneous channel capacity R_c , the covariance matrix of the transmitted vector \mathbf{x} at the transmitter is supposed to be a scaled identity matrix $\frac{P_t}{N_t} \mathbf{I}_{N_t}$. Given by [42], the mutual information per channel use is

$$\mathcal{I}(\mathbf{x}; \mathbf{y}) = \log_2 \left| \mathbf{I}_{N_r} + \frac{\rho}{N_t} \mathbf{W}\mathbf{W}^\dagger \right|. \quad (2.16)$$

As stated in [16, pp. 248-250], a band-limited channel of bandwidth W_c can be represented by samples taken $1/2W_c$ seconds apart, i.e., the channel is used at $2W_c$ channel uses per second as a time-discrete channel, and hence the channel capacity (bits/second) is

$$R_c = 2W_c \mathcal{I} = 2W_c \log_2 \left| \mathbf{I}_{N_r} + \frac{\rho}{N_t} \mathbf{H}\mathbf{H}^\dagger \right|. \quad (2.17)$$

Substituting (2.17) into the Shannon inequality (2.1), we have the optimum end-to-end distortion

$$D^*(\eta) = P_s \left| \mathbf{I}_{N_r} + \frac{\rho}{N_t} \mathbf{H}\mathbf{H}^\dagger \right|^{-\frac{2}{\eta}}. \quad (2.18)$$

Thereby, the optimum expected end-to-end distortion is

$$ED^*(\eta) = P_s \mathbb{E}_{\mathbf{H}} \left| \mathbf{I}_{N_r} + \frac{\rho}{N_t} \mathbf{H}\mathbf{H}^\dagger \right|^{-\frac{2}{\eta}}, \quad (2.19)$$

whose form is similar to the moment generating function of capacity in [94]. By the mathematical results given by Chiani *et al.* [94] for the expectation over an uncorrelated MIMO Gaussian channel \mathbf{H} , we have

$$ED_{\text{unc}}^*(\eta) = P_s K |\mathbf{U}(\eta)| \quad (2.20)$$

where $\mathbf{U}(\eta)$ is an $N_{\min} \times N_{\min}$ Hankel matrix with $(i, j)^{\text{th}}$ element given by

$$u_{ij}(\eta) = \int_0^\infty x^{N_{\max} - N_{\min} + j + i - 2} e^{-x} \left(1 + \frac{\rho}{N_t} x \right)^{-\frac{2}{\eta}} dx \quad (2.21)$$

and

$$K = \frac{1}{\prod_{k=1}^{N_{\min}} \Gamma(N_{\max} - k + 1) \Gamma(N_{\min} - k + 1)}. \quad (2.22)$$

By the integral solution (2.6), (2.21) can be written in the analytic form

$$u_{ij}(\eta) = \left(\frac{\rho}{N_t} \right)^{-d_{ij}} \Gamma(d_{ij}) \Psi \left(d_{ij}, d_{ij} + 1 - \frac{2}{\eta}; \frac{N_t}{\rho} \right), \quad (2.23)$$

This concludes our proof of the theorem. \square

2.4.2 Asymptotic optimum expected distortion

Theorem 1 tells us that the analytical form of ED_{unc}^* is a polynomial of ρ^{-1} . Therefore, at high SNR, the asymptotic ED_{unc}^* is in the form

$$ED_{\text{asy,unc}}^* = \mu_{\text{unc}}^*(\eta)\rho^{-\Delta_{\text{unc}}^*(\eta)} \quad (2.24)$$

where $\Delta_{\text{unc}}^*(\eta)$ is the *optimum distortion exponent* satisfying

$$\Delta_{\text{unc}}^*(\eta) = - \lim_{\rho \rightarrow \infty} \frac{\log ED_{\text{unc}}^*(\eta)}{\log \rho} \quad (2.25)$$

and μ_{unc}^* is the corresponding *optimum distortion factor* satisfying

$$\lim_{\rho \rightarrow \infty} \frac{\log \mu_{\text{unc}}^*(\eta)}{\log \rho} = 0. \quad (2.26)$$

The closed-form expressions of $\Delta_{\text{unc}}^*(\eta)$ and $\mu_{\text{unc}}^*(\eta)$ are given as follows.

Theorem 2 (Optimum Distortion Exponent for Uncorrelated MIMO Channel). *The optimum distortion exponent is*

$$\Delta_{\text{unc}}^*(\eta) = \sum_{k=1}^{N_{\min}} \min \left\{ \frac{2}{\eta}, 2k - 1 + |N_t - N_r| \right\}. \quad (2.27)$$

Proof. The optimum distortion exponent herein appears already in [38, 40]. However, a different proof is provided here.

Consider $u_{ij}(\eta)$ in Theorem 1. When ρ is large, N_t/ρ is small. We thus refer to Table 2.1 in [93] and see that, at a high SNR, $u_{ij}(\eta)$ approaches $e_{ij}(\eta)\rho^{-\Delta_{ij}(\eta)}$ with

$$\Delta_{ij}(\eta) = \min \left\{ \frac{2}{\eta}, i + j - 1 + |N_t - N_r| \right\} \quad (2.28)$$

and

$$\lim_{\rho \rightarrow \infty} \frac{\log e_{ij}(\eta)}{\log \rho} = 0. \quad (2.29)$$

Straightforwardly, at the asymptotically high SNR, the asymptotic form of $|\mathbf{U}(\eta)|$ is $|\mathbf{E}(\eta)|\rho^{-\Delta_{\text{unc}}^*(\eta)}$ with

$$\lim_{\rho \rightarrow \infty} \frac{\log |\mathbf{E}(\eta)|}{\log \rho} = 0. \quad (2.30)$$

$$\kappa_l(\beta, t, m, n) = \begin{cases} \Gamma(n-m+1) \frac{\Gamma(\beta-n+m-1)}{\Gamma(\beta)} \prod_{k=2}^t \Gamma(k) \Gamma(n-m+k) \\ \quad \times \frac{\Gamma(\beta-n+m-2k+2) \Gamma(\beta-n+m-2k+1)}{\Gamma(\beta-k+1) \Gamma(\beta-n+m-k+1)}, & t > 1; \\ \Gamma(n-m+1) \frac{\Gamma(\beta-n+m-1)}{\Gamma(\beta)}, & t = 1; \\ 1, & t = 0. \end{cases} \quad (2.32)$$

$$\kappa_h(\beta, t, m, n) = \begin{cases} \prod_{k=1}^t \Gamma(k) \Gamma(n-m-\beta+k), & t > 0; \\ 1, & t = 0. \end{cases} \quad (2.33)$$

By Lemma 1, we obtain that

$$\Delta_{\text{unc}}^*(\eta) = \sum_{k=1}^{N_{\min}} \min \left\{ \frac{2}{\eta}, 2k-1 + |N_t - N_r| \right\}. \quad (2.31)$$

This concludes our proof of this theorem. \square

Theorem 3 (Optimum Distortion Factor for Uncorrelated Channel). *Define two four-tuple functions $\kappa_l(\beta, t, m, n)$ and $\kappa_h(\beta, t, m, n)$ as (2.32) and (2.33) for $\beta \in \mathbb{R}^+$ and $t \in \{0, \mathbb{Z}^+\}$.*

$\mu_{\text{unc}}^*(\eta)$ is given as follows:

1. For $2/\eta \in (0, |N_t - N_r| + 1)$, referred to as high SCBR regime, the optimum distortion factor is

$$\mu_{\text{unc}}^*(\eta) = P_s N_t \Delta_{\text{unc}}^* \frac{\kappa_h\left(\frac{2}{\eta}, N_{\min}, N_{\min}, N_{\max}\right)}{\prod_{k=1}^{N_{\min}} \Gamma(N_{\max} - k + 1) \Gamma(N_{\min} - k + 1)}. \quad (2.34)$$

It monotonically decreases with N_{\max} .

2. For $2/\eta \in (N_t + N_r - 1, +\infty)$, referred to as low SCBR regime, the optimum distortion factor is

$$\mu_{\text{unc}}^*(\eta) = P_s N_t \Delta_{\text{unc}}^* \frac{\kappa_l\left(\frac{2}{\eta}, N_{\min}, N_{\min}, N_{\max}\right)}{\prod_{k=1}^{N_{\min}} \Gamma(N_{\max} - k + 1) \Gamma(N_{\min} - k + 1)}. \quad (2.35)$$

3. For $2/\eta \in [|N_t - N_r| + 1, N_t + N_r - 1]$, referred to as moderate SCBR regime, the optimum distortion factor is

$$\mu_{\text{unc}}^*(\eta) = \begin{cases} P_s N_t \Delta_{\text{unc}}^* \frac{\kappa_l(\frac{2}{\eta}, l, N_{\min}, N_{\max}) \kappa_h(\frac{2}{\eta} - 2l, N_{\min} - l, N_{\min}, N_{\max})}{\prod_{k=1}^{N_{\min}} \Gamma(N_{\max} - k + 1) \Gamma(N_{\min} - k + 1)}, \\ \quad \text{mod } \{\frac{2}{\eta} + 1 - |N_t - N_r|, 2\} \neq 0; \\ P_s N_t \Delta_{\text{unc}}^* \log \rho \frac{\kappa_l(\frac{2}{\eta}, l - 1, N_{\min}, N_{\max}) \kappa_h(\frac{2}{\eta} - 2l, N_{\min} - l, N_{\min}, N_{\max})}{\prod_{k=1}^{N_{\min}} \Gamma(N_{\max} - k + 1) \Gamma(N_{\min} - k + 1)}, \\ \quad \text{mod } \{\frac{2}{\eta} + 1 - |N_t - N_r|, 2\} = 0 \end{cases}, \quad (2.36)$$

$$\text{where } l = \left\lfloor \frac{\frac{2}{\eta} + 1 - |N_t - N_r|}{2} \right\rfloor.$$

Proof. From the proof of Theorem 2, we see that

$$\mu_{\text{unc}}^*(\eta) = \frac{P_s |\mathbf{E}(\eta)|}{\prod_{k=1}^{N_{\min}} \Gamma(N_{\max} - k + 1) \Gamma(N_{\min} - k + 1)} \quad (2.37)$$

where $\mathbf{E}(\eta)$ is an $N_{\min} \times N_{\min}$ matrix of $e_{ij}(\eta)$'s.

1. When $2/\eta \in (0, |N_t - N_r| + 1)$, given by (2.15) and Table 2.1, we have

$$e_{ij}(\eta) = N_t^{\frac{2}{\eta}} \Gamma(d_{ij} - \frac{2}{\eta}). \quad (2.38)$$

By Lemma 3,

$$|\mathbf{E}(\eta)| = N_t^{\Delta_{\text{unc}}^*} \kappa_h\left(\frac{2}{\eta}, N_{\min}, N_{\min}, N_{\max}\right). \quad (2.39)$$

In this case, $\Delta_{\text{unc}}^*(\eta) = 2N_{\min}/\eta$. Substituting (2.39) into (2.37), we obtain the optimum distortion factor in this case in the closed form

$$\mu_{\text{unc}}^*(\eta) = P_s N_t \Delta_{\text{unc}}^* \frac{\kappa_h(\frac{2}{\eta}, N_{\min}, N_{\min}, N_{\max})}{\prod_{k=1}^{N_{\min}} \Gamma(N_{\max} - k + 1) \Gamma(N_{\min} - k + 1)}. \quad (2.40)$$

In the light of Lemma 5, it monotonically decreases with N_{\max} .

2. When $2/\eta \in (N_t + N_r - 1, \infty)$, in terms of (2.15) and Table 2.1, we have

$$e_{ij}(\eta) = N_t^{d_{ij}} \Gamma(d_{ij}) \frac{\Gamma\left(\frac{2}{\eta} - d_{ij}\right)}{\Gamma\left(\frac{2}{\eta}\right)}. \quad (2.41)$$

In terms of Lemma 2 and Lemma 4, the determinant of $\mathbf{E}(\eta)$

$$|\mathbf{E}(\eta)| = N_t^{\Delta_{\text{unc}}^*} \kappa_l \left(\frac{2}{\eta}, N_{\min}, N_{\min}, N_{\max} \right). \quad (2.42)$$

In this case, $\Delta_{\text{unc}}^*(\eta) = N_t N_r$. Substituting (2.42) into (2.37), we obtain the optimum distortion factor in this case in the form

$$\mu_{\text{unc}}^* = P_s N_t^{\Delta_{\text{unc}}^*} \frac{\kappa_l \left(\frac{2}{\eta}, N_{\min}, N_{\min}, N_{\max} \right)}{\prod_{k=1}^{N_{\min}} \Gamma(N_{\max} - k + 1) \Gamma(N_{\min} - k + 1)}. \quad (2.43)$$

3. When $2/\eta \in [|N_t - N_r| + 1, N_t + N_r - 1]$, the analysis is relatively complex. Define a partition number

$$l = \left\lfloor \frac{\frac{2}{\eta} + 1 - |N_t - N_r|}{2} \right\rfloor \quad (2.44)$$

and partition the Hankel matrix $\mathbf{E}(\eta)$ in (2.14) as

$$\mathbf{E}(\eta) = \begin{pmatrix} \mathbf{A} & \mathbf{B} \\ \mathbf{B}^T & \mathbf{C} \end{pmatrix} \quad (2.45)$$

where \mathbf{A} is the $l \times l$ submatrix and \mathbf{C} is the $(N_{\min} - l) \times (N_{\min} - l)$ submatrix.

At a high SNR, in terms of Table 2.1, if $2l \neq \frac{2}{\eta} + 1 - |N_t - N_r|$, elements of \mathbf{A} and \mathbf{C} approximate

$$\tilde{a}_{ij} = N_t^{d_{ij}} \Gamma(d_{ij}) \frac{\Gamma(\frac{2}{\eta} - d_{ij})}{\Gamma(\frac{2}{\eta})} \rho^{-d_{ij}}, \quad (2.46)$$

$$\tilde{c}_{ij} = N_t^{\frac{2}{\eta}} \Gamma(d_{ij} - \frac{2}{\eta}) \rho^{-\frac{2}{\eta}}; \quad (2.47)$$

if $2l = \frac{2}{\eta} + 1 - |N_t - N_r|$, the form of \tilde{c}_{ij} is the same as (2.47) whereas the form of \tilde{a}_{ij} becomes

$$\tilde{a}_{ij} = \begin{cases} N_t^{d_{ij}} \Gamma(d_{ij}) \frac{\Gamma(\frac{2}{\eta} - d_{ij})}{\Gamma(\frac{2}{\eta})} \rho^{-d_{ij}}, & (i, j) \neq (l, l); \\ N_t^{\frac{2}{\eta}} \log \rho \rho^{-\frac{2}{\eta}}, & (i, j) = (l, l). \end{cases} \quad (2.48)$$

In terms of Schur determinant formula [95],

$$|\mathbf{E}(\eta)| = |\mathbf{A}| |\mathbf{C} - \mathbf{A}^*| \quad (2.49)$$

where $\mathbf{A}^* = \mathbf{B}^T \mathbf{A}^{-1} \mathbf{B}$. By the method similar to the derivation in Appendix 2.A, we know that at high SNR

$$\mathbf{C} - \mathbf{A}^* \sim \tilde{\mathbf{C}} \quad (2.50)$$

where $\tilde{\mathbf{C}}$ is composed of \tilde{c}_{ij} 's. Consequently,

$$|\mathbf{E}(\eta)| \sim |\tilde{\mathbf{A}}| |\tilde{\mathbf{C}}|. \quad (2.51)$$

Given the preceding derivation for the high and low SCBR regimes, we have

$$|\tilde{\mathbf{A}}| = \begin{cases} N_t^{l(l+N_{\max}-N_{\min})} \kappa_l(\frac{2}{\eta}, l, N_{\min}, N_{\max}) \rho^{-l(l+N_{\max}-N_{\min})}, \\ \text{if } 2l \neq \frac{2}{\eta} + 1 - |N_t - N_r|; \\ N_t^{l(l+N_{\max}-N_{\min})} \kappa_l(\frac{2}{\eta}, l-1, N_{\min}, N_{\max}) \log \rho \rho^{-l(l+N_{\max}-N_{\min})}, \\ \text{if } 2l = \frac{2}{\eta} + 1 - |N_t - N_r|, \end{cases} \quad (2.52)$$

$$|\tilde{\mathbf{C}}| = N_t^{\frac{2(N_{\min}-l)}{\eta}} \kappa_h(\frac{2}{\eta} - 2l, N_{\min} - l, N_{\min}, N_{\max}) \rho^{-\frac{2(N_{\min}-l)}{\eta}}. \quad (2.53)$$

Therefore, in this case,

$$\mu_{\text{unc}}^*(\eta) = \begin{cases} P_s N_t^{\Delta_{\text{unc}}^*} \frac{\kappa_l(\frac{2}{\eta}, l, N_{\min}, N_{\max}) \kappa_h(\frac{2}{\eta} - 2l, N_{\min} - l, N_{\min}, N_{\max})}{\prod_{k=1}^{N_{\min}} \Gamma(N_{\max} - l + 1) \Gamma(N_{\min} - k + 1)}, \\ 2l \neq \frac{2}{\eta} + 1 - |N_t - N_r|; \\ P_s N_t^{\Delta_{\text{unc}}^*} \log \rho \frac{\kappa_l(\frac{2}{\eta}, l-1, N_{\min}, N_{\max}) \kappa_h(\frac{2}{\eta} - 2l, N_{\min} - l, N_{\min}, N_{\max})}{\prod_{k=1}^{N_{\min}} \Gamma(N_{\max} - l + 1) \Gamma(N_{\min} - k + 1)}, \\ 2l = \frac{2}{\eta} + 1 - |N_t - N_r| \end{cases} \quad (2.54)$$

where the distortion exponent is

$$\Delta_{\text{unc}}^*(\eta) = l(l + |N_t - N_r|) + \frac{2(N_{\min} - l)}{\eta}. \quad (2.55)$$

This concludes our proof of this theorem. \square

2.5 Numerical analysis and discussion

Fig.2.1 shows numerical and simulation results on the optimum expected end-to-end distortion of Gaussian source transmission over uncorrelated

slow-fading MIMO channels in the high SCBR state and at the high SNR, $\rho = 30\text{dB}$. The number of antennas on one side (either the transmitter side or the receiver side) is fixed to five and the number of antennas on the other side is increased. ED_{unc}^* corresponding to (2.19) is evaluated by 10 000 realizations of \mathbf{H} and denoted by $ED_{\text{unc},\text{sim}}^*$.

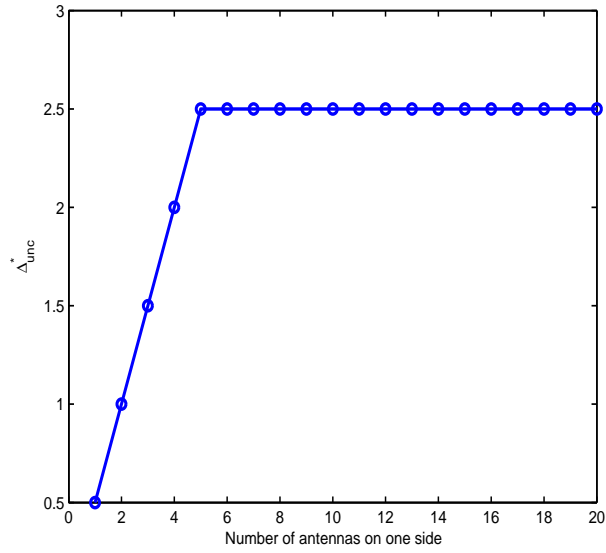
From Fig.2.1(b), we can see that $ED_{\text{unc},\text{sim}}^*$ monotonically decreases with the number of antennas on one side, which agrees with our intuition. There is an excellent agreement between $ED_{\text{unc},\text{asy}}^*$ and $ED_{\text{unc},\text{sim}}^*$, indicating that in this case, the behavior of ED_{unc}^* at high SNR can be explained by studying the distortion exponent Δ_{unc}^* and the distortion factor μ_{unc}^* .

In Fig.2.1(a), in terms of Theorem 2, Δ_{unc}^* increases with N_{min} and then keeps constant after N_{min} stops increasing, although the number of antennas on one side is increasing. In Fig.2.1(b), in terms of Theorem 3, μ_{unc}^* monotonically decreases with N_{max} . Therefore, when $N_{\text{min}} \leq 5$, ED_{unc}^* decreases because Δ_{unc}^* is increasing. The increase of Δ_{unc}^* dominates the monotonicity of ED_{unc}^* since the SNR is high. When the N_{min} is fixed to 5, ED_{unc}^* decreases because μ_{unc}^* is decreasing though Δ_{unc}^* keeps constant. Hence, we can see that, at the high SNR, the monotonicity of ED_{unc}^* with the number of antennas is either due to the increase of the distortion exponent or due to the decrease of the corresponding distortion factor.

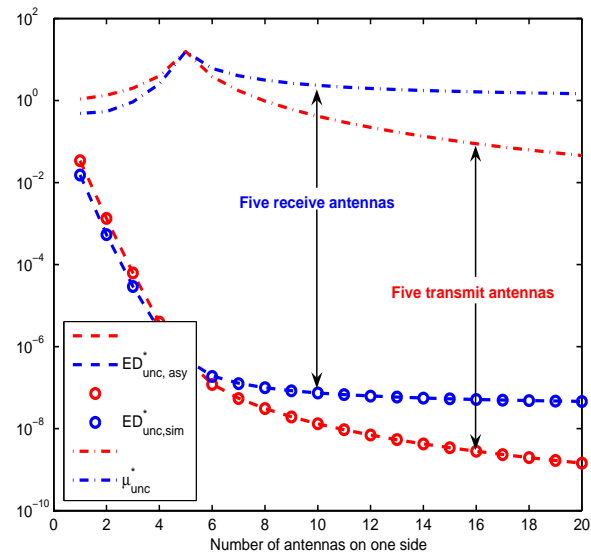
Moreover, from Fig.2.1, we can see that the commutation between the number of transmit antennas and the number of receive antennas impacts ED_{unc}^* . This impact comes from the effect of the commutation on the distortion factor μ_{unc}^* . As indicated by expressions in Theorem 3 and shown in Fig.2.1(b), between a couple of commutative antenna allocation schemes, $(N_t = N_{\text{min}}, N_r = N_{\text{max}})$ and $(N_t = N_{\text{max}}, N_r = N_{\text{min}})$, the former scheme whose number of transmit antennas is the smaller between the two antenna numbers suffers less distortion than the other. This is reasonable since under certain total transmit power constraint, the scheme allocated less transmit antennas achieves higher average transmit power per transmit antenna.

If a system is in the moderate or low SCBR regimes, Δ_{unc}^* monotonically increases with either of the two antenna numbers as Theorem 2 implies. Therefore, in the high SNR regime, in the moderate or low SCBR regimes, the optimum expected end-to-end distortion monotonically decreases with either of the two antenna numbers regardless of the tendency of μ_{unc}^* .

Fig.2.2-Fig.2.5 show the numerical and simulation results for the other four examples corresponding to different cases. Red circles represent the results of Monte Carlo simulations which are carried out by generating 10 000 realizations of \mathbf{H} and evaluating (2.19). Blue dashed lines represent $ED_{\text{asy},\text{unc}}^*$. Green lines represent the analytic form of ED_{unc}^* in Theorem



(a)



(b)

Figure 2.1: Uncorrelated channel, one of (N_t, N_r) is fixed to 5, $\eta = 4$, high SCBR.

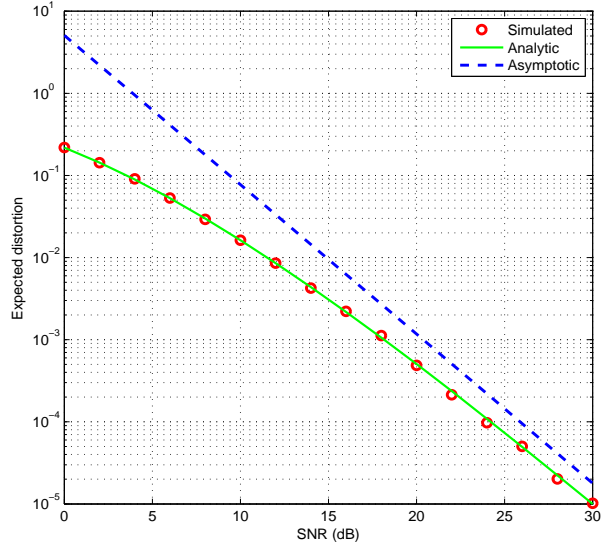


Figure 2.2: Uncorrelated channel, $N_t = 1$, $N_r = 2$, $\eta = 1.1$, high SCBR

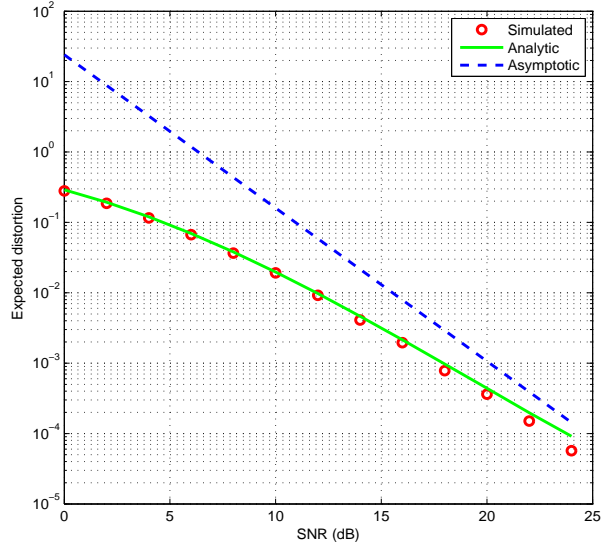


Figure 2.3: Uncorrelated channel, $N_t = 2$, $N_r = 2$, $\eta = 1.7$, moderate SCBR

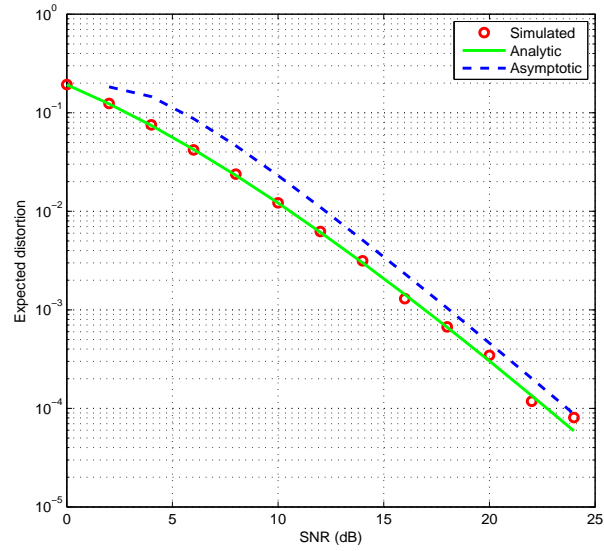


Figure 2.4: Uncorrelated channel, $N_t = 2$, $N_r = 2$, $\eta = 1$, moderate SCBR

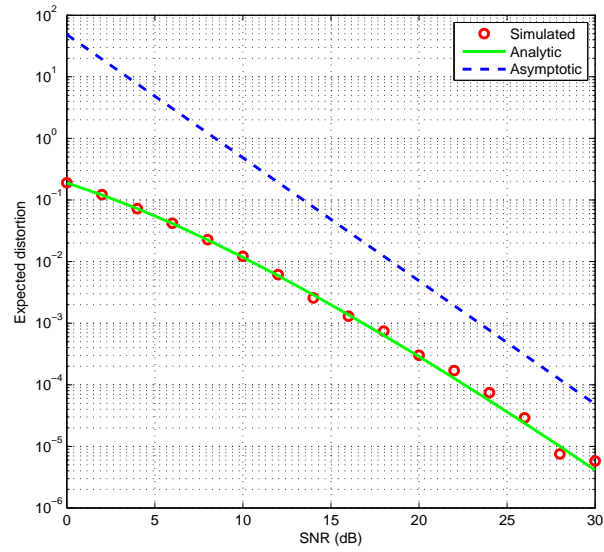


Figure 2.5: Uncorrelated channel, $N_t = 1$, $N_r = 2$, $\eta = 0.99$, low SCBR

1. It can be seen that the simulated results agree well with our analytic results. In Fig.2.2-Fig.2.5, we can see that, in the practical range of SNR, there are gaps between the curves of ED_{unc}^* and $ED_{\text{asy,unc}}^*$, which come from the impact of other terms in the polynomial of ED_{unc}^* .

2.6 Conclusion

In this chapter, assuming a continuous white noise source is transmitted over a spatially uncorrelated slow Rayleigh fading MIMO channel and the system is free of outage (e.g., the transmitter knows the instantaneous channel capacity by scalar feedback and does joint source-channel coding), we have derived the analytical expression of the optimum expected end-to-end distortion. On this basis, we have derived the asymptotic optimum expected distortion comprised of the optimum SNR distortion exponent and the corresponding distortion factor for all cases with respect to antenna numbers and source-to-channel band ratio. By our results, we have explained the behavior of the optimum expected end-to-end distortion of a MIMO system over an uncorrelated channel in the regime of high SNR, related to the behaviors of the SNR distortion exponent and the corresponding distortion factor.

Straightforwardly, the theorems in this chapter are upper bounds for the scenario that the transmitter has no knowledge on the channel and suffers outage accidents at a certain probability.

2.A Proof of Lemma 1

We shall prove this lemma recursively.

Define $p(n) = \min\{a, n\}$, subject to $a \in \mathbb{R}^+$ and $n \in \mathbb{Z}^+$. If $m_1 - m_2 = n_1 - n_2$, $m_1 > n_1$, and $m_2 > n_2$, then

$$p(m_1) - p(m_2) \leq p(n_1) - p(n_2). \quad (2.56)$$

In the case that $m = 2$, by definition,

$$\mathbf{W}_2(x) = \begin{pmatrix} c_{11}x^{p(2)} & c_{12}x^{p(3)} \\ c_{21}x^{p(3)} & c_{22}x^{p(4)} \end{pmatrix}. \quad (2.57)$$

Then

$$|\mathbf{W}_2(x)| = c_{11}c_{22}x^{p(2)+p(4)} - c_{12}c_{21}^2x^{2p(3)}. \quad (2.58)$$

By (2.56),

$$p(2) + p(4) \leq 2p(3). \quad (2.59)$$

Consequently, when $m = 2$,

$$\begin{aligned} \lim_{x \rightarrow 0} \frac{\log|\mathbf{W}_2(x)|}{\log x} &= p(2) + p(4) \\ &= \sum_{i=1}^2 \min\{a, 2i\}. \end{aligned} \quad (2.60)$$

Suppose when $m = k - 1$, $k \in \mathbb{Z}^+ \cap [3, +\infty)$,

$$\lim_{x \rightarrow 0} \frac{\log|\mathbf{W}_{k-1}(x)|}{\log x} = \sum_{i=1}^{k-1} \min\{a, 2i\}. \quad (2.61)$$

When $m = k$, $\mathbf{W}_k(x)$ can be written as

$$\begin{pmatrix} \mathbf{W}_{k-1}(x) & \mathbf{b}_k(x) \\ \mathbf{b}_k^T(x) & c_{kk}x^{p(2k)} \end{pmatrix} \quad (2.62)$$

where the column vector

$$\mathbf{b}_k(x) = \begin{pmatrix} c_{1k}x^{p(k+1)} \\ \vdots \\ c_{k-1,k}x^{p(2k-1)} \end{pmatrix}. \quad (2.63)$$

Hence, in terms of Schur determinant formula [95],

$$\begin{aligned} \lim_{x \rightarrow 0} \frac{\log |\mathbf{W}_k(x)|}{\log x} &= \lim_{x \rightarrow 0} \frac{\log [|\mathbf{W}_{k-1}(x)| |\mathbf{W}_{k-1}^*(x)|]}{\log x} \\ &= \lim_{x \rightarrow 0} \frac{\log |\mathbf{W}_{k-1}(x)|}{\log x} + \lim_{x \rightarrow 0} \frac{\log \det \mathbf{W}_{k-1}^*(x)}{\log x} \end{aligned} \quad (2.64)$$

where $\mathbf{W}_{k-1}^*(x)$ is the Schur complement of $\mathbf{W}_{k-1}(x)$,

$$\mathbf{W}_{k-1}^*(x) = c_{2k} x^{p(2k)} - \mathbf{b}_k^T(x) \mathbf{W}_{k-1}^{-1}(x) \mathbf{b}_k(x). \quad (2.65)$$

Since $\mathbf{W}_{k-1}(x) \mathbf{W}_{k-1}^{-1}(x) = \mathbf{I}$, $\mathbf{W}_{k-1}^{-1}(x)$ is of the form

$$\begin{pmatrix} c'_{11} x^{-p(2)} & \dots & c'_{1k} x^{-p(k)} \\ \vdots & \ddots & \vdots \\ c'_{k1} x^{-p(k)} & \dots & c'_{k-1,k-1} x^{-p(2k-2)} \end{pmatrix}. \quad (2.66)$$

Consequently,

$$\begin{aligned} &\lim_{x \rightarrow 0} \frac{\log [\mathbf{b}_k^T(x) \mathbf{W}_{k-1}^{-1}(x) \mathbf{b}_k(x)]}{\log x} \\ &= \min\{p(2k-1) - p(k) + p(k+1), \quad p(2k-1) - p(k+1) + p(k+2), \\ &\quad \dots, \quad p(2k-1) - p(2k-2) + p(2k-1)\} \\ &\stackrel{(a)}{=} p(2k-1) - p(2k-2) + p(2k-1) \\ &\stackrel{(b)}{\geq} p(2k) \end{aligned} \quad (2.67)$$

where both steps (a) and (b) follow the inequality (2.56). Therefore, by (2.64) and (2.65),

$$\lim_{x \rightarrow 0} \frac{\log \det \mathbf{W}(x)}{\log x} = \sum_{i=1}^k \min\{a, 2i\}, \quad (2.68)$$

which concludes this proof.

2.B Proof of Lemma 2

Each summand in $|\mathbf{W}(x)|$, which is a product of the elements $w_{1j_1}, \dots, w_{mj_m}$, can be written as

$$x^{\sum_{k=1}^m (k+j_k)} \prod_{k=1}^m c_{k+j_k} \quad (2.69)$$

where the numbers $\{j_1, j_2, \dots, j_m\}$ is a permutation of $\{1, 2, \dots, m\}$. Then, each summand has the same degree $m(m+1)$, which concludes the proof.

2.C Proof of Lemma 3

By definition,

$$\mathbf{W} = \begin{pmatrix} \Gamma(a+1) & \cdots & \Gamma(a+m) \\ \vdots & \ddots & \vdots \\ \Gamma(a+m) & \cdots & \Gamma(a+2m-1) \end{pmatrix}. \quad (2.70)$$

For calculating the determinant of \mathbf{W} , we do Gaussian elimination by elementary row operations from bottom to top for obtaining the equivalent upper triangular \mathbf{L} [96]. Below-diagonal elements are eliminated from the first column to the last column.

Let \mathbf{W}_l denote the matrix after the below-diagonal elements of the l^{th} column are eliminated. Then the $(i, j)^{\text{th}}$ element of \mathbf{W}_l subject to $i \geq j > l$ is of the form

$$w_{l,i,j} = \theta_{l,i,j} \Gamma(a+i+j-1-l). \quad (2.71)$$

Hence, after below-diagonal elements of the $(l-1)^{\text{th}}$ column are eliminated, for the elements subject to $i > l$ and $j = l$,

$$w_{l-1,i-1,l} = \theta_{l-1,i-1,l} \Gamma(a+i-1), \quad (2.72)$$

$$w_{l-1,i,l} = \theta_{l-1,i,l} \Gamma(a+i). \quad (2.73)$$

Consequently, for eliminating the $(i, l)^{\text{th}}$ element of \mathbf{W}_{l-1} to obtain \mathbf{W}_l , the multiplied coefficient for the row operation in the Gaussian elimination on the i^{th} row

$$c_{l,i} = -\frac{\theta_{l-1,i,l}}{\theta_{l-1,i-1,l}} (a+i-1). \quad (2.74)$$

That is, $w_{l,i,j}$ is obtained as follows:

$$\begin{aligned} w_{l,i,j} &= w_{l-1,i,j} + c_{l,i} w_{l-1,i-1,j} \\ &= \left[\theta_{l-1,i,j} (a+i+j-l-1) - \theta_{l-1,i-1,j} \frac{\theta_{l-1,i,l}}{\theta_{l-1,i-1,l}} (a+i-1) \right] \\ &\quad \times \Gamma(a+i+j-l-1). \end{aligned} \quad (2.75)$$

Comparing the RHS of the above equation to (2.71), we get

$$\theta_{l,i,j} = \theta_{l-1,i,j} (a+i+j-l-1) - \theta_{l-1,i-1,j} \frac{\theta_{l-1,i,l}}{\theta_{l-1,i-1,l}} (a+i-1). \quad (2.76)$$

Before doing any operation on \mathbf{W} , $\theta_{0,i,j} = 1$. Then, by (2.76), we obtain $\theta_{1,i,j} = j - 1$ and $\theta_{2,i,j} = \Gamma(j)/\Gamma(j - 2)$. Supposing

$$\theta_{l,i,j} = \frac{\Gamma(j)}{\Gamma(j - l)}. \quad (2.77)$$

then by (2.76) we have

$$\theta_{l+1,i,j} = \frac{\Gamma(j)}{\Gamma(j - l - 1)}. \quad (2.78)$$

Therefore, our conjecture is right. Hence,

$$\theta_{i-1,i,i} = \Gamma(i). \quad (2.79)$$

and the i^{th} diagonal entry of \mathbf{L} ,

$$w_{i-1,i,i} = \Gamma(i)\Gamma(a + i). \quad (2.80)$$

Consequently,

$$|\mathbf{W}_m| = \prod_{k=1}^m \Gamma(k)\Gamma(a + k), \quad (2.81)$$

which concludes this proof.

2.D Proof of Lemma 4

This proof is similar to Appendix 2.C.

By definition,

$$\mathbf{W} = \begin{pmatrix} \Gamma(a + 1)\Gamma(b - 1) & \cdots & \Gamma(a + m)\Gamma(b - m) \\ \vdots & \ddots & \vdots \\ \Gamma(a + m)\Gamma(b - m) & \cdots & \Gamma(a + 2m - 1)\Gamma(b - 2m + 1) \end{pmatrix}. \quad (2.82)$$

The $(i, j)^{\text{th}}$ element of \mathbf{W}_l subject to $i \geq j > l$ is of the form

$$w_{l,i,j} = \theta_{l,i,j} \Gamma(a + i + j - 1 - l)\Gamma(b - i - j + 1). \quad (2.83)$$

Consequently, the multiplied coefficient

$$c_{l,i} = -\frac{\theta_{l-1,i,l}(a + i - 1)}{\theta_{l-1,i-1,l}(b - i - l + 1)}. \quad (2.84)$$

and

$$\begin{aligned}
w_{l,i,j} &= w_{l-1,i,j} + c_{l,i} w_{l-1,i-1,j} \\
&= \left[\theta_{l-1,i,j} (a+i+j-l-1) - \frac{\theta_{l-1,i-1,j} \theta_{l-1,i,l} (a+i-1) (b-i-j+1)}{\theta_{l-1,i-1,l} (b-i-l+1)} \right] \\
&\quad \Gamma(a+i+j-l-1) \Gamma(b-i-j+1).
\end{aligned} \tag{2.85}$$

Comparing the RHS of the above expression to (2.83), we have

$$\theta_{l,i,j} = \theta_{l-1,i,j} (a+i+j-l-1) - \theta_{l-1,i-1,j} \frac{\theta_{l-1,i,l} (a+i-1) (b-i-j+1)}{\theta_{l-1,i-1,l} (b-i-l+1)} \tag{2.86}$$

Before doing any operation on \mathbf{W} , $\theta_{0,i,j} = 1$. Then, by (2.86), we obtain

$$\theta_{1,i,j} = \frac{(j-1)(a+b-1)}{(b-i)}, \tag{2.87}$$

$$\theta_{2,i,j} = \frac{(j-1)(j-2)(a+b-1)(a+b-2)}{(b-i)(b-i-1)}. \tag{2.88}$$

Supposing

$$\theta_{l,i,j} = \prod_{k=1}^l \frac{(j-k)(a+b-k)}{(b-i-l+k)}. \tag{2.89}$$

then by (2.86) we have

$$\theta_{l+1,i,j} = \prod_{k=1}^{l+1} \frac{(j-k)(a+b-k)}{(b-i-l+k)}. \tag{2.90}$$

Therefore, our conjecture is right. So, for $i \geq 2$, the i^{th} diagonal element of the equivalent upper triangular \mathbf{L} ,

$$w_{i-1,i,i} = \Gamma(a+b) \Gamma(i) \Gamma(a+i) \frac{\Gamma(b-2i+2) \Gamma(b-2i+1)}{\Gamma(a+b-i+1) \Gamma(b-i+1)}. \tag{2.91}$$

Consequently,

$$\begin{aligned}
|\mathbf{W}| &= \Gamma(a+1) \Gamma(b-1) \Gamma^{m-1}(a+b) \\
&\quad \prod_{k=2}^m \Gamma(k) \Gamma(a+k) \frac{\Gamma(b-2k+2) \Gamma(b-2k+1)}{\Gamma(a+b-k+1) \Gamma(b-k+1)},
\end{aligned} \tag{2.92}$$

which concludes this proof.

2.E Proof of Lemma 5

$f(n)$ can be written as

$$f(n) = \frac{\Gamma(n-a)}{\Gamma(n)} \cdots \frac{\Gamma(n-m+1-a)}{\Gamma(n-m+1)}. \quad (2.93)$$

We thus have

$$f(n+1) - f(n) = \left(\frac{n-a}{n} \cdots \frac{n-m+1-a}{n-m+1} - 1 \right) f(n). \quad (2.94)$$

It is seen that $\frac{n-a}{n} \cdots \frac{n-m+1-a}{n-m+1} < 1$ and $f(n) > 0$. Hence, $f(n+1) - f(n) < 0$, *i.e.*, $f(n)$ is monotonically decreasing.

For $g(n)$,

$$\begin{aligned} g(n+1) - g(n) &= \left[(n+1)^{am} \frac{n-a}{n} \cdots \frac{n-m+1-a}{n-m+1} - n^{am} \right] f(n) \\ &\leq \left[(n+1)^{am} \left(\frac{n-a}{n} \right)^m - n^{am} \right] f(n) \end{aligned} \quad (2.95)$$

If

$$(n+1)^a \frac{n-a}{n} < n^a, \quad (2.96)$$

then we have $g(n+1) - g(n) < 0$.

Define a function $h(x)$,

$$\begin{aligned} h(x) &= (x-a)(x+1)^a - x^{a+1} \\ &= (x+1)^{a+1} - x^{a+1} - (a+1)(x+1)^a, \quad x > a \end{aligned} \quad (2.97)$$

In terms of mean value theory [97], for $\phi(x) = x^{a+1}$, there exists ξ which lets

$$\phi'(\xi) = (x+1)^{a+1} - x^{a+1}, \quad x < \xi < x+1 \quad (2.98)$$

where $\phi'(\xi)$ is the first derivative.

As

$$\phi''(x) = a(a+1)x^{a-1} > 0, \quad (2.99)$$

$\phi'(x)$ is monotonically increasing and thus

$$\phi'(\xi) < \phi'(x+1). \quad (2.100)$$

So, $h(x) < 0$.

Then, we have

$$\frac{x-a}{x} < \left(\frac{x}{x+1} \right)^a. \quad (2.101)$$

When $x = n$,

$$(n+1)^a \frac{n-a}{n} < n^a \quad (2.102)$$

Consequently, $g(n+1) - g(n) < 0$, that is, $g(n)$ is monotonically decreasing.

Chapter 3

End-to-End Distortion: Correlated MIMO Channel

3.1 Introduction

In this chapter, we extend our investigation on the optimum expected end-to-end distortion to the case of spatially-correlated slow-fading channel.

In practice, a spatially-correlated MIMO channel is more general than an uncorrelated MIMO channel. Intuitively, for a correlated MIMO channel, we ought to obtain the result that the spatial correlation increases ED^* as it decreases the channel capacity and the results of the correlated case converges to the uncorrelated case when the correlation matrix approaches an identity matrix.

The system model in this chapter is similar to the description of the system model in Section 2.2 in Chapter 2. However, we herein assume the channel is spatially correlated on the receiver side and uncorrelated on the transmitter side. The correlation matrix $\mathbf{\Sigma} = \mathbb{E}\{\mathbf{H}\mathbf{H}^\dagger\}$, which is assumed to be a full-rank matrix, i.e. $N_r \leq N_t$, with distinct eigenvalues. Its dual case is that the channel is spatially uncorrelated at the receiver and correlated at the transmitter.

The remainder of this chapter is organized as follows. In Section 3.2, we give mathematical definitions, properties and lemmas as mathematical preliminaries for subsequent derivations. Section 3.3 is dedicated to our main

results. Numerical results are shown in Section 3.4 with analysis. Finally, Section 3.5 concludes the contributions of this chapter.

3.2 Mathematical preliminaries

The mathematical definition and lemmas below will be used in derivations and results thereafter.

For the function $\Psi(a, c; x)$, besides its definition and properties clarified in Section 2.3 in Chapter 2, in this chapter, we shall use other properties stated by Bateman [93, pp. 257-261] as below:

- If c is not an integer,

$$\begin{aligned} \Psi(a, c; x) &= \frac{\Gamma(1-c)}{\Gamma(a-c+1)} \Phi(a, c; x) \\ &+ \frac{\Gamma(c-1)}{\Gamma(a)} x^{1-c} \Phi(a-c+1, 2-c; x) \end{aligned} \quad (3.1)$$

where $\Phi(a, c; x)$ is another confluent hypergeometric function,

$$\Phi(a, c; x) = \sum_{r=0}^{\infty} \frac{(a)_r}{(c)_r} \frac{x^r}{r!}. \quad (3.2)$$

Note that $(a)_n = \Gamma(a+n)/\Gamma(a)$.

- if c is a positive integer,

$$\begin{aligned} \Psi(a, n+1; x) &= \frac{(-1)^{n-1}}{n! \Gamma(a-n)} \left\{ \Phi(a, n+1; x) \log x \right. \\ &+ \sum_{r=0}^{\infty} \frac{(a)_r}{(n+1)_r} [\psi(a+r) - \psi(1+r) - \psi(1+n+r)] \frac{x^r}{r!} \left. \right\} \\ &+ \frac{(n-1)!}{\Gamma(a)} \sum_{r=0}^{n-1} \frac{(a-n)_r}{(1-n)_r} \frac{x^{r-n}}{r!} \quad n = 0, 1, 2, \dots \end{aligned} \quad (3.3)$$

The last sum is to be omitted if $n = 0$.

-

$$\Psi(a, c; x) = x^{1-c} \Psi(a-c+1, 2-c; x). \quad (3.4)$$

Hence, when c is a non-positive integer, we can obtain the form of $\Psi(a, c; x)$ from (3.3) and (3.4), which is similar to (3.3),

$$\begin{aligned} \Psi(a, c; x) &= \frac{(-1)^{-c}}{(1-c)! \Gamma(a)} \left\{ \Phi(a+1-c, 2-c; x) x^{1-c} \log x \right. \\ &+ \sum_{r=0}^{\infty} \frac{(a+1-c)_r}{(2-c)_r} [\psi(a+1-c+r) - \psi(1+r) \\ &\left. - \psi(2-c+r)] \frac{x^{r+1-c}}{r!} \right\} + \frac{\Gamma(1-c)}{\Gamma(a+1-c)} \sum_{r=0}^{-c} \frac{(a)_r}{(c)_r} \frac{x^r}{r!} \end{aligned} \quad (3.5)$$

The other two mathematic lemma that we shall use are as below.

Lemma 6. Define an $m \times m$ Toeplitz matrix \mathbf{W} whose $(i, j)^{\text{th}}$ element is $\Gamma(a+i-j)$, $1 \leq i, j \leq m$, $a \in \mathbb{R}$. Then

$$|\mathbf{W}| = (-1)^{\frac{m(m-1)}{2}} \prod_{k=1}^m \Gamma(k) \Gamma(a+k-m). \quad (3.6)$$

Proof. The derivation is very similar to Appendix 2.C. However, for deriving Lemma 6, we use Gaussian elimination by column operations from the right to the left, instead of row operations from the bottom to the top in Appendix 2.C. After the Gaussian elimination, the left upper-diagonal triangle-matrix becomes a zero triangle-matrix. Consequently, the determinant of \mathbf{W} is

$$|\mathbf{W}| = (-1)^{\frac{m(m-1)}{2}} \prod_{k=1}^m \Gamma(k) \Gamma(a+k-m). \quad (3.7)$$

□

Lemma 7. Let $(a)_n$ denote $\Gamma(a+n)/\Gamma(a)$, $a \in \mathbb{R}$, $n \in \mathbb{Z}^+$. Then

$$(a+1)_n = (-1)^n (-a-n)_n \quad (3.8)$$

Proof. It is derived in terms of the feature of the Gamma function $\Gamma(x)$,

$$\Gamma(1-z)\Gamma(z) = \frac{\pi}{\sin(\pi z)}. \quad (3.9)$$

□

3.3 Main results

3.3.1 Optimum expected distortion at any SNR

Theorem 4 (Optimum Expected Distortion for MIMO Correlated Channel). *The optimum expected end-to-end distortion for MIMO systems over correlated channels*

$$ED_{\text{cor}}^*(\eta) = \frac{P_s |\mathbf{G}(\eta)|}{\prod_{k=1}^{N_{\min}} \sigma_k^{|N_t - N_r| + 1} \Gamma(N_{\max} - k + 1) \prod_{1 \leq m < n \leq N_{\min}} (\sigma_n - \sigma_m)}. \quad (3.10)$$

where $\mathbf{G}(\eta)$ is an $N_{\min} \times N_{\min}$ matrix whose $(i, j)^{\text{th}}$ entry given by

$$g_{ij}(\eta) = \left(\frac{\rho}{N_t} \right)^{-d_j} \Gamma(d_j) \Psi \left(d_j, d_j + 1 - \frac{2}{\eta}; \frac{N_t}{\sigma_i \rho} \right). \quad (3.11)$$

$d_j = |N_t - N_r| + j$. $\boldsymbol{\sigma} = \{\sigma_1, \sigma_2, \dots, \sigma_{N_{\min}}\}$ with $0 < \sigma_1 < \sigma_2 < \dots < \sigma_{N_{\min}}$ denoting the ordered eigenvalues of the correlation matrix $\boldsymbol{\Sigma}$.

Proof. Following the proof of Theorem 1, by the mathematical results given by Chiani *et al.* in [94] for spatially correlated \mathbf{H} , we have

$$ED_{\text{cor}}^*(\eta) = P_s K_{\boldsymbol{\Sigma}} |\mathbf{G}(\eta)| \quad (3.12)$$

where $\mathbf{G}(\eta)$ is an $N_{\min} \times N_{\min}$ matrix with $(i, j)^{\text{th}}$ elements given by

$$g_{ij}(\eta) = \int_0^\infty x^{|N_t - N_r| + j - 1} e^{-x/\sigma_i} \left(1 + \frac{\rho}{N_t} x\right)^{-\frac{2}{\eta}} dx \quad (3.13)$$

and

$$K_{\boldsymbol{\Sigma}} = \frac{|\boldsymbol{\Sigma}|^{-N_{\max}}}{|\mathbf{V}_2(\boldsymbol{\sigma})| \prod_{k=1}^{N_{\min}} \Gamma(N_{\max} - k + 1)} \quad (3.14)$$

where $\mathbf{V}_2(\boldsymbol{\sigma})$ is a Vandermonde matrix given by

$$\mathbf{V}_2(\boldsymbol{\sigma}) \triangleq \mathbf{V}_1 \left(-\{\sigma_1^{-1}, \dots, \sigma_{N_{\min}}^{-1}\} \right) \quad (3.15)$$

and the Vandermonde matrix $\mathbf{V}_1(\mathbf{x})$ is defined as

$$\mathbf{V}_1(\mathbf{x}) \triangleq \begin{bmatrix} 1 & 1 & \dots & 1 \\ x_1 & x_2 & \dots & x_{N_{\min}} \\ \vdots & \vdots & \ddots & \vdots \\ x_1^{N_{\min}-1} & x_2^{N_{\min}-1} & \dots & x_{N_{\min}}^{N_{\min}-1} \end{bmatrix}. \quad (3.16)$$

Due to the property of Vandermonde matrix [95], the determinant of $\mathbf{V}_2(\boldsymbol{\sigma})$

$$|\mathbf{V}_2(\boldsymbol{\sigma})| = \prod_{1 \leq m < n \leq N_{\min}} (-\sigma_j^{-1} + \sigma_i^{-1}) \quad (3.17)$$

$$= \prod_{1 \leq m < n \leq N_{\min}} \sigma_m^{-1} \sigma_n^{-1} (\sigma_n - \sigma_m) \quad (3.18)$$

$$= \prod_{k=1}^{N_{\min}} \sigma_k^{1-N_{\min}} \prod_{1 \leq m < n \leq N_{\min}} (\sigma_n - \sigma_m) \quad (3.19)$$

$$= \prod_{k=1}^{N_{\min}} \sigma_k^{1-N_{\min}} |\mathbf{V}_1(\boldsymbol{\sigma})|. \quad (3.20)$$

Thereby,

$$K_{\Sigma} = \frac{1}{\prod_{k=1}^{N_{\min}} \sigma_k^{|N_t - N_r| + 1} \Gamma(N_{\max} - k + 1) \prod_{1 \leq m < n \leq N_{\min}} (\sigma_n - \sigma_m)} \quad (3.21)$$

In terms of the integral equation (2.6), (3.13) can be written in the analytic form

$$g_{ij}(\eta) = \left(\frac{\rho}{N_t}\right)^{-d_j} \Gamma(d_j) \Psi\left(d_j, d_j + 1 - \frac{2}{\eta}; \frac{N_t}{\sigma_i \rho}\right). \quad (3.22)$$

This concludes our proof of this theorem. \square

3.3.2 Asymptotic optimum expected distortion

Theorem 4 tells us that the analytical expression of ED_{cor}^* is a polynomial of ρ^{-1} . Therefore, at high SNR, the asymptotic ED_{cor}^* is of the form

$$ED_{\text{asy,cor}}^* = \mu_{\text{cor}}^*(\eta) \rho^{-\Delta_{\text{cor}}^*(\eta)} \quad (3.23)$$

where $\Delta_{\text{cor}}^*(\eta)$ is the *optimum distortion exponent* satisfying

$$\Delta_{\text{cor}}^*(\eta) = - \lim_{\rho \rightarrow \infty} \frac{\log ED_{\text{cor}}^*(\eta)}{\log \rho} \quad (3.24)$$

and μ_{cor}^* is the corresponding *optimum distortion factor* satisfying

$$\lim_{\rho \rightarrow \infty} \frac{\log \mu_{\text{cor}}^*(\eta)}{\log \rho} = 0. \quad (3.25)$$

The closed-form expressions of $\Delta_{\text{cor}}^*(\eta)$ and μ_{cor}^* are given as follows.

Theorem 5 (Optimum Distortion Exponent for MIMO Correlated Channel). *The optimum distortion SNR exponent Δ_{cor}^* in the optimum expected end-to-end distortion in a system over a spatially correlated MIMO channel is the same as the optimum distortion SNR exponent Δ_{unc}^* in a system over an uncorrelated MIMO channel, that is,*

$$\Delta_{\text{cor}}^*(\eta) = \sum_{k=1}^{N_{\min}} \min \left\{ \frac{2}{\eta}, 2k - 1 + |N_t - N_r| \right\} \quad (3.26)$$

Proof. Let $\tilde{\mathbf{G}}$ denote the asymptotic form of \mathbf{G} at a high SNR. Since g_{ij} is a polynomial of ρ^{-1} given by (3.11) and the preliminaries in Section 3.2, in terms of Table 2.1, $|\tilde{\mathbf{G}}|$ can be written as $\sum_{m=1}^M |\tilde{\mathbf{G}}_m|$ where

$$|\tilde{\mathbf{G}}_m| = u_m \rho^{-\Delta_{\text{cor}}^*}, \quad (3.27)$$

i.e., they have the same degree over ρ^{-1} . Each element of $\tilde{\mathbf{G}}_m$ is a monomial of ρ^{-1} denoted by $\tilde{g}_{m,ij}$. In terms of Table 2.1 and the preliminaries in Section 3.2, we learn that $\tilde{g}_{m,ij}$'s form is one of $\sigma_i^{-r_{m,j}} a(j, r_{m,j}) \rho^{-(d_j+r_{m,j})}$ (Form 1) and $\sigma_i^{d_j-\frac{2}{\eta}} c_j \log^\epsilon \rho \rho^{-\frac{2}{\eta}}$ (Form 2), where $r_{m,j}$ is a non-negative integer, $\epsilon = 0$ or 1, and

$$a(j, r_{m,j}) = N_t^{d_j+r_{m,j}} \frac{\Gamma(\frac{2}{\eta} - d_j) \Gamma(d_j + r_{m,j})}{\Gamma(\frac{2}{\eta}) \Gamma(r_{m,j} + 1) (d_j + 1 - \frac{2}{\eta})_{r_{m,j}}} \quad (3.28)$$

$$c_j = N_t^{\frac{2}{\eta}} \Gamma(d_j - \frac{2}{\eta}). \quad (3.29)$$

If the elements of first l columns of $\tilde{\mathbf{G}}_m$ are of Form 1 and other elements are of Form 2, $\tilde{\mathbf{G}}_m$ can be partitioned as

$$\tilde{\mathbf{G}}_m = \left(\tilde{\mathbf{G}}_{m,1} \quad \tilde{\mathbf{G}}_{m,2} \right) \quad (3.30)$$

where $\tilde{\mathbf{G}}_{m,1}$ is of size $N_{\min} \times l$ and $\tilde{\mathbf{G}}_{m,2}$ is of size $N_{\min} \times (N_{\min} - l)$. Since $\tilde{\mathbf{G}}_m$ is a full-rank matrix, $\tilde{\mathbf{G}}_{m,1}$ and $\tilde{\mathbf{G}}_{m,2}$ ought to be full rank as well. Apparently, $\tilde{\mathbf{G}}_{m,2}$ is a full-rank matrix; whereas, for $\tilde{\mathbf{G}}_{m,1}$, if there exist $r_{m,j_1} = r_{m,j_2}$ for $j_1 \neq j_2$, $\tilde{\mathbf{G}}_{m,1}$ would not be full rank, because in that case, its submatrix constructed by the two columns with individual indices j_1 and j_2 would be rank-one. Thus, each $r_{m,j}$ must be distinct.

Now let us figure out l . Define a distortion exponent function as

$$\gamma(n) = \begin{cases} \sum_{k=1}^n d_k + \sum_{k=0}^{n-1} k + \frac{2(N_{\min}-n)}{\eta}, & n \in \mathbb{Z} \cap (0, N_{\min}]; \\ \frac{2N_{\min}}{\eta}, & n = 0. \end{cases} \quad (3.31)$$

Apparently, $\gamma(n)$ is on the curve of the two-order function $f(x)$,

$$f(x) = x^2 + \left(|N_t - N_r| - \frac{2}{\eta} \right) x + \frac{2N_{\min}}{\eta} \quad (3.32)$$

which is a symmetric convex function and whose minimum value is given by $x = \frac{\frac{2}{\eta} - |N_t - N_r|}{2}$. Since $n = l$ gives the minimum $\gamma(n)$, when $2/\eta \in (0, |N_t - N_r| + 1)$, $l = 0$; when $2/\eta \in (N_t + N_r - 1, +\infty)$, $l = N_{\min}$; when $\eta \in [|N_t - N_r| + 1, N_t + N_r - 1]$, there exists an l who gives the minimum $\gamma(n)$. Note that when $2/\eta = |N_t - N_r| + 1$, $\gamma(0) = \gamma(1)$; when $2/\eta = N_t + N_r - 1$, $\gamma(N_{\min} - 1) = \gamma(N_{\min})$.

For the case of $\eta \in [|N_t - N_r| + 1, N_t + N_r - 1]$, we should have

$$\gamma(l) \leq \gamma(l - 1) \quad (3.33)$$

and

$$\gamma(l) \leq \gamma(l + 1), \quad (3.34)$$

which gives

$$\frac{2}{\eta} - 1 - |N_t - N_r| \leq 2l \leq \frac{2}{\eta} + 1 - |N_t - N_r|. \quad (3.35)$$

Hence, for $\eta \in [|N_t - N_r| + 1, N_t + N_r - 1]$,

$$l = \left\lfloor \frac{\frac{2}{\eta} + 1 - |N_t - N_r|}{2} \right\rfloor \quad \text{or} \quad \left\lceil \frac{\frac{2}{\eta} - 1 - |N_t - N_r|}{2} \right\rceil \quad (3.36)$$

and

$$\begin{aligned} \Delta_{\text{cor}}^*(\eta) &= \gamma(l) \\ &= l(l + |N_r - N_t|) + \frac{2(N_{\min} - l)}{\eta} \\ &= \sum_{k=1}^{N_{\min}} \min \left\{ \frac{2}{\eta}, 2k - 1 + |N_t - N_r| \right\}. \end{aligned} \quad (3.37)$$

Note that $\gamma\left(\left\lfloor \frac{\frac{2}{\eta} + 1 - |N_t - N_r|}{2} \right\rfloor\right) = \gamma\left(\left\lceil \frac{\frac{2}{\eta} - 1 - |N_t - N_r|}{2} \right\rceil\right)$. With the results for the other two cases, this concludes our proof. \square

Theorem 6 (Optimum Distortion Factor for MIMO Correlated Channel). *The optimum distortion factor $\mu_{\text{cor}}^*(\eta)$ is given as follows.*

1. For $2/\eta \in (0, |N_t - N_r| + 1)$, the optimum distortion factor is

$$\mu_{\text{cor}}^*(\eta) = \prod_{k=1}^{N_{\min}} \sigma_k^{-\frac{2}{\eta}} \mu_{\text{unc}}^*(\eta). \quad (3.38)$$

2. For $2/\eta \in (N_t + N_r - 1, +\infty)$, the optimum distortion factor is

$$\mu_{\text{cor}}^*(\eta) = \prod_{k=1}^{N_{\min}} \sigma_k^{-N_{\max}} \mu_{\text{unc}}^*(\eta). \quad (3.39)$$

3. For $2/\eta \in [|N_t - N_r| + 1, N_t + N_r - 1]$, the optimum distortion factor is

$$\begin{aligned} \mu_{\text{cor}}^*(\eta) = & \frac{(-1)^{\frac{l(l-1)}{2}} |\mathbf{V}_3(\boldsymbol{\sigma})|}{\prod_{k=1}^{N_{\min}} \sigma_k^{|N_t - N_r| + 1} \prod_{1 \leq m < n \leq N_{\min}} (\sigma_n - \sigma_m)} \\ & \times \prod_{k=1}^{N_{\min} - l} \frac{(k)_l}{(|N_t - N_r| - \frac{2}{\eta} + l + k)_l} \mu_{\text{unc}}^*(\eta) \end{aligned} \quad (3.40)$$

where $l = \lfloor \frac{\frac{\eta}{2} + 1 - |N_r - N_t|}{2} \rfloor$ and each element of $\mathbf{V}_3(\boldsymbol{\sigma})$

$$v_{3,ij} = \sigma_i^{-\min\{j-1, \frac{2}{\eta} - d_j\}}. \quad (3.41)$$

Proof. From the proofs of Theorem 4 and Theorem 5, we have

$$\mu_{\text{cor}}^* = \frac{P_s |\boldsymbol{\Sigma}|^{-N_{\max}} \sum_{m=1}^M u_m}{\prod_{k=1}^{N_{\min}} \Gamma(N_{\max} - k + 1) |\mathbf{V}_2(\boldsymbol{\sigma})|} \quad (3.42)$$

where u_m is defined in (3.27).

1. Consider the case of $2/\eta \in (0, |N_t - N_r| + 1)$. We have $M = 1$ and

$$\tilde{g}_{1,ij} = \sigma_i^{d_j - \frac{2}{\eta}} c_j \rho^{-\frac{2}{\eta}}, \quad i = 1, \dots, N_{\min}, \quad j = 1, \dots, N_{\min} \quad (3.43)$$

where d_j is defined in Theorem 4 and u_j is defined in (3.29). Thereby,

$$u_1 = N_t^{\frac{2N_{\min}}{\eta}} |\mathbf{V}_1(\boldsymbol{\sigma})| \prod_{j=1}^{N_{\min}} \Gamma(d_j - \frac{2}{\eta}) \prod_{i=1}^{N_{\min}} \sigma_i^{|N_t - N_r| + 1 - \frac{2}{\eta}}. \quad (3.44)$$

So, in this case,

$$\begin{aligned} \mu_{\text{cor}}^*(\eta) &= \frac{|\boldsymbol{\Sigma}|^{-N_{\max}} |\mathbf{V}_1(\boldsymbol{\sigma})| \prod_{i=1}^{N_{\min}} \sigma_i^{|N_t - N_r| + 1 - \frac{2}{\eta}}}{|\mathbf{V}_2(\boldsymbol{\sigma})|} \\ &\times \frac{P_s N_t^{\frac{2N_{\min}}{\eta}} \prod_{j=1}^{N_{\min}} \Gamma(d_j - \frac{2}{\eta})}{\prod_{k=1}^{N_{\min}} \Gamma(N_{\max} - k + 1)} \\ &= \prod_{k=1}^{N_{\min}} \sigma_k^{-\frac{2}{\eta}} \mu_{\text{unc}}^*(\eta). \end{aligned} \quad (3.45)$$

Note that $\mathbf{V}_1(\boldsymbol{\sigma})$ and $\mathbf{V}_2(\boldsymbol{\sigma})$ are Vandermonde matrices defined by (3.16) and (3.15) respectively, in the proof of Theorem 4.

2. Consider the case of $2/\eta \in (N_t + N_r - 1, +\infty)$. We have $M = N_{\min}!$ and

$$\begin{aligned} \tilde{g}_{m,ij} &= \sigma_i^{-r_{m,j}} a(j, r_{m,j}) \rho^{-d_j - r_{m,j}}, \quad m = 1, \dots, M, \quad i = 1, \dots, N_{\min}, \\ &\quad j = 1, \dots, N_{\min} \end{aligned} \quad (3.46)$$

where

$$\begin{aligned} a(j, r_{m,j}) &= N_t^{d_j + r_{m,j}} \frac{\Gamma(d_j) \Gamma(\frac{2}{\eta} - d_j) (d_j)_{r_{m,j}}}{\Gamma(\frac{2}{\eta}) \Gamma(r_{m,j} + 1) (d_j + 1 - \frac{2}{\eta})_{r_{m,j}}} \\ &= N_t^{d_j + r_{m,j}} \frac{\Gamma(\frac{2}{\eta} - d_j) \Gamma(d_j + r_{m,j})}{\Gamma(\frac{2}{\eta}) \Gamma(r_{m,j} + 1) (d_j + 1 - \frac{2}{\eta})_{r_{m,j}}} \end{aligned} \quad (3.47)$$

By Lemma 7,

$$\left(d_j + 1 - \frac{2}{\eta} \right)_{r_{m,j}} = (-1)^{r_{m,j}} \left(\frac{2}{\eta} - d_j - r_{m,j} \right)_{r_{m,j}}. \quad (3.48)$$

Substitute (3.48) to (3.47), we have

$$a(j, r_{m,j}) = (-1)^{r_{m,j}} N_t^{d_j + r_{m,j}} \frac{\Gamma(d_j + r_{m,j}) \Gamma(\frac{2}{\eta} - d_j - r_{m,j})}{\Gamma(\frac{2}{\eta}) \Gamma(r_{m,j} + 1)}. \quad (3.49)$$

Hence,

$$\begin{aligned}
 u_m &= (-1)^{\sum_j r_{m,j}} \text{sgn}(\mathbf{r}_m) |\mathbf{V}_2(\boldsymbol{\sigma})| \prod_{j=1}^{N_{\min}} a(j, r_{m,j}) \\
 &= \text{sgn}(\mathbf{r}_m) |\mathbf{V}_2(\boldsymbol{\sigma})| \prod_{j=1}^{N_{\min}} N_t^{d_j+r_{m,j}} \frac{\Gamma(d_j+r_{m,j})\Gamma(\frac{2}{\eta}-d_j-r_{m,j})}{\Gamma(\frac{2}{\eta})\Gamma(r_{m,j}+1)}
 \end{aligned} \tag{3.50}$$

Note that \mathbf{r}_m is a permutation of $\{0, 1, \dots, N_{\min} - 1\}$ and $\text{sgn}(\mathbf{r}_m)$ denotes the signature of the permutation \mathbf{r}_m : $+1$ if \mathbf{r}_m is an even permutation and -1 if \mathbf{r}_m is an odd permutation. Consequently, in the light of Leibniz formula [95],

$$\sum_{m=1}^M u_m = \frac{|\mathbf{V}_2(\boldsymbol{\sigma})|}{\prod_{k=1}^{N_{\min}} \Gamma(k)} |\mathbf{Q}| \tag{3.51}$$

where each element of \mathbf{Q} is

$$q_{ij} = N_t^{d_{ij}} \Gamma(d_{ij}) \frac{\Gamma(\frac{2}{\eta} - d_{ij})}{\Gamma(\frac{2}{\eta})}. \tag{3.52}$$

Note that d_{ij} is defined in the description of Theorem 1. Comparing (3.52) to (2.41), we find that q_{ij} and e_{ij} are identical. Therefore,

$$\mu_{\text{cor}}^*(\eta) = \prod_{k=1}^{N_{\min}} \sigma_k^{-N_{\max}} \mu_{\text{unc}}^*(\eta). \tag{3.53}$$

3. Consider the case of $2/\eta \in [|N_t - N_r| - 1, N_t + N_r + 1]$. In terms of the proof of Theorem 5 and the preliminaries in Section 3.2, when $\text{mod} \{2/\eta + 1 - |N_t - N_r|, 2\} \neq 0$, $M = l!$,

$$\tilde{g}_{m,ij} = \begin{cases} \sigma_i^{-r_{m,j}} a(j, r_{m,j}) \rho^{-d_j - r_{m,j}}, & j \leq l; \\ \sigma_i^{d_j - \frac{2}{\eta}} c_j \rho^{-\frac{2}{\eta}}, & j \geq l + 1; \end{cases} \tag{3.54}$$

when $\text{mod} \{2/\eta + 1 - |N_t - N_r|, 2\} = 0$, $M = (l - 1)!$,

$$\tilde{g}_{m,ij} = \begin{cases} \sigma_i^{-r_{m,j}} a(j, r_{m,j}) \rho^{-d_j - r_{m,j}}, & j \leq l - 1; \\ \sigma_i^{-l+1} (-1)^{l-1} \frac{N_t^{\frac{2}{\eta}}}{\Gamma(l)} \log \rho \rho^{-\frac{2}{\eta}}, & j = l; \\ \sigma_i^{d_j - \frac{2}{\eta}} c_j \rho^{-\frac{2}{\eta}}, & j \geq l + 1. \end{cases} \tag{3.55}$$

Note that $a(j, r_{m,j})$ and c_j are given by (3.28) and (3.29) respectively; when $\text{mod } \{2/\eta + 1 - |N_t - N_r|, 2\} \neq 0$, \mathbf{r}_m is a permutation of $\{0, 1, \dots, l-1\}$; when $\text{mod } \{2/\eta + 1 - |N_t - N_r|, 2\} = 0$, \mathbf{r}_m is a permutation of $\{0, 1, \dots, l-2\}$. Thus,

$$u_m = \begin{cases} \text{sgn}(\mathbf{r}_m) |\mathbf{V}_3(\boldsymbol{\sigma})| \prod_{j=1}^l a(j, r_{m,j}) \prod_{j=l+1}^{N_{\min}} N_t^{\frac{2}{\eta}} \Gamma(d_j - \frac{2}{\eta}), \\ \quad \text{mod } \{2/\eta + 1 - |N_t - N_r|, 2\} \neq 0; \\ \text{sgn}(\mathbf{r}_m) |\mathbf{V}_3(\boldsymbol{\sigma})| (-1)^{l-1} N_t^{\frac{2(N_{\min}-l+1)}{\eta}} \log \rho \\ \quad \times \prod_{j=1}^{l-1} a(j, r_{m,j}) \prod_{j=l+1}^{N_{\min}} \Gamma(d_j - \frac{2}{\eta}), \\ \quad \text{mod } \{2/\eta + 1 - |N_t - N_r|, 2\} = 0. \end{cases} \quad (3.56)$$

where each element of $\mathbf{V}_3(\boldsymbol{\sigma})$,

$$v_{3,ij} = \sigma_i^{-\min\{j-1, \frac{2}{\eta} - d_j\}}. \quad (3.57)$$

Comparing to the proof of Theorem 3 for the same case of η , we have

$$\begin{aligned} \mu_{\text{cor}}^*(\eta) &= \frac{(-1)^{\frac{l(l-1)}{2}} |\mathbf{V}_3(\boldsymbol{\sigma})|}{\prod_{k=1}^{N_{\min}} \sigma_k^{|N_t - N_r| + 1} \prod_{1 \leq m < n \leq N_{\min}} (\sigma_n - \sigma_m)} \\ &\quad \times \prod_{k=1}^{N_{\min}-l} \frac{(k)_l}{(|N_t - N_r| - \frac{2}{\eta} + l + k)_l} \mu_{\text{unc}}^*(\eta). \end{aligned} \quad (3.58)$$

□

Theorem 7 (Convergence).

$$\lim_{\boldsymbol{\Sigma} \rightarrow \mathbf{I}} \mu_{\text{cor}}^*(\eta) = \mu_{\text{unc}}^*(\eta). \quad (3.59)$$

Proof. When $2/\eta \in (0, |N_t - N_r| + 1)$ or $2/\eta \in (N_t + N_r - 1, +\infty)$, in terms of Theorem 6, straightforwardly, $\lim_{\boldsymbol{\Sigma} \rightarrow \mathbf{I}} \mu_{\text{cor}}^*(\eta) = \mu_{\text{unc}}^*(\eta)$.

Consider the case of $2/\eta \in [|N_t - N_r| - 1, N_t + N_r + 1]$. By Taylor expansion and Lemma 7, the elements of $\mathbf{V}_3(\boldsymbol{\sigma})$

$$\begin{aligned} v_{3,ij} &= \sum_{n=0}^{\infty} \frac{(-p_j - n + 1)_n}{n!} (\sigma_i - 1)^n \\ &= \sum_{n=0}^{\infty} \frac{(-1)^n (p_j)_n}{n!} (\sigma_i - 1)^n \end{aligned} \quad (3.60)$$

where $p_j = \min\{j - 1, \frac{2}{\eta} - d_j\}$.

Thereby, when $\boldsymbol{\sigma}$ approaches a vector of ones,

$$|\mathbf{V}_3(\boldsymbol{\sigma})| = \sum_{m=1}^{(N_{\min}-1)!} |\mathbf{V}_{3,m}(\boldsymbol{\sigma})| \quad (3.61)$$

where the elements of $\mathbf{V}_{3,m}(\boldsymbol{\sigma})$

$$v_{3,m,ij} = \begin{cases} 1, & j = 1; \\ \frac{(-1)^{s_{m,j}} (p_j)_{s_{m,j}} (\sigma_i - 1)^{s_{m,j}}}{s_{m,j}!}, & j \geq 1. \end{cases} \quad (3.62)$$

Note that $\mathbf{s}_m = \{s_{m,2}, \dots, s_{m,N_{\min}}\}$ is a permutation of $\{1, 2, \dots, N_{\min} - 1\}$.

The determinant of $\mathbf{V}_{3,m}(\boldsymbol{\sigma})$

$$|\mathbf{V}_{3,m}(\boldsymbol{\sigma})| = (-1)^{n_1} |\mathbf{V}_1(\boldsymbol{\sigma} - \mathbf{1})| \text{sgn}(\mathbf{s}_m) \prod_{k=2}^{N_{\min}} \frac{1}{\Gamma(p_k)\Gamma(k)} \prod_{j=2}^{N_{\min}} \Gamma(s_{m,j} + p_j) \quad (3.63)$$

where $n_1 = \frac{N_{\min}(N_{\min}-1)}{2}$. In the light of Leibniz formula [95] and

$$|\mathbf{V}_1(\boldsymbol{\sigma} - \mathbf{a})| = |\mathbf{V}_1(\boldsymbol{\sigma})|, \quad \mathbf{a} = \{a, \dots, a\}, \quad (3.64)$$

$|\mathbf{V}_3(\boldsymbol{\sigma})|$ can be written in the form

$$|\mathbf{V}_3(\boldsymbol{\sigma})| = (-1)^{\frac{N_{\min}(N_{\min}-1)}{2}} |\mathbf{V}_1(\boldsymbol{\sigma})| |\mathbf{W}| \prod_{k=2}^{N_{\min}} \frac{1}{\Gamma(p_k)\Gamma(k)} \quad (3.65)$$

where \mathbf{W} is an $(N_{\min} - 1) \times (N_{\min} - 1)$ matrix with elements

$$w_{ij} = \Gamma(i + p_{j+1}) = \begin{cases} \Gamma(i + j), & j \leq l - 1 \\ \Gamma\left(\frac{2}{\eta} - |N_t - N_r| - 1 + i - j\right), & j \geq l. \end{cases} \quad (3.66)$$

By partial Gaussian elimination, \mathbf{W} can be transformed to \mathbf{W}' with a $(N_{\min} - l) \times (l - 1)$ left-lower submatrix of zeros. Partition \mathbf{W}' as

$$\mathbf{W}' = \begin{pmatrix} \mathbf{W}'_1 & \mathbf{W}'_2 \\ \mathbf{W}'_3 & \mathbf{W}'_4 \end{pmatrix}, \quad (3.67)$$

where \mathbf{W}'_3 is the submatrix of zeros, the elements of \mathbf{W}'_1 are

$$w'_{1,ij} = \Gamma(i + j - 1), \quad 1 \leq i, j \leq l - 1, \quad (3.68)$$

and the elements of \mathbf{W}'_4 are

$$w'_{4,ij} = \left(\frac{2}{\eta} - |N_t - N_r| - j - l \right)_{l-1} \Gamma\left(\frac{2}{\eta} - |N_t - N_r| - l + i - j\right), \quad (3.69)$$

$$l \leq i, j \leq N_{\min} - 1.$$

$$|\mathbf{W}| = |\mathbf{W}'_1| |\mathbf{W}'_4| \quad (3.70)$$

By Lemma 3,

$$|\mathbf{W}'_1| = \prod_{k=1}^{l-1} \Gamma(k) \Gamma(k+1). \quad (3.71)$$

By Lemma 6,

$$|\mathbf{W}'_4| = (-1)^{n_2} \prod_{j=l}^{N_{\min}-1} \left(\frac{2}{\eta} - |N_t - N_r| - j - l \right)_{l-1} \prod_{k=1}^{N_{\min}-l} \Gamma(k) \Gamma\left(\frac{2}{\eta} - N_{\max} + k\right). \quad (3.72)$$

where $n_2 = \frac{(N_{\min}-l)(N_{\min}-l-1)}{2}$.

Consequently, in terms of Theorem 5,

$$\begin{aligned} \lim_{\Sigma \rightarrow \mathbf{1}} \mu_{\text{cor}}^* &= (-1)^{n_1+n_2+n_3} \prod_{k=1}^{N_{\min}-l} \frac{\Gamma\left(\frac{2}{\eta} - N_{\max} + k\right)}{\Gamma\left(\frac{2}{\eta} - |N_t - N_r| - k - 2l + 1\right)} \\ &\quad \times \frac{\Gamma\left(|N_t - N_r| - \frac{2}{\eta} + l + k\right)}{\Gamma\left(|N_t - N_r| - \frac{2}{\eta} + 2l + k\right)} \mu_{\text{unc}}^* \end{aligned} \quad (3.73)$$

where $n_3 = \frac{l(l-1)}{2}$. Since for any function $f(x)$,

$$\prod_{k=1}^{N_{\min}-l} f(a + N_{\min} - k - l + 1) = \prod_{k'=1}^{N_{\min}-l} f(a + k') \quad (3.74)$$

where $k' = N_{\min} - k - l + 1$,

$$\lim_{\Sigma \rightarrow \mathbf{1}} \mu_{\text{cor}}^*(\eta) = (-1)^{n_1+n_2+n_3} \prod_{k=1}^{N_{\min}-l} \frac{\left(\frac{2}{\eta} - N_{\max} + k - l\right)_l}{\left(N_{\max} - \frac{2}{\eta} - k + 1\right)_l} \mu_{\text{unc}}^*(\eta). \quad (3.75)$$

By Lemma 7,

$$\left(\frac{2}{\eta} - N_{\max} + k - l\right)_l = (-1)^l \left(N_{\max} - \frac{2}{\eta} - k + 1\right)_l \quad (3.76)$$

Thus,

$$\lim_{\Sigma \rightarrow \mathbf{I}} \mu_{\text{cor}}^*(\eta) = (-1)^{n_1+n_2+n_3+n_4} \mu_{\text{unc}}^*(\eta). \quad (3.77)$$

where $n_4 = l(N_{\text{min}} - l + 1)$. As

$$(-1)^{n_1+n_2+n_3+n_4} = (-1)^{n_1-n_2+n_3+n_4} = 1, \quad (3.78)$$

we have

$$\lim_{\Sigma \rightarrow \mathbf{I}} \mu_{\text{cor}}^*(\eta) = \mu_{\text{unc}}^*(\eta). \quad (3.79)$$

This concludes our proof. \square

3.4 Numerical analysis and discussion

The analytical framework we have derived is general and valid for the correlated cases with all eigenvalues of the correlation matrix Σ distinct to each other. To give an example, we consider a well-known correlation model as in [94]: the exponential correlation with $\Sigma = \{r^{|i-j|}\}_{i,j=1,\dots,N_r}$ and $r \in (0, 1)$ [98].

Fig.3.1-Fig.3.4 illustrates the ED^* on a power-one white noise source transmitted in different cases. Red circles represent results of Monte Carlo simulations which are carried out by generating 10 000 realizations of \mathbf{H} and evaluating (2.19). Green lines represent the analytic form of ED_{cor}^* in Theorem 4 or ED_{unc}^* in Theorem 1. Blue dashed lines represent the asymptotic optimum distortion ED_{asy}^* .

$$ED_{\text{asy}}^* = \begin{cases} \mu_{\text{unc}}^* \rho^{-\Delta_{\text{unc}}^*}, & r = 0 \\ \mu_{\text{cor}}^* \rho^{-\Delta_{\text{cor}}^*}, & r > 0. \end{cases} \quad (3.80)$$

In Fig.3.1, we see that there is an agreement between ED^* and ED_{asy}^* in the high SNR regime. As we have analyzed in the preceding section, at a high SNR, due to the same optimum SNR distortion exponent, the optimum distortions of systems with different correlation matrices have the same descendent slope. The optimum distortion increases with r . The line of the uncorrelated case ($r = 0$) is the lowest among the five. For reaching the same optimum distortion in the high SNR regime above 15 dB, there is about 8 dB difference of SNR between the cases of $r = 0.99$ and the case of $r = 0$. This agrees with our intuition since spatial correlation decreases

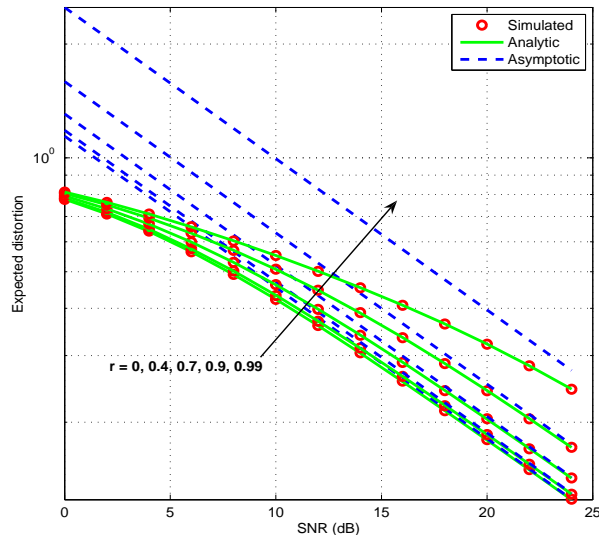


Figure 3.1: Uncorrelated and correlated channels, $N_t = 4$, $N_r = 2$, $\eta = 10$, high SCBR

channel capacity. For systems in the high SCBR regime at high SNR, the optimum distortion exponents are the same. The difference comes from different distortion factors involved by correlation coefficients.

Fig.3.2-Fig.3.4 show that, in some cases, due to the effect of other terms in the polynomial of ED^* , there are gaps between ED^* and ED_{asy}^* in the given range of SNR.

3.5 Conclusion

In this chapter, we have investigated the optimum expected end-to-end distortion in an analog-source transmission system over a correlated MIMO channel. The analytical expression of the optimum expected end-to-end distortion and its asymptotic form have been given. We have proved that the optimum distortion exponent for the case of correlated-fading channel is the same as that for the case of uncorrelated-fading channel. At a high SNR, the degradation of the optimum asymptotic expected end-to-end distortion caused by correlation is seen only in the optimum distortion factor. We have

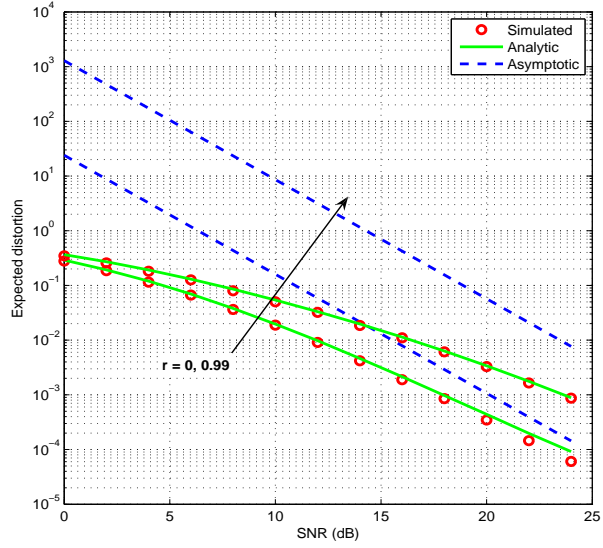


Figure 3.2: Uncorrelated and correlated channels, $N_t = 2$, $N_r = 2$, $\eta = 1.7$, moderate SCBR

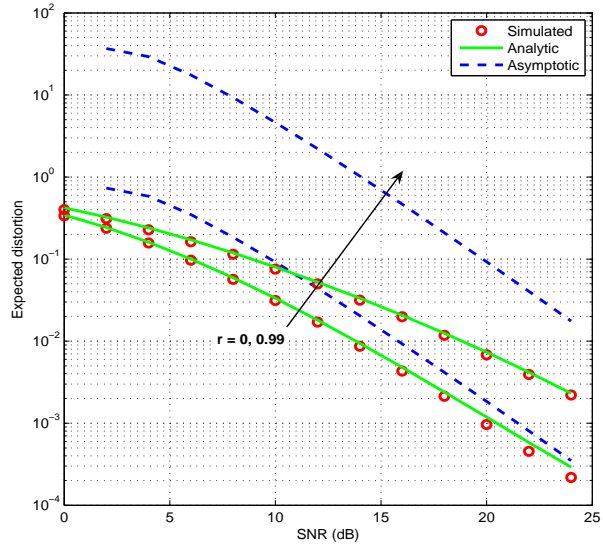


Figure 3.3: Uncorrelated and correlated channels, $N_t = 2$, $N_r = 2$, $\eta = 2$, moderate SCBR

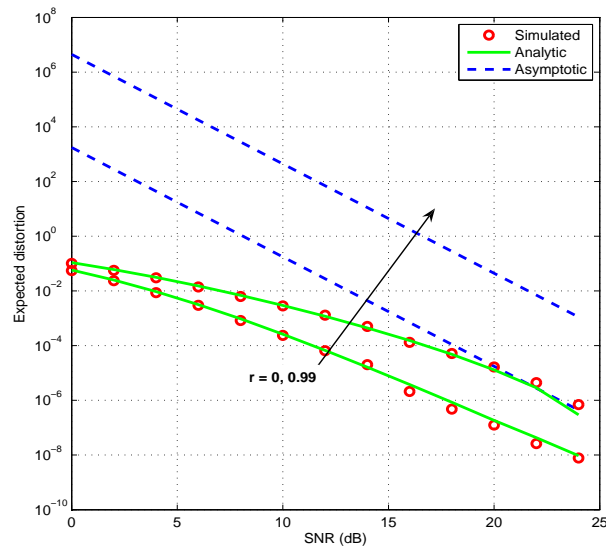


Figure 3.4: Uncorrelated and correlated channels, $N_t = 2$, $N_r = 2$, $\eta = 0.6657$, low SCBR

proved that, corresponding to our intuition, when the correlation matrix approaches an identity matrix, the optimum asymptotic expected end-to-end distortion for the case of correlated-fading MIMO channel converges to the one for the case of uncorrelated-fading MIMO channel.

Chapter 4

End-to-End Distortion: With Time Interleaving

4.1 Introduction

In this chapter, we extend our investigation on the optimum expected end-to-end distortion to the case of long-frame system over block-fading channel.

For a time-varying fading channel, it is well known that time-interleaving techniques can be used to exploit time diversity and thereby benefits the error probability [2, 11, 99–106]. However, so far, no much work has been done on the impact of time diversity on the reproduced analog (continuous-amplitude) source.

In practice, an analog source is to be transmitted in frames to whose length coding and decoding are subject. A frame can span over several fading blocks to exploit the time diversity. Obviously, to be in time and tractable, the frame length cannot be infinite. Thereby, for transmitting over a block-fading channel, the number of time diversity branches to be exploited is limited. We are particularly interested in the mechanism of how time interleaving benefits reproducing an analog source conveyed via a block-fading channel in length-limited frames.

In Chapter 2 and Chapter 3, we have analyzed the optimum expected end-to-end distortion ED^* of short-frame systems without time diversity. In this chapter, our investigation shall base on the fact that the ideal time-

interleaving inside a length-limited frame over a block-fading channel is equivalent to separating the source sequence to transmit via several parallel independent coherent channels. The channel is assumed to be uncorrelated. The analysis for the case of correlated channel would be straightforward, though this thesis does not give the details.

Coincidentally, Gunduz and Erkip have derived the relation between the optimum distortion exponent and time diversity the same as we will show in the following. However, via introducing the multiplicative optimum distortion factor, we obtain more results on the impact of time diversity giving a further guidance on system design.

The remainder of this chapter is organized as follows. The system model for ideal interleaving frame transmission is described in Section 4.2. Section 4.3 is dedicated to our main results. The effect of utilizing time diversity branches is illustrated in Section 4.4. Finally, Section 4.5 concludes the contributions of this chapter.

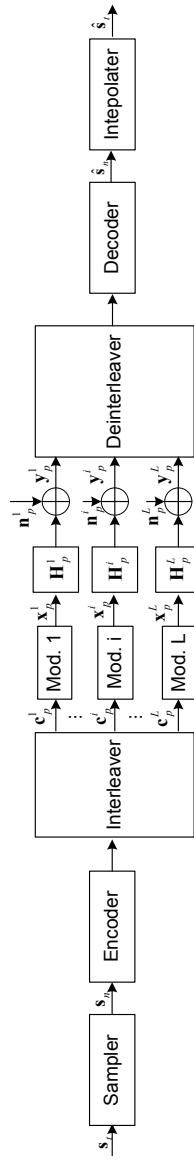


Figure 4.1: Block diagram of the transmission model with perfect interleaving

4.2 System Model

Consider a flat block-fading MIMO channel of bandwidth W_c with N_t inputs and N_r outputs. Assuming there are L fading-blocks in one frame, i.e, L time diversity branches in one frame, with ideal interleaving, we can regard the time-varying spatially-uncorrelated MIMO channel in one-frame transmission as L parallel statistically-independent memory-less coherent MIMO channels. Fig.4.1 is the block diagram of the transmission model. Suppose a white noise source \mathbf{s}_t of bandwidth W_s and average power P_s is to be conveyed. First, it is sampled (over Nyquist sampling rate) into a time-discrete source \mathbf{s}_n . After separate or joint source-channel coding with ideal interleaving, the transmission can be regarded as L source symbols to be transmitted over L parallel channels at time p simultaneously. For each equivalent coherent channel, the channel model is represented as

$$\mathbf{y}_p^i = \mathbf{H}_i \mathbf{x}_p^i + \mathbf{n}_p^i, \quad 1 \leq i \leq L. \quad (4.1)$$

where all elements of \mathbf{H}_i are i.i.d. $\mathcal{CN}(0, 1)$ random variables and all elements of \mathbf{n}_p^i are zero-mean i.i.d. complex random variables with variance σ_n^2 . Suppose $\|\mathbf{x}_p^i\|_2^2 = P_t$, the average SNR at each receive antenna $\rho = P_t/\sigma_n^2$. At the receiver, after de-interleaving and decoding, the estimate of the time-discrete source, $\hat{\mathbf{s}}_n$, is obtained. Finally, the analog source is reconstructed to $\hat{\mathbf{s}}_t$ via interpolation.

4.3 Main Results

4.3.1 Optimum expected distortion at any SNR

Theorem 8 (Optimum Expected Distortion with Time Interleaving). *The optimum expected end-to-end distortion in a MIMO system over an uncorrelated block-fading channel with perfect time interleaving is*

$$ED_{\text{int}}^*(\eta) = P_s^{1-L} [ED_{\text{unc}}^*(L\eta)]^L. \quad (4.2)$$

Proof. Since the channel can be regarded as parallel channels as Fig.4.1 shows, the mutual information of the channel per channel use is

$$\begin{aligned} \mathcal{I} &= \frac{1}{L} \sum_{i=1}^L \mathcal{I}_i \\ &= \frac{1}{L} \sum_{i=1}^L \log \left| \mathbf{I}_{N_r \times N_r} + \frac{\rho}{N_t} \mathbf{H}_i \mathbf{H}_i^\dagger \right| \end{aligned} \quad (4.3)$$

where \mathcal{I}_i is the mutual information per channel use for the i -th channel in the equivalent parallel channel bank.

Analogous to the proof of Theorem 1, according to Shannon's inequality [23], we have

$$W_s \log \frac{P_s}{D} \leq \frac{2W_c}{L} \sum_{i=1}^L \log \left| \mathbf{I}_{N_r \times N_r} + \frac{\rho}{N_t} \mathbf{H}_i \mathbf{H}_i^\dagger \right|. \quad (4.4)$$

Consequently,

$$\begin{aligned} ED_{\text{int}}^* &= P_s \left(\mathbb{E}_{\mathbf{H}} \left| \mathbf{I}_{N_r \times N_r} + \frac{\rho}{N_t} \mathbf{H}_i \mathbf{H}_i^\dagger \right|^{-\frac{2}{L\eta}} \right)^L \\ &= P_s \left(\frac{ED_{\text{unc}}^*(L\eta)}{P_s} \right)^L \\ &= P_s^{1-L} ED_{\text{unc}}^*{}^L(L\eta). \end{aligned} \quad (4.5)$$

This concludes our proof. \square

4.3.2 Asymptotic optimum expected distortion

At a high SNR, the asymptotic ED_{int}^* is of the form

$$ED_{\text{asy,int}}^* = \mu_{\text{int}}^*(\eta) \rho^{-\Delta_{\text{int}}^*(\eta)}. \quad (4.6)$$

Given (4.2), we have

$$ED_{\text{asy,int}}^*(\eta) = P_s^{1-L} ED_{\text{asy,unc}}^*{}^L(L\eta). \quad (4.7)$$

Therefore, the optimum distortion exponent is

$$\Delta_{\text{int}}^*(\eta) = L\Delta_{\text{unc}}^*(L\eta), \quad (4.8)$$

as in [41] and the optimum distortion factor is

$$\mu_{\text{int}}^*(\eta) = P_s^{1-L} \mu_{\text{unc}}^*{}^L(L\eta) \quad (4.9)$$

4.4 Interleaving Impact Analysis

In this section, we analyze the interleaving impact on $ED_{\text{asy,int}}^*$. The definition of different SCBR regimes are: $2/L\eta \in (N_t + N_r - 1, +\infty)$ is defined as *low SCBR regime*; $2/L\eta \in (0, |N_t - N_r| + 1)$ is defined as *high SCBR regime*;

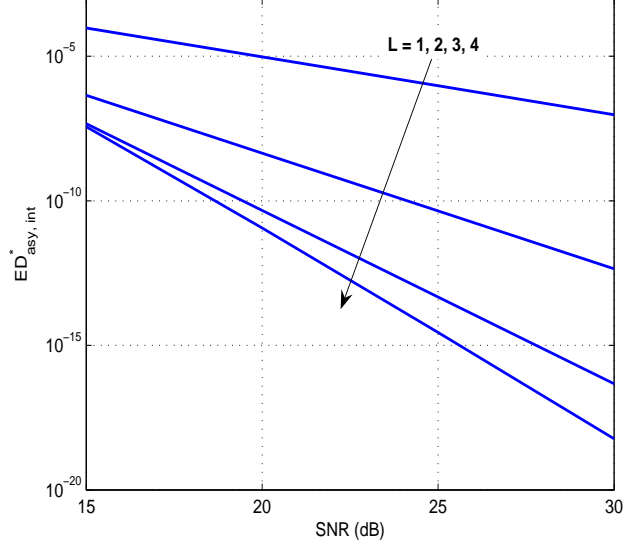


Figure 4.2: With time interleaving, $N_t = 2$, $N_r = 1$, $\eta = 0.25$, low SCBR

$2/L\eta \in [|N_t - N_r| + 1, N_t + N_r - 1]$ is defined as *moderate SCBR regime*. Note that in the following numerical analysis, $P_s = 1$.

When the time diversity branches $L \leq \left\lceil \frac{2}{\eta(|N_t - N_r| + 1)} \right\rceil$, the system is either in the low SCBR regime or in the moderate SCBR regime. In both cases, Δ_{int}^* increases with L , which leads $ED_{\text{asy,int}}^*$ to decrease with L in the high SNR regime. Fig.4.2 illustrates the relationship between $ED_{\text{asy,int}}^*$ and L in the low SCBR regime. We can see that increasing L decreases $ED_{\text{asy,int}}^*$ and makes the line of $ED_{\text{asy,int}}^*$ decay faster, which corresponds to the increase of Δ_{int}^* .

When $L > \left\lceil \frac{2}{\eta(|N_t - N_r| + 1)} \right\rceil$, the system is in the high SCBR regime. In this case, Δ_{int}^* is fixed to $2N_{\min}/\eta$ and thus has nothing to do with L . So, let us study the behavior of μ_{int}^* with L .

Given Theorem 3 in Chapter 2, equations (4.8) and (4.9), when the system is in the high SCBR regime, the optimum distortion factor

$$\mu_{\text{int}}^* = P_s N_t^{\frac{2N_{\min}}{\eta}} \left(\prod_{k=1}^{N_{\min}} \frac{\Gamma(|N_t - N_r| - \frac{2}{\eta L} + k)}{\Gamma(|N_t - N_r| + k)} \right)^L. \quad (4.10)$$

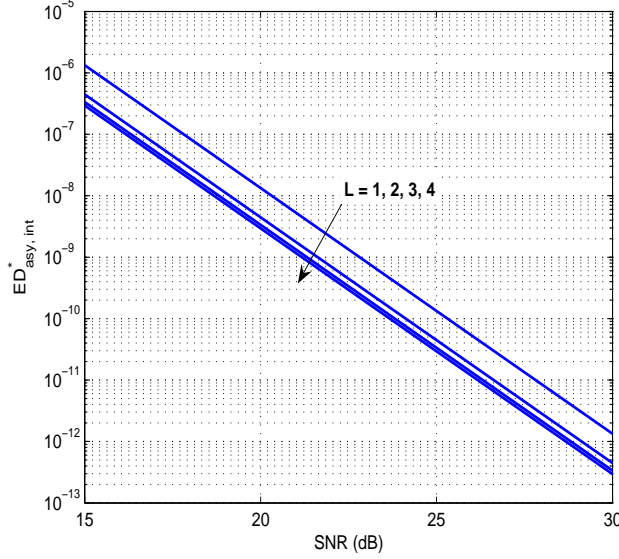


Figure 4.3: With time interleaving, $N_t = 4$, $N_r = 2$, $\eta = 1$, high SCBR

Let

$$\varphi(L) = \prod_{k=1}^{N_{\min}} \frac{\Gamma(|N_t - N_r| - \frac{2}{\eta L} + k)}{\Gamma(|N_t - N_r| + k)}. \quad (4.11)$$

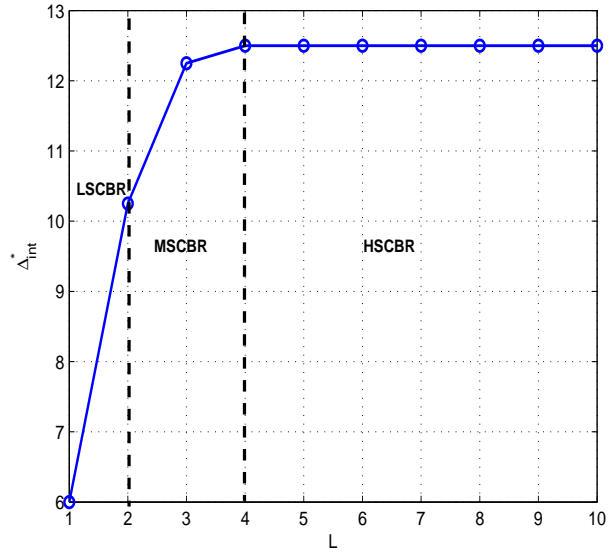
Since $0 < \varphi(L) < 1$ and $\frac{d}{dL}\varphi(L) > 0$, the derivative of the μ_{int}^* with respect to L

$$\frac{d}{dL}\mu_{\text{int}}^* = P_s N_t^{\frac{2N_{\min}}{\eta}} \varphi(L)^L \ln \varphi(L) \cdot \frac{d}{dL}\varphi(L) < 0. \quad (4.12)$$

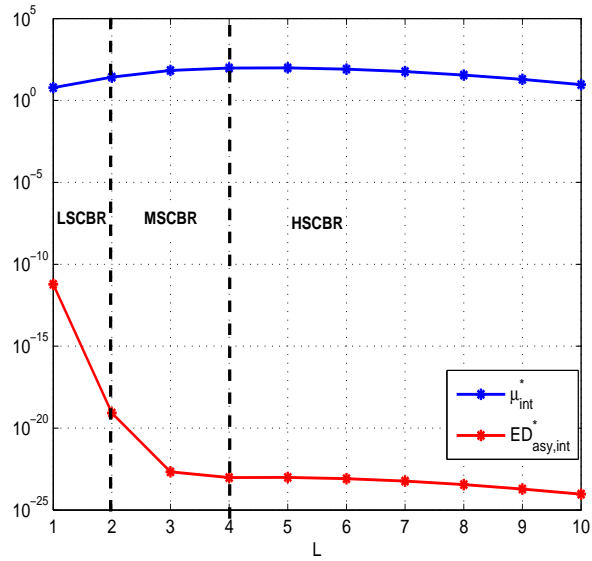
Consequently, the corresponding distortion factor μ_{int}^* decreases with L in the high SCBR regime and thereby $ED_{\text{asy,int}}^*$ also decreases. Fig.4.3 illustrates the relationship between $ED_{\text{asy,int}}^*$ and L in the high SCBR state. We can see that increasing L decreases $ED_{\text{asy,int}}^*$ but does not change the slope.

For a system initially in the low SCBR regime, if we increase L continuously, the SCBR regime would migrate from the *low* to the *moderate* and then to the *high*. We refer to the point of L where the systems migrates from the moderate SCBR regime to the high SCBR regime as *transit point*, which is

$$L^* = \left\lceil \frac{2}{\eta(|N_t - N_r| + 1)} \right\rceil. \quad (4.13)$$



(a)



(b)

Figure 4.4: SCBR state transition with time diversity branches. $N_t = 2$, $N_r = 3$, $\eta = 0.32$, and $\rho = 20\text{dB}$.

Fig.4.4 illustrates the transition process. In Fig.4.4(a) and Fig.4.4(b), the ranges of low, moderate and high SCBR regimes are denoted by LSCBR, MSCBR and HSCBR, respectively. The transit point L^* in this case is 4. We can see that $ED_{\text{asy,int}}^*$ decreases with L , but after L^* , because increasing L only affects μ_{int}^* , the benefit of increasing L becomes insignificant.

4.5 Conclusion

In this chapter, considering transmitting a white Gaussian source $s(t)$ over a block-fading uncorrelated MIMO channel via an outage-free long-frame system, we have investigated the impact of time diversity on the optimum end-to-end distortion. Based on our preceding results for the case of flat uncorrelated channel, we have derived the analytical expression of the optimum expected end-to-end distortion and its closed-form asymptotic expression with respect to the time diversity order. We have proved that the optimum asymptotic expected end-to-end distortion, consisting of the optimum distortion exponent and the multiplicative optimum distortion factor, is monotonically decreasing with the time diversity order. However, the optimum distortion exponent keeps constant when the time diversity order is greater than the transit point. Our analysis on the optimum asymptotic expected end-to-end distortion reflects the behavior of the optimum expected end-to-end distortion. Analogous to our analysis in this chapter, the results for the case of correlated channel are straightforward.

Chapter 5

Analog Channel Feedback

5.1 Introduction

In this chapter, we consider feeding back MIMO channel estimation by linear analog approaches.

We suppose that linear analog transmission over a MIMO channel can also benefit from the spatial diversity coming along with degrees of spatial freedom and it could be obtained by space-time block coding at the transmitter and the corresponding combination at the receiver. Since in a linear analog system, for a unit-norm source, mean-squared error (MSE) is the reciprocal of the received SNR and it is the primary metric for analog-source transmission, we believe that, for MIMO systems, the matched filter bound (MFB) on received SNR (SNR_{MFB}) is a plausible performance target.

We see that for linear analog transmission, due to its linearity, in the expression of expected MSE (i.e., distortion), the spatial diversity does not show in the distortion exponent over the transmit SNR but in the distortion factor aside, and the absolute value of the negative exponent is always one. It is known that a nonlinear transmission method can achieve a higher absolute value of the distortion exponent [25, 34, 38, 46, 77]. However, taking the distortion factor into account, a nonlinear scheme may not perform better than a linear scheme for any SNR but for impractical sufficiently high SNR, as we indicated in Chapter 1.

Furthermore, under a strict latency constraint, a linear analog transmis-

sion method would perform better than a quantization transmission method, even on the distortion exponent.

In linear analog transmission, supposing that the full transmit power is used to radiate, the analog source vector is to be scaled and meet the transmit power constraint. Thereby, for recovering the source vector at the receiver, a scaling factor should be transmitted in another way. Namely, in this case, only the direction of the source vector can be transmitted in the linear analog method. In this chapter, for simplicity, in this case, for measuring MSE, we assume that the scaling factor is transmitted in another way and known at the receiver perfectly.

Alternatively, in some scenarios, the receiver only needs to know the directions of the source vectors. e.g., in downlink zero-forcing beamforming (ZFBF) techniques after user selection, only the channel directions are to be known at the base station. In these cases, the transmitter does not need to know the scaling factor, purely linear analog transmission sufficing. The metric in these cases would be direction error.

If we suppose the channel direction information is to be used in ZFBF, we could measure the performance of a feedback scheme by the signal-to-interference ratio (SIR) in downlink, which indicates the degradation of the ZFBF approach due to the noises in the training and feedback procedures. The upper bound on the SIR would be the SIR under the assumption that there is only noise in the downlink channel training procedure but not in the uplink feedback procedure.

The remainder of this chapter is organized as follows. In Section 5.2, we introduce the orthogonal space-time block coding (OSTBC) to linear analog transmission and compare it with the random vector quantization (RVQ) approach. In Section 5.3, we describe a linear analog channel feedback scheme with OSTBC and compare it with a linear analog channel feedback scheme with circulant STBC (CSTBC). The SIR in a ZFBF scheme with our analog channel feedback approach with OSTBC is investigated in Section 5.4. Finally, this chapter is concluded in Section 5.5.

5.2 Space-time coding in analog transmission

In this section, orthogonal space-time coding (OSTBC)(see, e.g., [107–115]) is introduced to linear analog transmission. It can help a MIMO system benefit from spatial diversity and reach the matched filter bound (MFB) on received SNR. The examples are given to show the performance of the linear analog approach with OSTBC compared with the RVQ approach with respect to average direction error and average MSE.

5.2.1 Channel model

Assume a frequency-flat block-fading MIMO channel with N_t inputs and N_r outputs. The channel model is

$$\mathbf{Y} = \mathbf{X}_s \mathbf{H} + \mathbf{W} \quad (5.1)$$

where \mathbf{H} is the $N_t \times N_r$ channel matrix known at the receiver and unknown at the transmitter, \mathbf{X}_s is the $L_b \times N_t$ space-time block codeword matrix subject to the transmit power constraint P_t per channel use and \mathbf{s} is the input symbol sequence of L_s symbols with individual source power P_{s_i} , $1 \leq i \leq L_s$, \mathbf{W} is the $L_b \times N_r$ noise matrix whose elements are i.i.d. as $\mathcal{CN}(0, \sigma_w^2)$, and \mathbf{Y} is the $L_b \times N_r$ matrix of received symbols.

5.2.2 MFB on receive SNR

For linear coding in analog transmission, the matched filter bound (MFB), which refers to maximum spatial diversity combining, is different from the one in digital transmission with respect to affected objects. It is well-known that in digital transmission, MFB is an exponentially upper bound on the probability of error [116] and can be achieved by orthogonal space-time coding with maximum likelihood (ML) detection or other means. For linear receivers in analog transmission, MFB is a multiplicative coefficient upper bound on received SNR which closely relates to MSE.

Assume L_s continuous-amplitude complex source symbols are to be transmitted linearly via a length- L_b data block. At the receiver, if the matched filter bound (MFB) on received SNR is achieved, the total power on the received block would be $L_b P_t \|\mathbf{H}\|_F^2$, exploiting the maximum spatial diversity of the MIMO channel for linear systems. For reaching the MFB, each source symbol ought to be transmitted at least once via each transmit antenna, i.e., in the block, there are at least N_t replicas for each symbol. Consequently,

the MFB on average SNR per source symbol is

$$\text{SNR}_{\text{MFB}} = \frac{L_b P_t \|\mathbf{H}\|_F^2}{N_t L_s \sigma_n^2}. \quad (5.2)$$

5.2.3 OSTBC achieves SNR_{MFB}

It is well known that the orthogonality of an OSTBC completely decouples a MIMO channel into many parallel and independent subchannels. Nevertheless, as far as we know, the orthogonality of the effective channel had been actually in intuition until recently Shang and Xia made it clear by their persuasive explanation in [117] (though it is not their main contribution therein) based on the general construction of OSTBC proposed by Liang in [111]. We shall introduce Shang-Xia's derivation with more details as follows.

In terms of Liang's Proposition 2 in [111], an OSTBC \mathcal{O}_s can be written in the construction form

$$\mathcal{O}_s = (\mathbf{A}_1 \mathbf{s} + \mathbf{B}_1 \mathbf{s}^* \quad \mathbf{A}_2 \mathbf{s} + \mathbf{B}_2 \mathbf{s}^* \quad \cdots \quad \mathbf{A}_{N_t} \mathbf{s} + \mathbf{B}_{N_t} \mathbf{s}^*) \quad (5.3)$$

where $\mathbf{s} \in \mathbb{C}^{L_s}$, $\mathbf{A}_1, \mathbf{A}_2, \dots, \mathbf{A}_{N_t}$ and $\mathbf{B}_1, \mathbf{B}_2, \dots, \mathbf{B}_{N_t}$ satisfy complex Hurwitz-Randon matrix equations [118, 119],

$$\begin{cases} \mathbf{A}_i^\dagger \mathbf{A}_i + \mathbf{B}_i^\top \mathbf{B}_i^* &= \mathbf{I}_{L_s \times L_s}, \quad i = 1, 2, \dots, N_t \\ \mathbf{A}_i^\dagger \mathbf{A}_j + \mathbf{B}_j^\top \mathbf{B}_i^* &= \mathbf{0}, \quad 1 \leq i < j \leq N_t \\ \mathbf{A}_i^\dagger \mathbf{B}_j + \mathbf{B}_j^\top \mathbf{A}_i^* &= \mathbf{0}, \quad i, j = 1, 2, \dots, N_t. \end{cases} \quad (5.4)$$

Substituting \mathcal{O}_s into (5.1), we have

$$\mathbf{Y} = \mathcal{O}_s \mathbf{H} + \mathbf{W}. \quad (5.5)$$

As an extension to the solution in [117] for the MISO case, we multiply both sides of (5.5) by $\sum_{i=1}^{N_t} h_{ij}^* \mathbf{A}_i^\dagger$ and also the conjugate of both its sides by $\sum_{i=1}^{N_t} h_{ij} \mathbf{B}_i^\top$ for each column of \mathbf{y}_j , and sum the resulting $2N_r$ equations

$$\begin{aligned} & \sum_{j=1}^{N_r} \sum_{i=1}^{N_t} (h_{ij}^* \mathbf{A}_i^\dagger \mathbf{y}_j + h_{ij} \mathbf{B}_i^\top \mathbf{y}_j^*) \\ &= \sum_{j=1}^{N_r} \left(\sum_{i=1}^{N_t} h_{ij}^* \mathbf{A}_i^\dagger \sum_{i_1=1}^{N_t} (\mathbf{A}_{i_1} \mathbf{s} + \mathbf{B}_{i_1} \mathbf{s}^*) h_{i_1 j} + \sum_{i=1}^{N_t} h_{ij} \mathbf{B}_i^\top \sum_{i_1=1}^{N_t} (\mathbf{A}_{i_1}^* \mathbf{s}^* + \mathbf{B}_{i_1}^* \mathbf{s}) h_{i_1 j}^* \right. \\ & \quad \left. + \sum_{i=1}^{N_t} (h_{ij}^* \mathbf{A}_i^\dagger \mathbf{w}_j + h_{ij} \mathbf{B}_i^\top \mathbf{w}_j^*) \right). \end{aligned} \quad (5.6)$$

The valid part in the processed received signal is

$$\begin{aligned}
& \sum_{j=1}^{N_r} \left(\sum_{i=1}^{N_t} h_{ij}^* \mathbf{A}_i^\dagger \sum_{i_1=1}^{N_t} (\mathbf{A}_{i_1} \mathbf{s} + \mathbf{B}_{i_1} \mathbf{s}^*) h_{i_1 j} + \sum_{i=1}^{N_t} h_{ij} \mathbf{B}_i^T \sum_{i_1=1}^{N_t} (\mathbf{A}_{i_1}^* \mathbf{s}^* + \mathbf{B}_{i_1}^* \mathbf{s}) h_{i_1 j}^* \right) \\
&= \sum_{j=1}^{N_r} \left(\sum_{i=1}^{N_t} |h_{ij}|^2 (\mathbf{A}_i^\dagger \mathbf{A}_i + \mathbf{B}_i^T \mathbf{B}_i^*) \mathbf{s} + \sum_{\substack{i, i_1=N_t \\ i, i_1=1, i \neq i_1}} h_{ij}^* h_{i_1 j} (\mathbf{A}_i^\dagger \mathbf{A}_{i_1} + \mathbf{B}_{i_1}^T \mathbf{B}_i^*) \mathbf{s} \right. \\
&\quad \left. + \sum_{\substack{i, i_1=N_t \\ i, i_1=1, i \neq i_1}} h_{ij}^* h_{i_1 j} (\mathbf{A}_i^\dagger \mathbf{B}_{i_1} + \mathbf{B}_{i_1}^T \mathbf{A}_i^*) \mathbf{s}^* \right) \\
&\stackrel{(a)}{=} \sum_{j=1}^{N_r} \|\mathbf{h}_j\|^2 \mathbf{s} \\
&= \|\mathbf{H}\|_{\mathbb{F}}^2 \mathbf{s}
\end{aligned} \tag{5.7}$$

where the step (a) comes from (5.4), presenting the orthogonality of the effective channel.

Alternatively, regarding the MISO subchannel for the j^{th} receive antenna, the subchannel model can be represented as

$$\begin{aligned}
\begin{pmatrix} \mathbf{y}_j \\ \mathbf{y}_j^* \end{pmatrix} &= \begin{pmatrix} \mathcal{O}_s \mathbf{h}_j + \mathbf{w}_j \\ \mathcal{O}_s^* \mathbf{h}_j^* + \mathbf{w}_j^* \end{pmatrix} \\
&= \begin{pmatrix} \sum_{i=1}^{N_t} h_{ij} \mathbf{A}_i & \sum_{i=1}^{N_t} h_{ij} \mathbf{B}_i \\ \sum_{i=1}^{N_t} h_{ij}^* \mathbf{B}_i^* & \sum_{i=1}^{N_t} h_{ij}^* \mathbf{A}_i^* \end{pmatrix} \begin{pmatrix} \mathbf{s} \\ \mathbf{s}^* \end{pmatrix} + \begin{pmatrix} \mathbf{w}_j \\ \mathbf{w}_j^* \end{pmatrix}.
\end{aligned} \tag{5.8}$$

Given (5.4), we have

$$\begin{aligned}
& \begin{pmatrix} \sum_{i=1}^{N_t} h_{ij}^* \mathbf{A}_i^\dagger & \sum_{i=1}^{N_t} h_{ij} \mathbf{B}_i^T \end{pmatrix} \begin{pmatrix} \mathbf{y}_j \\ \mathbf{y}_j^* \end{pmatrix} \\
&= \begin{pmatrix} \|\mathbf{h}_j\|^2 \mathbf{I}_{L_s \times L_s} & \mathbf{0}_{L_s \times L_s} \end{pmatrix} \begin{pmatrix} \mathbf{s} \\ \mathbf{s}^* \end{pmatrix} + \begin{pmatrix} \sum_{i=1}^{N_t} h_{ij}^* \mathbf{A}_i^\dagger & \sum_{i=1}^{N_t} h_{ij} \mathbf{B}_i^T \end{pmatrix} \begin{pmatrix} \mathbf{w}_j \\ \mathbf{w}_j^* \end{pmatrix} \\
&= \|\mathbf{h}_j\|^2 \mathbf{s} + \sum_{i=1}^{N_t} h_{ij}^* \mathbf{A}_i^\dagger \mathbf{w}_j + \sum_{i=1}^{N_t} h_{ij} \mathbf{B}_i^T \mathbf{w}_j^*.
\end{aligned} \tag{5.9}$$

Given (5.8) and (5.9), for the MISO subchannel for the j^{th} receive antenna, the effective subchannel matrix is

$$\mathbf{H}'_j = \begin{pmatrix} \sum_{i=1}^{N_t} h_{ij} \mathbf{A}_i \\ \sum_{i=1}^{N_t} h_{ij}^* \mathbf{B}_i^* \end{pmatrix}, \tag{5.10}$$

which is a scaled $2L_b \times L_s$ non-square orthogonal matrix,

$$\mathbf{H}'_j \dagger \mathbf{H}'_j = \|\mathbf{h}_j\|^2 \mathbf{I}_{L_s \times L_s}. \quad (5.11)$$

Given (5.7) and (5.9), the noise in the processed signal

$$\mathbf{w}' = \sum_{j=1}^{N_r} \sum_{i=1}^{N_t} (h_{ij}^* \mathbf{A}_i \dagger \mathbf{w}_j + h_{ij} \mathbf{B}_i^T \mathbf{w}_j^*). \quad (5.12)$$

Thus, in the case that noise elements are i.i.d. $\mathcal{CN}(0, \sigma_w^2)$, the correlation matrix of noise

$$\mathbb{E} \left[\mathbf{w}' \mathbf{w}' \dagger \right] = \|\mathbf{H}\|_F^2 \sigma_w^2 \mathbf{I}_{L_s \times L_s}. \quad (5.13)$$

Consequently, for the source symbol s_i , the received SNR is

$$\rho_i = \frac{P_{s_i} \|\mathbf{H}\|_F^2}{\sigma_w^2}. \quad (5.14)$$

By the structure of \mathcal{O}_s (5.3) and the condition (5.4), the signal energy from the m^{th} transmit antenna is

$$\begin{aligned} P_m &= \|\mathbf{A}_m \mathbf{s} + \mathbf{B}_m \mathbf{s}^*\|^2 \\ &= \|\mathbf{s}\|^2, \quad m = 1, \dots, N_t. \end{aligned} \quad (5.15)$$

Hence,

$$N_t \|\mathbf{s}\|^2 = L_b P_t \quad (5.16)$$

which gives

$$\|\mathbf{s}\|^2 = \frac{L_b P_t}{N_t}, \quad (5.17)$$

i.e.,

$$\sum_{i=1}^{L_s} P_{s_i} = \frac{L_b P_t}{N_t}. \quad (5.18)$$

Substituting (5.17) into the sum of (5.14), we have

$$\text{SNR}_{\text{OSTBC}} = \frac{\sum_{i=1}^{L_s} \rho_i}{L_s} = \frac{L_b P_t \|\mathbf{H}\|_F^2}{N_t L_s \sigma_w^2}, \quad (5.19)$$

which is exactly SNR_{MFB} (5.2) for MIMO systems.

When a long latency is allowed, based on the derived result above for MIMO systems, straightforwardly, repeating OSTBC or repeating the input vector to construct an OSTBC of larger size and then equalizing symbols by mean estimation can also achieve SNR_{MFB} .

5.2.4 OSTBC analog vs. RVQ digital

In recent literature, as a digital approach, random vector quantization (RVQ) is proposed to feed back the channel information (see [68, 77, 120, 121], etc.). An interesting common point between RVQ and linear analog transmission is that both of them can only be used to transmit an analog vector's direction. If the amplitude of the vector is also required, it is assumed to be sent in another way.

In spite of the disadvantages of RVQ as a digital approach, introduced in Chapter 1, we will compare the performance of the linear analog approach with OSTBC to RVQ with respect to average direction error and average MSE.

Average direction error comparison

As described in [68, 77, 120, 121], for multiuser zero-forcing beamforming (ZFBF) at the base station, in some cases, e.g., after user selection, the base station only needs to know the directions of channel vectors. Although most discussions on ZFBF assume only one antenna at each user end, it is not difficult to implement it to the case with multiple antennas at each user end. In this case, the feedback procedure can be considered as transmitting the direction of an analog vector over a MIMO channel. The metric can be the average direction error

$$\mathbb{E}(\phi^2) = \mathbb{E} \left[1 - \left| \frac{\mathbf{s}\hat{\mathbf{s}}^\dagger}{\|\mathbf{s}\|\|\hat{\mathbf{s}}\|} \right|^2 \right] \quad (5.20)$$

where \mathbf{s} is the row source vector of L_s complex elements and $\hat{\mathbf{s}}$ is the recovered source vector at the receiver.

In the RVQ approach, a unit vector quantization codebook \mathcal{W} is generated randomly, including 2^B isotropically i.i.d. unit vectors \mathbf{w}_i , $i = 1, \dots, 2^B$. The codeword \mathbf{w}_k satisfying

$$\mathbf{w}_k = \arg \max_{\mathbf{w}_i \in \mathcal{W}} \left| \frac{\mathbf{s}}{\|\mathbf{s}\|} \mathbf{w}_i^\dagger \right|^2 \quad (5.21)$$

is selected and its index is sent. It is known that [120, 121]

$$\mathbb{E} \left[1 - \left| \frac{\mathbf{s}}{\|\mathbf{s}\|} \mathbf{w}_k^\dagger \right|^2 \right] = 2^B \beta \left(2^B, \frac{L_s}{L_s - 1} \right) \quad (5.22)$$

where $\beta(x, y)$ is the beta function defined as $\beta(x, y) = \frac{\Gamma(x)\Gamma(y)}{\Gamma(x+y)}$ [122], and for an arbitrary unit vector \mathbf{w}_i , $1 - \left| \frac{\mathbf{s}}{\|\mathbf{s}\|} \mathbf{w}_i^\dagger \right|^2$ is a beta distributed random variable, $\mathcal{B}(L_s - 1, 1)$, with

$$\mathbb{E} \left[1 - \left| \frac{\mathbf{s}}{\|\mathbf{s}\|} \mathbf{w}_i^\dagger \right|^2 \right] = \frac{L_s - 1}{L_s}. \quad (5.23)$$

Assume the transmission is over L_b channel uses without channel coding and using 2^b -QAM modulation. The size of the codebook is 2^{bL_b} , i.e., $B = bL_b$. Denote the probability of wrong decision on the code index at the receiver by P_e . The average direction error by the RVQ method

$$\mathbb{E} [\phi_{\text{RVQ}}^2] = 2^B \beta \left(2^B, \frac{L_s}{L_s - 1} \right) (1 - P_e) + \frac{L_s - 1}{L_s} P_e. \quad (5.24)$$

Assume a length-two unit source vector \mathbf{s} is transmitted over a two-input two-output Rayleigh fading channel over two channel uses and the channel is perfectly known at the receiver but not known at the transmitter. Suppose both the RVQ method and the linear analog method with OSTBC are using Alamouti coding and the corresponding MRC at the receiver. Fig. 5.2 illustrates the comparison of the linear analog transmission method with OSTBC to the RVQ transmission method in terms of the average direction error. For the RVQ method without channel coding, the probabilities of wrong decision P_e are estimated by simulation (10,000 trials) and shown in Table 5.1 and Fig. 5.1. Then, its average direction errors are calculated in terms of (5.24). For the linear analog method with OSTBC, the average direction errors are evaluated by simulations (10,000 trials).

In Fig. 5.2, we can see that, in the assumed scenario, with respect to average direction error, when the SNR is greater than 7dB, the linear analog method with OSTBC performs better than the uncoded QPSK-modulated RVQ method; when SNR is greater than 20dB, the OSTBC linear analog method performs better than the 16QAM-modulated RVQ method. Though it seems that in a specific range of SNR, the OSTBC linear analog method performs always worse than the RVQ method with the optimal modulation in that SNR range (the difference would be 5dB), we should not forget that the complexity of the RVQ method is much higher than that of the linear analog method, e.g., the 16QAM scheme in our scenario requires processing on a randomly-varying codebook of size 2^8 , and the 64QAM scheme requires processing on a randomly-varying codebook of size 2^{12} . Additionally,

Table 5.1: Wrong decision ratios of QPSK, 16QAM and 64QAM modulation schemes

ρ (dB)	$P_{e,QPSK}$	$P_{e,16QAM}$	$P_{e,64QAM}$
0	0.013341	0.20756	0.39076
5	0.000706	0.074239	0.27534
10	0.000012	0.01096	0.13196
15	≈ 0	0.000553	0.0307
20	≈ 0	0.000008	0.002518
25	≈ 0	0.000001	0.000078
30	≈ 0	≈ 0	0.000002

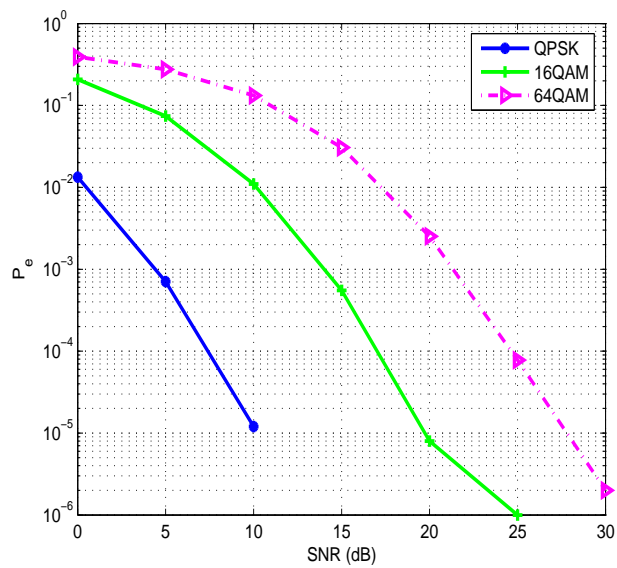


Figure 5.1: Wrong decision ratios of QPSK, 16QAM and 64QAM modulation schemes

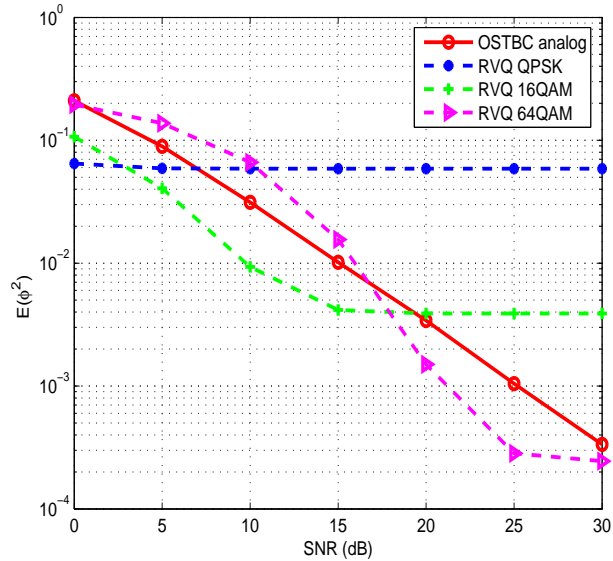


Figure 5.2: Average direction error comparison: OSTBC vs. RVQ

for rate-adaptive digital transmission in practice, we need to also consider the system overhead and the method of letting the transmitter reliably know the SNR range of the feedback channel.

Average MSE comparison

If the channel feedback is used to rebuild the channel matrix, then average MSE is a plausible metric to measure the performance of a channel feedback scheme. Concerning minimizing the MSE, the RVQ approach in [68, 77, 120, 121] is to be modified as follows, referred to as *real RVQ* (RRVQ) herein.

Assume a unit vector quantization code book \mathcal{W} is generated randomly, including 2^B isotropically i.i.d unit vectors \mathbf{w}_i , $i = 1, \dots, 2^B$. Since our target is to minimize the MSE, the selection criterion is to select a codeword \mathbf{w}_k satisfying $\mathbf{w}_k = \arg \min_{\mathbf{w}_i \in \mathcal{W}} \|\mathbf{s} - \|\mathbf{s}\|\mathbf{w}_i\|^2$. We have

$$\|\mathbf{s} - \|\mathbf{s}\|\mathbf{w}_i\|^2 = \|\mathbf{s}\|^2 \left(2 - 2\operatorname{Re} \left[\mathbf{w}_i^\dagger \frac{\mathbf{s}}{\|\mathbf{s}\|} \right] \right). \quad (5.25)$$

Then,

$$\mathbf{w}_k = \arg \max_{\mathbf{w}_i \in \mathcal{W}} \operatorname{Re} \left[\mathbf{w}_i^\dagger \frac{\mathbf{s}}{\|\mathbf{s}\|} \right]. \quad (5.26)$$

Let z denote the inner product between a channel direction and an arbitrary quantization vector, $z_i = \left| \mathbf{w}_i^\dagger \frac{\mathbf{s}}{\|\mathbf{s}\|} \right|^2$. Namely,

$$\operatorname{Re} \left[\mathbf{w}_i^\dagger \frac{\mathbf{s}}{\|\mathbf{s}\|} \right] = \sqrt{z_i} \cos \theta_i \quad (5.27)$$

where z_i is beta distributed $\mathcal{B}(1, L_s - 1)$ [120, 121], and θ_i is uniform distributed $\mathcal{U}[-\pi, \pi]$. Consequently, the index selection criterion can be written as

$$k = \arg \max_{i=1, \dots, 2^B} \sqrt{z_i} \cos \theta_i. \quad (5.28)$$

Consider transmitting an analog source vector \mathbf{s} composed of L_s complex values over an M -input N -output slow-fading channel by the uncoded RRVQ approach. Let

$$\gamma = \operatorname{Re} \left[\mathbf{w}_k^\dagger \frac{\mathbf{s}}{\|\mathbf{s}\|} \right] \quad (5.29)$$

where \mathbf{w}_k is the selected codeword in \mathcal{W} . The average MSE of the recovered source at the receiver by the uncoded RRVQ approach

$$\begin{aligned} \mathbb{E} [\epsilon_{\text{RRVQ}}^2] &= \mathbb{E} \|\hat{\mathbf{s}} - \mathbf{s}\|^2 \\ &= 2\|\mathbf{s}\|^2 (1 - \mathbb{E}[\gamma]) P_c + 2\|\mathbf{s}\|^2 (1 - P_c) \\ &= 2\|\mathbf{s}\|^2 (1 - \mathbb{E}[\gamma] P_c) \end{aligned} \quad (5.30)$$

where P_c is the probability of correct decision.

Assume a length-four unit source vector \mathbf{s} is transmitted over a two-input two-output Rayleigh fading channel over four channel uses with perfect CSIR and unknown CSIT. Suppose both the RRVQ method and the linear analog method with OSTBC use Alamouti coding and the corresponding MRC at the receiver. Fig.5.3 illustrates the comparison of the linear analog transmission method with OSTBC with the RVQ transmission method with respect to average mean squared error.

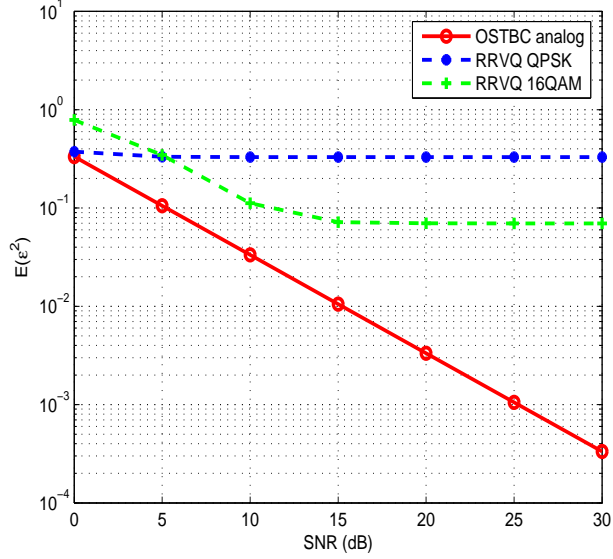


Figure 5.3: Average MSE comparison: OSTBC vs. RRVQ

Table 5.2: $\mathbb{E}[\gamma]$

	$B = 8$	$B = 16$
$\mathbb{E}(\gamma)$	0.8352	0.9670

Since the linear analog approach with OSTBC achieves SNR_{MFB} , in this case, the average MSE on \hat{s}

$$\begin{aligned}
 \mathbb{E}[\epsilon_{\text{OSTBC}}^2] &= \mathbb{E}_H \left[\frac{1}{\text{SNR}_{\text{MFB}}} \right] \\
 &= \mathbb{E}_H \left[\frac{2}{\|\mathbf{H}\|_F^2 \rho} \right] \\
 &= \frac{1}{3\rho}
 \end{aligned} \tag{5.31}$$

For the RRVQ method, since the probability of wrong decision P_e for transmitting two uncoded QAM symbols over two channel uses are given by Table 5.1, straightforwardly,

$$P_c = (1 - P_e)^2. \tag{5.32}$$

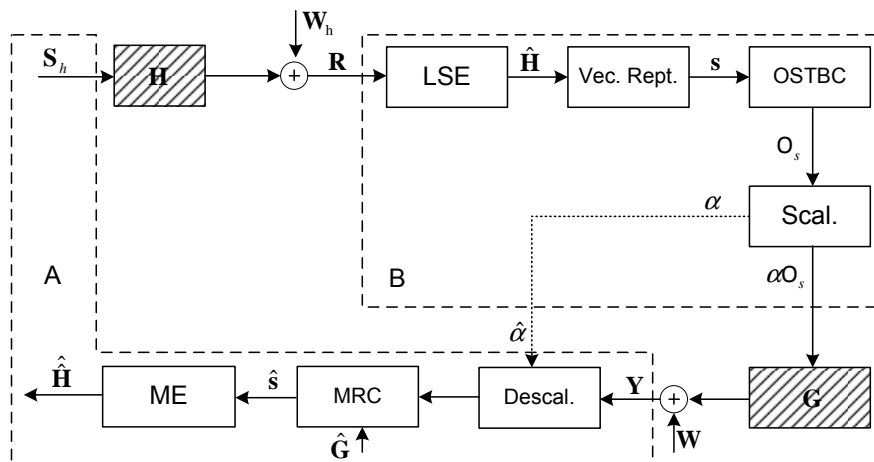


Figure 5.4: Linear analog channel feedback scheme

The values of $\mathbb{E}(\gamma)$ in the case of $L_s = 4$ are evaluated by simulations (1000 trials) and given by Table 5.2. $\mathbb{E}[\epsilon_{\text{RRVQ}}^2]$ is then calculated in terms of (5.30).

Fig.5.3 shows that, with respect to average MSE, in the assumed scenario, the linear analog method with OSTBC is not only of much lower computational complexity but also performs better than uncoded QPSK- and 16QAM-modulated RRVQ methods. Note that due to its high complexity, we did not simulate the RRVQ methods with modulation complexity higher than 16QAM, which means to calculate $\mathbb{E}[\gamma]$ for $B \geq 20$.

5.3 CSIT acquisition by analog channel feedback

5.3.1 Scheme description and channel model

Consider a peer-to-peer MIMO system with analog channel feedback for acquiring the channel state information at the transmitter (CSIT) over a slow-fading MIMO channel, N_a antennas at the transmitter A, and N_b antennas at the receiver B. Fig.5.4 shows the framework of the linear analog channel feedback scheme with orthogonal space-time coding. The complete procedure of four stages and the corresponding channel models are described as follows:

The first stage is referred to as *transmit channel training stage*. In this stage, in the pilot time slot, a $N_a \times \beta_h N_a$ training matrix \mathbf{S}_h , composed of β_h

$N_a \times N_a$ identity matrices, is sent by A under the transmit power constraint P_a per channel use; the receiver B does least square estimation (LSE) on the received signal matrix \mathbf{R} and obtains the estimated channel matrix $\hat{\mathbf{H}}$.

The channel model of the transmit channel training stage is

$$\mathbf{R}_h = \sqrt{P_a} \mathbf{H} \mathbf{S}_h + \mathbf{W}_h \quad (5.33)$$

where \mathbf{R}_h is the received signal at B, \mathbf{H} is the complex channel gain matrix, \mathbf{W}_h is the additive noise matrix at B, and $\mathbf{S}_h \mathbf{S}_h^\dagger = \beta_h \mathbf{I}$.

By LSE, the complex channel gain matrix estimation is

$$\hat{\mathbf{H}} = \frac{\mathbf{R}_h \mathbf{S}_h^\dagger}{\beta_h \sqrt{P_a}}. \quad (5.34)$$

The second stage is referred to as *feedback preparing stage*. In this stage, $\hat{\mathbf{H}}$ is regarded as a column source vector of $N_a N_b$ complex values, denoted by $\hat{\mathbf{h}}$. Assume the feedback latency is L_b channel uses and a L_s/L_b -rate OSTBC \mathcal{O}_s of size $L_b \times N_b$ is used. Let $\beta_s = \frac{L_s}{N_a N_b}$. The length- L_s basis source vector \mathbf{s} is composed of $\beta_s \hat{\mathbf{h}}$ as

$$\mathbf{s} = \begin{pmatrix} \hat{\mathbf{h}} \\ \vdots \\ \hat{\mathbf{h}} \end{pmatrix}. \quad (5.35)$$

Then, the OSTBC \mathcal{O}_s is set. \mathcal{O}_s is scaled to meet the block power constraint $L_b P_b$ before feedback. Given (5.17), the scaling factor is

$$\begin{aligned} \alpha &= \sqrt{\frac{L_b P_b}{N_b \|\mathbf{s}\|^2}} \\ &= \sqrt{\frac{L_b P_b}{\beta_s N_b \|\hat{\mathbf{h}}\|^2}} \end{aligned} \quad (5.36)$$

Third stage is referred to as *feedback channel training stage*. In this stage, in the pilot time slot, a $N_b \times \beta_g N_b$ training matrix \mathbf{S}_g , composed of $\beta_g N_b \times N_b$ identity matrices, is sent by B under the transmit power constraint P_b per channel use. A does LSE on the received signal matrix \mathbf{R}_g and obtains the channel matrix estimation $\hat{\mathbf{G}}$.

The channel model of the feedback channel training stage is

$$\mathbf{R}_g = \sqrt{P_b} \mathbf{G} \mathbf{S}_g + \mathbf{W}_g \quad (5.37)$$

where \mathbf{R}_g is the received signal at A, \mathbf{G} is the complex feedback channel gain matrix, and \mathbf{W}_g is the additive noise matrix at A.

By LSE, the estimated complex feedback channel gain matrix is

$$\hat{\mathbf{G}} = \frac{\mathbf{R}_g \mathbf{S}_g^\dagger}{\sqrt{P_b}}. \quad (5.38)$$

The fourth stage is referred to as *CSIT acquiring stage*. In this stage, B sends the scaled OSTBC to A; at A, the received signals are processed, such as descaling, maximum ratio combining (MRC), and mean estimation, to obtain the transmit channel gain matrix estimation $\hat{\mathbf{H}}$. Herein, we suppose the scaling factor α is transmitted to A in some unlinear way.

The channel model of the CSIT acquiring stage is

$$\mathbf{Y} = \alpha \mathcal{O}_s \mathbf{G} + \mathbf{W} \quad (5.39)$$

where \mathbf{Y} is the received signal at A, \mathbf{G} is the complex feedback channel gain matrix, and \mathbf{W} is the additive noise matrix at A.

After descaling, by MRC given by (5.6), the source vector estimation is

$$\hat{\mathbf{s}} = \frac{1}{\hat{\alpha}} \sum_{j=1}^{N_a} \left(\sum_{i=1}^{N_b} \hat{g}_{ij}^* \mathbf{A}_i^\dagger \quad \sum_{i=1}^{N_b} \hat{g}_{ij} \mathbf{B}_i^T \right) \begin{pmatrix} \mathbf{y}_j \\ \mathbf{y}_j^* \end{pmatrix}. \quad (5.40)$$

By mean estimation on $\hat{\mathbf{s}}$, the estimated channel gain vector is

$$\hat{\mathbf{h}} = \frac{1}{\beta_s} \sum_{k=1}^{\beta_s} \begin{pmatrix} \hat{s}_{(k-1)N_a N_b + 1} \\ \vdots \\ \hat{s}_{k N_a N_b} \end{pmatrix}, \quad (5.41)$$

which is used to reconstruct the channel matrix estimation $\hat{\mathbf{H}}$.

5.3.2 Mean squared error evaluation

Considering mean square error (MSE) as the primary metric in analog source transmission, in this subsection, we analyze the performance of the aforementioned linear analog channel feedback scheme with OSTBC with respect to MSE, and compare its performance to a linear analog channel feedback scheme with circulant STBC (CSTBC).

In this chapter, the MSE metric is

$$\begin{aligned} \epsilon^2 &= \mathbb{E} \|\hat{\mathbf{H}} - \mathbf{H}\|_F^2 \\ &= \mathbb{E} \|\hat{\mathbf{h}} - \mathbf{h}\|^2 \end{aligned} \quad (5.42)$$

MSE analysis for OSTBC channel feedback

In the channel training stage, given (5.33) and (5.34), we have

$$\hat{\mathbf{H}} = \mathbf{H} + \frac{\sum_{k=1}^{\beta_h} \mathbf{W}_{h,k}}{\beta_h \sqrt{P_a}} \quad (5.43)$$

where $\mathbf{W}_{h,k}$ are $N_b \times N_a$ submatrices of \mathbf{W}_h ,

$$\mathbf{W}_h = \left(\mathbf{W}_{h,1} \quad \dots \quad \mathbf{W}_{h,\beta_f} \right). \quad (5.44)$$

Correspondingly, the vector reshaped from $\hat{\mathbf{H}}$

$$\hat{\mathbf{h}} = \mathbf{h} + \frac{\sum_{k=1}^{\beta_h} \mathbf{w}_{h,k}}{\beta_h \sqrt{P_a}} \quad (5.45)$$

where $\mathbf{w}_{h,k}$'s are column vectors reshaped from $\mathbf{W}_{h,k}$ -s.

For simplicity, assume there is no error in estimating \mathbf{G} and acquiring the scaling factor α , i.e., $\hat{\mathbf{G}} = \mathbf{G}$ and $\hat{\alpha} = \alpha$. By the results in the subsection 5.2.3,

$$\hat{\mathbf{s}} = \|\mathbf{G}\|_{\mathbf{F}}^2 \mathbf{s} + \frac{1}{\alpha} \mathbf{w}' \quad (5.46)$$

where

$$\mathbf{w}' = \sum_{j=1}^{N_a} \sum_{i=1}^{N_b} (g_{ij}^* \mathbf{A}_i^\dagger \mathbf{w}_j + g_{ij} \mathbf{B}_i^T \mathbf{w}_j^*). \quad (5.47)$$

Consequently,

$$\hat{\mathbf{h}} = \hat{\mathbf{h}} + \frac{1}{\beta_s \alpha \|\mathbf{G}\|_{\mathbf{F}}^2} \sum_{k=1}^{\beta_s} \mathbf{w}'_k \quad (5.48)$$

where \mathbf{w}'_k 's are subvectors of \mathbf{w}' ,

$$\mathbf{w}' = \begin{pmatrix} \mathbf{w}'_1 \\ \vdots \\ \mathbf{w}'_{\beta_s} \end{pmatrix}. \quad (5.49)$$

Hence,

$$\hat{\mathbf{h}} - \mathbf{h} = \frac{\sum_{k=1}^{\beta_h} \mathbf{w}_{h,k}}{\beta_h \sqrt{P_a}} + \frac{1}{\alpha \beta_s \|\mathbf{G}\|_{\mathbf{F}}^2} \sum_{k=1}^{\beta_s} \mathbf{w}'_k. \quad (5.50)$$

Under the assumption that the elements of \mathbf{W}_h are i.i.d. $\mathcal{CN} \sim (0, \sigma_{w_h}^2)$ and the elements of \mathbf{W} are i.i.d. $\mathcal{CN} \sim (0, \sigma_w^2)$, given (5.13) and (5.36), the MSE

$$\begin{aligned}
\epsilon_{\text{OSTBC}}^2 &= \mathbb{E} \|\hat{\mathbf{h}} - \mathbf{h}\|^2 \\
&= \frac{\mathbb{E} \|\sum_{k=1}^{\beta_h} \mathbf{w}_{h,k}\|^2}{\beta_h^2 P_a} + \mathbb{E} \left(\frac{1}{\alpha^2} \right) \frac{1}{\beta_s^2 (\|\mathbf{G}\|_{\text{F}}^2)^2} \mathbb{E} \|\sum_{k=1}^{\beta_s} \mathbf{w}'_k\|^2 \\
&= \frac{N_a N_b \sigma_{w_h}^2}{\beta_h P_a} + \left(\|\mathbf{H}\|_{\text{F}}^2 + \frac{N_a N_b \sigma_{w_h}^2}{\beta_h P_a} \right) \frac{N_a N_b^2 \sigma_w^2}{L_b P_b \|\mathbf{G}\|_{\text{F}}^2} \\
&= \frac{N_a N_b}{\beta_h \rho_h} + \left(\|\mathbf{H}\|_{\text{F}}^2 + \frac{N_a N_b}{\beta_h \rho_h} \right) \frac{N_a N_b^2}{L_b \|\mathbf{G}\|_{\text{F}}^2 \rho}
\end{aligned} \tag{5.51}$$

where $\rho_h = P_a / \sigma_{w_h}^2$ and $\rho = P_b / \sigma_w^2$.

MSE analysis for CSTBC channel feedback

In linear analog transmission, circulant STBC (CSTBC) is an alternative approach of space-time block coding on analog sources, whose rate is one. For conveying an analog vector source \mathbf{s} of N_t complex elements, $\mathbf{s} = (s_1, s_2, \dots, s_{N_t})^{\text{T}}$, over a MIMO channel with N_t transmit antennas and N_r receive antennas, the channel model of the linear analog transmission approach with CSTBC is

$$\mathbf{Y} = \mathcal{C}_s \mathbf{H} + \mathbf{W} \tag{5.52}$$

where \mathbf{Y} is the received signal matrix of size $N_t \times N_r$, \mathbf{H} is the channel matrix of size $N_t \times N_r$, \mathbf{W} is the noise matrix, and \mathcal{C}_s is the CSTBC,

$$\mathcal{C}_s = \begin{pmatrix} s_1 & s_{N_t} & \dots & s_3 & s_2 \\ s_2 & s_1 & s_{N_t} & & s_3 \\ \vdots & s_2 & s_1 & \ddots & \vdots \\ s_{N_t-1} & & \ddots & \ddots & s_{N_t} \\ s_{N_t} & s_{N_t-1} & \dots & s_2 & s_1 \end{pmatrix}. \tag{5.53}$$

Given (5.52), we can see that the channel model can also be written as

$$\mathbf{Y} = \begin{pmatrix} \mathbf{H}'_1 & \dots & \mathbf{H}'_{N_r} \end{pmatrix} \mathbf{s} + \mathbf{W} \tag{5.54}$$

where

$$\mathbf{H}'_j = \begin{pmatrix} h_{1j} & h_{N_t j} & \dots & h_{3j} & h_{2j} \\ h_{2j} & h_{1j} & h_{N_t j} & & h_{3j} \\ \vdots & h_{2j} & h_{1j} & \ddots & \vdots \\ h_{N_t-1,j} & & \ddots & \ddots & h_{N_t j} \\ h_{N_t j} & h_{N_t-1,j} & \dots & h_{2j} & h_{1j} \end{pmatrix}, \quad j = 1, \dots, N_r. \quad (5.55)$$

It is easy to see that the effective subchannel matrix \mathbf{H}'_j is also a circulant matrix.

Under the assumption that \mathbf{H}'_j 's are invertible matrices, the MRC at the receiver is

$$\begin{aligned} \hat{\mathbf{s}} &= \frac{1}{N_r} \sum_{j=1}^{N_r} \mathbf{H}'_j{}^{-1} \mathbf{y}_j \\ &= \mathbf{s} + \frac{1}{N_r} \sum_{j=1}^{N_r} \mathbf{H}'_j{}^{-1} \mathbf{w}_j \end{aligned} \quad (5.56)$$

where \mathbf{y}_j 's are subvectors of \mathbf{Y} ,

$$\mathbf{Y} = (\mathbf{y}_1 \quad \dots \quad \mathbf{y}_{N_r}), \quad (5.57)$$

and \mathbf{w}_j 's are subvectors of \mathbf{W} ,

$$\mathbf{W} = (\mathbf{w}_1 \quad \dots \quad \mathbf{w}_{N_r}). \quad (5.58)$$

Under the power constraint P_t per channel use, i.e.,

$$\|\mathbf{s}\|^2 = P_t, \quad (5.59)$$

the received SNR

$$\text{SNR}_{\text{CSTBC}} = \frac{N_r^2 P_t}{\sigma_w^2 \sum_{j=1}^{N_r} \text{tr}\{(\mathbf{H}'_j{}^\dagger \mathbf{H}'_j)^{-1}\}}. \quad (5.60)$$

By the properties of circulant matrices [123],

$$\text{tr}\{(\mathbf{H}'_j{}^\dagger \mathbf{H}'_j)^{-1}\} = \frac{N_t}{\|\mathbf{h}_j\|^2}. \quad (5.61)$$

Consequently,

$$\text{SNR}_{\text{CSTBC}} = \frac{N_r^2 P_t}{N_t \sigma_w^2 \sum_{j=1}^{N_r} \frac{1}{\|\mathbf{h}_j\|^2}}. \quad (5.62)$$

Consider a linear analog channel feedback scheme using CSTBC. Assume $L_b = \beta_s N_a N_b$. The channel estimation data block fed back by the receiver B is

$$\mathcal{C} = \left(\mathcal{C}_{11} \quad \mathcal{C}_{12} \quad \dots \quad \mathcal{C}_{1\beta_s} \quad \mathcal{C}_{N_a 1} \quad \dots \quad \mathcal{C}_{N_a \beta_s} \right) \quad (5.63)$$

where \mathcal{C}_{ij} , $i = 1, \dots, N_a$, $j = 1, \dots, \beta_s$, is a CSTBC constructed from the column channel vector estimation $\hat{\mathbf{h}}_j$.

The scaling factor

$$\alpha = \sqrt{\frac{N_a P_b}{\|\mathbf{h}\|^2}}. \quad (5.64)$$

The receive processing at transmitter A is

$$\hat{\mathbf{h}}_j = \frac{1}{\alpha \beta_s N_a} \sum_{k=1}^{\beta_s} \sum_{i=1}^{N_a} \hat{\mathbf{G}}_i'^{-1} \mathbf{y}_{i,j,k}, \quad j = 1, \dots, N_a \quad (5.65)$$

where $\mathbf{y}_{i,j,k}$ is the corresponding subvector in the receive matrix \mathbf{Y} and $\hat{\mathbf{G}}_i'$ is the effective circulant matrix of the subchannel vector estimation $\hat{\mathbf{g}}_i$, $i = 1, \dots, N_a$.

Under the same assumption as for deriving (5.51), the MSE of the CSTBC method

$$\epsilon_{\text{CSTBC}}^2 = \frac{N_a N_b}{\beta_h \rho_h} + \left(\|\mathbf{H}\|_F^2 + \frac{N_a N_b}{\beta_h \rho_h} \right) \frac{N_b^2 \sum_{i=1}^{N_a} \frac{1}{\|\mathbf{g}_i\|^2}}{L_b N_a \rho} \quad (5.66)$$

where $\rho_h = P_a / \sigma_{w_h}^2$ and $\rho = P_b / \sigma_w^2$.

OSTBC vs. CSTBC

Comparing (5.62) to (5.19), in the light of the inequality between the harmonic mean and the arithmetic mean, we have

$$\text{SNR}_{\text{CSTBC}} \leq \text{SNR}_{\text{MFB}}. \quad (5.67)$$

The equality holds only when $\|\mathbf{h}_1\|^2 = \dots = \|\mathbf{h}_{N_r}\|^2$.

Comparing (5.66) to (5.51), similarly to the above,

$$\epsilon_{\text{CSTBC}}^2 \geq \epsilon_{\text{OSTBC}}^2. \quad (5.68)$$

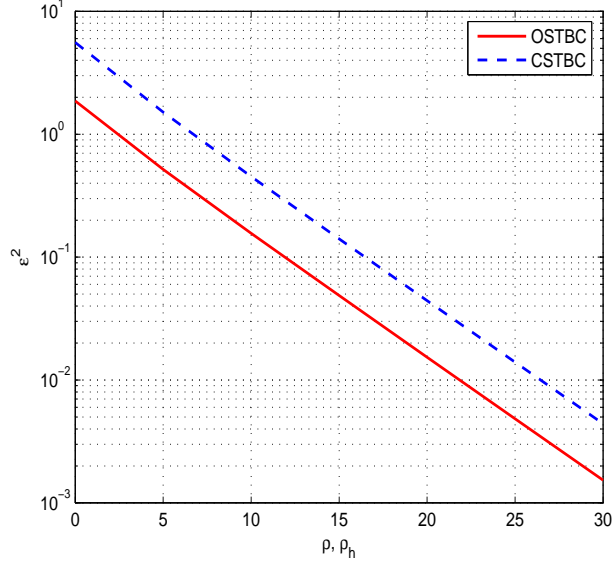


Figure 5.5: MSE comparison: OSTBC vs. CSTBC

The equality holds only when $\|\mathbf{h}_1\|^2 = \dots = \|\mathbf{h}_{N_a}\|^2$.

Assume $N_a = N_b = 2$, $\beta_h = 10$, $L_b = 4$, $\rho_h = \rho$, and random generated deterministic transmit and feedback channels,

$$\mathbf{H} = \begin{pmatrix} 0.3028 + 0.5169i & 0.0285 + 0.4023i \\ 0.6333 + 0.4086i & 0.4788 - 0.1808i \end{pmatrix}, \quad (5.69)$$

$$\mathbf{G} = \begin{pmatrix} -0.2669 - 1.0431i & -0.2092 - 0.1655i \\ 0.0838 + 1.0207i & 0.2226 - 0.2482i \end{pmatrix}. \quad (5.70)$$

Fig.5.5 illustrates that, in this case, for achieving the same MSE, the OSTBC linear analog scheme requires 5dB less SNR than the CSTBC scheme.

Assume complex elements in \mathbf{H} and \mathbf{G} are symmetric i.i.d. distributed $\mathcal{CN}(0, 1)$. We have

$$\|\mathbf{H}\|_F^2 \sim \chi^2(2N_a N_b), \quad (5.71)$$

$$\frac{1}{\|\mathbf{G}\|_F^2} \sim \text{Inv-}\chi^2(2N_a N_b), \quad (5.72)$$

$$\frac{1}{\|\mathbf{g}_j\|^2} \sim \text{Inv-}\chi^2(2N_b). \quad (5.73)$$

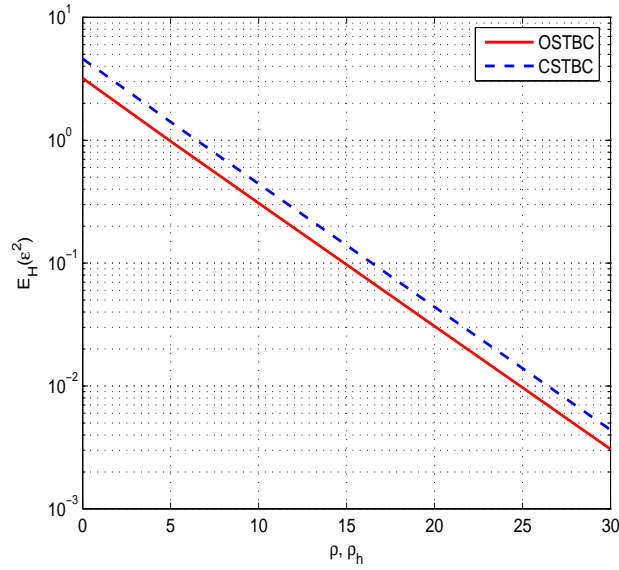


Figure 5.6: Average MSE comparison: OSTBC vs. CSTBC

Hence,

$$\mathbb{E}\|\mathbf{H}\|_{\text{F}}^2 = 2N_a N_b, \quad (5.74)$$

$$\mathbb{E}\frac{1}{\|\mathbf{G}\|_{\text{F}}^2} = \frac{1}{2N_a N_b - 2}, \quad (5.75)$$

$$\mathbb{E}\frac{1}{\|\mathbf{g}_j\|^2} = \frac{1}{2N_b - 2}. \quad (5.76)$$

Consequently, when $N_b \geq 2$, the average MSE

$$\mathbb{E}(\epsilon_{\text{OSTBC}}^2) = \frac{N_a N_b}{\beta_h \rho_h} + \left(2N_a N_b + \frac{N_a N_b}{\beta_h \rho_h}\right) \frac{N_a N_b^2}{2L_b(N_a N_b - 1)\rho}, \quad (5.77)$$

$$\mathbb{E}(\epsilon_{\text{CSTBC}}^2) = \frac{N_a N_b}{\beta_h \rho_h} + \left(2N_a N_b + \frac{N_a N_b}{\beta_h \rho_h}\right) \frac{N_b^2}{2L_b(N_b - 1)\rho}, \quad (5.78)$$

$$\mathbb{E}(\epsilon_{\text{OSTBC}}^2) \leq \mathbb{E}(\epsilon_{\text{CSTBC}}^2). \quad (5.79)$$

Fig.5.6 shows that, for the same scenario as the precedent example for evaluating MSE in the case of certain deterministic channels, the average MSE gap between the linear channel feedback schemes with OSTBC and CSTBC is about 2 dB.

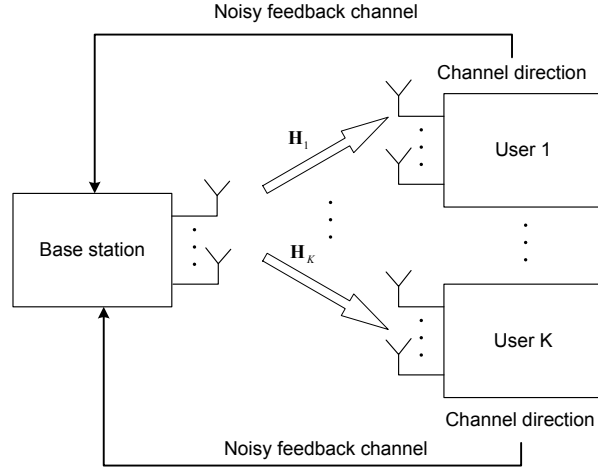


Figure 5.7: Multiuser MIMO downlink channel with channel feedback

From (5.77) and (5.78), we see that, when $\beta_h \rho_h$ is so large that $\frac{N_a N_b}{\beta_h \rho_h}$ approaches to zero, the ratio of the average MSE of the CSTBC scheme to the OSTBC scheme

$$\frac{\mathbb{E}(\epsilon_{\text{CSTBC}}^2)}{\mathbb{E}(\epsilon_{\text{OSTBC}}^2)} \sim 1 + \frac{1}{N_b - 1} \left(1 - \frac{1}{N_a}\right). \quad (5.80)$$

5.4 Multiuser MIMO downlink beamforming with analog channel feedback

5.4.1 Scheme description

As shown in Fig.5.8, we consider a K -user MIMO downlink system with zero-beamforming precoding (ZFBF) at the base station, N_{u_i} antennas at the user i , and N_b antennas at the base station.

The received signals via the downlink can be represented by

$$\begin{pmatrix} \mathbf{y}_1 \\ \vdots \\ \mathbf{y}_K \end{pmatrix} = \begin{pmatrix} \mathbf{H}_1 \\ \vdots \\ \mathbf{H}_K \end{pmatrix} (\mathbf{v}_1 \cdots \mathbf{v}_K) \begin{pmatrix} u_1 \\ \vdots \\ u_K \end{pmatrix} + \begin{pmatrix} \mathbf{w}_1 \\ \vdots \\ \mathbf{w}_K \end{pmatrix} \quad (5.81)$$

5.4 Multiuser MIMO downlink beamforming with analog channel feedback 91

where \mathbf{H}_i is user i 's channel matrix of size $N_{u_i} \times N_b$, \mathbf{v}_i is user i 's length- N_b precoding vector, u_i is user i 's data symbol to be transmitted, $\mathbf{y}_1 \dots \mathbf{y}_K$ are each user's received vectors, and \mathbf{w}_i is the additive noise vector for user i .

Ideally, if the transmitter perfectly know the directions of the row vectors in \mathbf{H}_i 's, we should have

$$\mathbf{H}_i \mathbf{v}_j = 0_{N_{u_i}}, \quad i \neq j, \quad 1 \leq i, j \leq K. \quad (5.82)$$

which indicates that inter-user interferences are prevented by precoding at the base station.

Hence, our scheme of multiuser MIMO downlink ZFBF with OSTBC analog channel feedback is as follows: in the first stage, for each user, user i learns its downlink channel by common training procedure; in the second stage, user i considers the channel estimation $\hat{\mathbf{H}}_i$ as a source vector of $N_b N_{u_i}$ complex analog symbols to be transmitted and accordingly construct an OSTBC of size $L_b \times N_{u_i}$ where L_b is the feedback latency given by the system according to the time resource allocated to the feedback procedure; $\hat{\mathbf{H}}_i$ is row-wise normalized and scaled according to the block power constraint $L_b P_{b_i}$; in the third stage, K users are supposed to transmit data spread by different OVFS for avoiding inter-user interferences [75], and the base station learns the feedback channel by feedback training and processes the received signal to obtain the row-wise-normalized channel matrix estimations $\hat{\mathbf{H}}_i$; in the fourth stage, the base station generates the unit beamforming vectors \mathbf{v}_i -s satisfying

$$\hat{\mathbf{H}}_j \mathbf{v}_i = 0_{N_{u_j}}, \quad i \neq j, \quad 1 \leq i, j \leq K \quad (5.83)$$

and uses them in ZFBF.

From the above description, we can see that the condition on the number of antennas at the base station is

$$N_b \geq \max\{M_1, \dots, M_K\} \quad (5.84)$$

with

$$M_i = \sum_{j=1, j \neq i}^K N_{u_j} + 1, \quad 1 \leq i, j \leq K. \quad (5.85)$$

5.4.2 Signal-to-interference ratio evaluation

Although ideally, all inter-user interferences can be eliminated by ZFBF, such perfectness cannot happen in practice. Even for learning \mathbf{H}_i -s at user

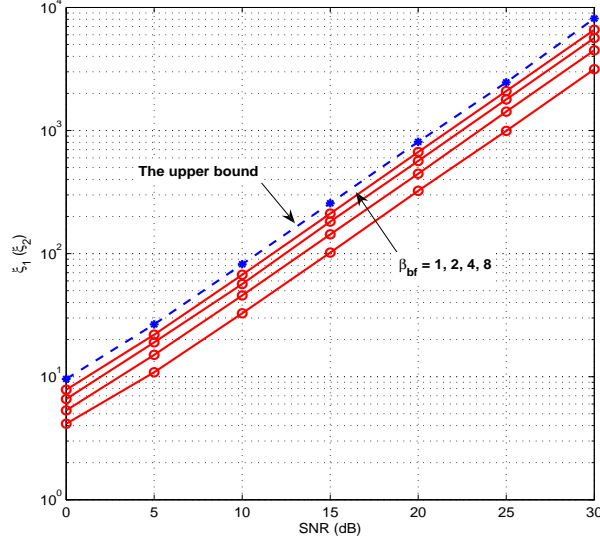


Figure 5.8: Average SIR comparison: OSTBC analog channel feedback with different latencies and upper bound

ends by training, there are estimation errors caused by the noise in the common training procedure. Additionally, there are the noise in the feedback training procedure for learning the feedback channel and the noise in the channel direction feedback procedure. Therefore, in practice, the beamforming vectors are distorted due to noises and thus cause inter-user interferences $\mathbf{H}_i \hat{\mathbf{v}}_j$ -s ($i \neq j$) which are not zero vectors due to the imperfectness of $\hat{\mathbf{v}}_j$. The average signal-to-interference ratio (SIR) of each user

$$\xi_k = \mathbb{E} \left[\frac{u_k^\dagger \hat{\mathbf{v}}_k^\dagger \mathbf{H}_k^\dagger \mathbf{H}_k \hat{\mathbf{v}}_k u_k}{\sum_{i \neq k} u_i^\dagger \hat{\mathbf{v}}_i^\dagger \mathbf{H}_k^\dagger \mathbf{H}_k \hat{\mathbf{v}}_i u_i} \right], \quad k = 1, \dots, K \quad (5.86)$$

can be a metric for evaluating channel feedback schemes.

Suppose there are one base station with three antennas and two users with two antennas each. Assume that the channels are MIMO Rayleigh fading with i.i.d. channel gains $\mathcal{CW}(0, 1)$ and source symbols u_1 and u_2 are i.i.d distributed. In terms of (5.86), the average SIR

$$\xi_1 = \xi_2 = \mathbb{E} \left[\frac{\|\mathbf{H}_1 \mathbf{v}_1\|^2}{\|\mathbf{H}_1 \mathbf{v}_2\|^2} \right]. \quad (5.87)$$

Fig.5.8 shows the simulation results (50,000 trials) when $\beta_h = \beta_g = 4$ and $\beta_s = 1, 2, 4, 8$. The upper bound of φ_i is represented by the blue dashed line, which is the average SIR in the case under the assumption that there is no noise in the feedback channel but only the noise in training the downlink channel, i.e., $\hat{\mathbf{H}}_i \neq \mathbf{H}_i$ but $\hat{\hat{\mathbf{H}}}_i = \hat{\mathbf{H}}_i$. We see that, when $\beta_s = 2$, the average SIR of OSTBC linear analog feedback scheme is about 2.5dB away from the upper bound; when $\beta_s = 8$, the performance of OSTBC linear analog feedback scheme is very close to the upper bound.

5.5 Conclusion

Considering the low complexity and reliability of linear analog transmission, we have introduced the orthogonal space-time block coding (OSTBC) to linear analog channel feedback to exploit the spatial diversity in an MIMO channel. We have proved that the linear analog approach with OSTBC can achieve the matched filter bound (MFB) on received SNR.

By simulations, we have compared the performance of the linear analog approach with OSTBC with the RVQ approach with respect to average MSE and average direction error. In the example where the average direction errors are measured, we have seen the self-adaptability to channel of the linear analog approach with OSTBC. In the example where the average direction errors are measured, we have seen that the linear analog method with OSTBC performs always better than the real RVQ method. Therefore, we could conclude that, in some cases, additionally considering the relative high computational complexity of the RVQ approach, in the sense of application, the linear analog transmission with OSTBC is more appropriate for analog vector source transmission via a MIMO channel.

Subsequently, we have described two complete linear analog channel feedback schemes for acquiring CSIT at the transmitter with linear analog channel feedback methods with OSTBC and CSTBC respectively. MSE and average MSE of these two schemes have been analyzed and compared. It has been shown that a scheme with OSTBC performs always better than a scheme with CSTBC due to the inequality of Pythagorean means.

For investigating the performance of linear analog channel feedback with OSTBC, assuming multiuser MIMO downlink ZFBF is employed at the base station, for a two-user case, we have simulated SIR's for the linear analog channel feedback schemes with OSTBC with different latencies and compared them to the upper bound. The simulation results have shown that, in our example, the performance of the MU-MIMO ZFBF system

using linear analog channel feedback with OSTBC is quite close to the upper bound.

Chapter 6

Layered Multiplexing

6.1 Introduction

In this chapter, we consider a layered-multiplexing scheme for short-block multi-layer transmission with hybrid automatic repeat request(HARQ) feedback.

Referring to the strategy of rateless coding over AWGN channels [88–90], a binary source packet is divided into several equal-length subpackets. These subpackets are channel coded and modulated to layers individually. Then, these layers are linearly combined to a block and sent. The receiver tries to decode all multiplexed layers. If decoding is not successful, the receiver will indicate the transmitter to resend a new linear combination of layers by ARQ feedback. This rateless coding strategy is to deal with the uncertainty of a channel and ensure the reliability of the transmission when there is no CSIT.

The key issue in the above-described rateless coding strategy is: how to let decoding at the receiver benefit from multiple block transmissions?

In [88–90], Erez et al. proposed to use random dither layer-time coding at the transmitter and MRC at the receiver to sum up all long-term block SNRs which have nothing to do with inter-layer interference and noise realizations but noise variances. This approach is effective for long-block cases but not for short-block cases. In short-block cases, the decoder relies more on interference and noise realizations. Then, in these cases, a more practical

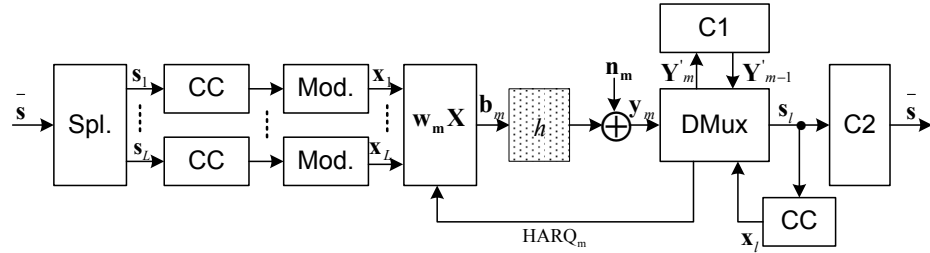


Figure 6.1: A multi-layer system with HARQ

way for benefiting from multiple block transmissions is to reduce the inter-layer interference by some layer-time coding scheme at the transmitter and the corresponding processing at the receiver, which we will propose in this chapter.

Another easy improvement to the strategy is that, when some layers are successfully decoded at the receiver, we can use a HARQ signal instead of an ARQ signal to indicate the transmitter not to combine decoded layers in the next block transmission and thus the other undecoded layers could benefit from allocated powers and less inter-layer interference.

The remainder of this chapter is organized as follows. In Section 6.2, the channel model and the general framework of a multi-layer transmission system with HARQ are given. The details of our Walsh layer-time coding scheme with HARQ feedback are presented in Section 6.3. The simulation result of comparison to comparable denser modulation schemes are shown in Section 6.4. Finally, this chapter is concluded in Section 6.5.

Note that the multi-layer transmission considered in this chapter is supposed to be over an AWGN SISO channel. With space-time coding and decoding, our scheme could be employed in MIMO systems.

6.2 General description and channel model

Consider transmitting a N -bit binary packet \bar{s} via a multi-layer system with HARQ as shown in Fig.6.1. \bar{s} is split into L subpackets $\{s_l : 1 \leq l \leq L\}$ (Spl.). The L subpackets are individually channel coded at rate r ($r \leq 1$) into N/rL bits (CC) and unit-energy phase-modulated into layers $\{x_l : 1 \leq l \leq L\}$ (Mod.) each of which is composed of T unit-energy phase-modulated symbols $\{x_{lt} : 1 \leq t \leq T\}$. Namely, if K -PSK modulation is used,

$$N = rLT \log_2 K. \quad (6.1)$$

Subsequently, $\{\mathbf{x}_l : 1 \leq l \leq L\}$ are multiplexed into one block \mathbf{b}_m by linear combination for the m^{th} block transmission

$$\mathbf{b}_m = \mathbf{w}_m \mathbf{X} \quad (6.2)$$

where

$$\mathbf{X} = \begin{pmatrix} \mathbf{x}_1 \\ \vdots \\ \mathbf{x}_L \end{pmatrix} \quad (6.3)$$

and the \mathbf{w}_m is the length- L layer-multiplexing vector, i.e. the m^{th} row vector of the layer-time code matrix \mathbf{W} .

Letting P denote the peak power constraint per channel use, we have

$$|\mathbf{w}_m \mathbf{X}_{.t}|^2 \leq P \quad (6.4)$$

with $\mathbf{X}_{.t}$ the t^{th} column of the matrix \mathbf{X} .

Since the column vector $\mathbf{X}_{.t}$ is composed of L unit-energy random variables, we have

$$|\mathbf{w}_m \mathbf{X}_{.t}|^2 \leq \|\mathbf{w}_m\|_1^2. \quad (6.5)$$

By Jensen's inequality [124],

$$\left(\frac{\|\mathbf{w}_m\|_1}{L}\right)^2 \leq \frac{\|\mathbf{w}_m\|_F^2}{L}. \quad (6.6)$$

Consequently, to ensure the power constraint is satisfied for arbitrary $\mathbf{X}_{.t}$, the following condition on \mathbf{w}_m is proposed,

$$\|\mathbf{w}_m\|_2^2 \leq \frac{P}{L}. \quad (6.7)$$

Under the assumption that the delay constraint is MT , a *block group* \mathbf{B} of size $M \times T$ is supposed to be transmitted over a slow-fading AWGN SISO channel through multiple transmissions with HARQ feedback. The received signals can be represented by

$$\mathbf{Y} = h \mathbf{B} + \mathbf{N} \quad (6.8)$$

where h is the channel coefficient constant for the whole procedure of transmitting \mathbf{B} , \mathbf{N} is the $M \times T$ noise matrix whose elements are i.i.d. $\mathcal{CN}(0, \sigma_n^2)$, and \mathbf{Y} is the received matrix of size $M \times T$. (6.8) can be also written as

$$\mathbf{Y} = h \mathbf{W} \mathbf{X} + \mathbf{N} \quad (6.9)$$

where

$$\mathbf{Y} = \begin{pmatrix} \mathbf{y}_1 \\ \vdots \\ \mathbf{y}_M \end{pmatrix}, \quad \mathbf{W} = \begin{pmatrix} \mathbf{w}_1 \\ \vdots \\ \mathbf{w}_M \end{pmatrix}, \quad \mathbf{N} = \begin{pmatrix} \mathbf{n}_1 \\ \vdots \\ \mathbf{n}_M \end{pmatrix}. \quad (6.10)$$

At the receiver, for the m^{th} block transmission, with the relevant information \mathbf{y}'_{m-1} from previous block transmissions (stored in Cache 1 (C1)), the receiver tries to demultiplex layers from the received vector \mathbf{y}_m (DMux). The successfully-decoded subpacket \mathbf{s}_l is not only output to Cache 2 (C2) for rebuilding $\bar{\mathbf{s}}$, but also re-channel-coded into the layer \mathbf{x}_l (CC at the receiver) for the module DMux to decode rest layers. The indices of undecoded layers are fed back to the transmitter by HARQ signals (HARQ $_m$). Meanwhile, the relevant information \mathbf{y}'_m from this transmission is saved in C1 for helping process the next retransmission.

6.3 Process description

In this section, we first introduce Walsh matrix into layer-time coding and then present the main features and details of our layer-multiplexing scheme in different stages.

6.3.1 Walsh layer-time coding

Walsh matrices are the Hadamard matrices of dimension 2^k for $k \in \mathbb{N}$. They are given by the following recursive formula

$$\begin{aligned} \mathbf{W}_a(2) &= \begin{bmatrix} 1 & 1 \\ 1 & -1 \end{bmatrix}, \\ \mathbf{W}_a(2^k) &= \begin{bmatrix} \mathbf{W}_a(2^{k-1}) & \mathbf{W}_a(2^{k-1}) \\ \mathbf{W}_a(2^{k-1}) & -\mathbf{W}_a(2^{k-1}) \end{bmatrix}. \end{aligned} \quad (6.11)$$

We suggest to use Walsh matrices as layer-time codes is not because of their orthogonality but because of their feature from the generating process. From the formula (6.11), we can see that, if we employ a column-wise scaled Walsh matrix as a layer-time code matrix whose columns are considered as layers and rows are considered as time, the inter-layer interferences can be eliminated or alleviated by adding rows up. Note that OVSF code matrices have the same property since it is a variation of Walsh matrix with the row order changed.

6.3.2 In the first transmission

In the first transmission, the target of layer-power allocation is to ensure that no retransmission is required when all *instantaneous channel SNR*'s in the block, $\rho_{h,1t} = \min\{|h|^2/|n_{1t}|^2\}$, $1 \leq t \leq T$, are higher than a specific threshold $\bar{\rho}$.

The power allocation scheme is similar to the method in [90] except with some different concerns. Assume all layered symbols x_{lt} have the same SNR threshold $\bar{\rho}$ ensuring correct demodulation and \mathbf{y}_1 is processed by successive interference cancelation (SIC) in the sequence from the top layer \mathbf{x}_L to the bottom layer \mathbf{x}_1 . Let P_l denote the allocated power for x_{lt} , $1 \leq l \leq L$, $1 \leq t \leq T$. The instantaneous SINR of x_{lt} in the first transmission,

$$\rho_l = \frac{|h|^2 P_l}{|h \sum_{l'=1}^{l-1} \sqrt{P_{l'}} x_{l't} + n_{1t}|^2}. \quad (6.12)$$

By Jansen's inequality [124]

$$|h \sum_{l'=1}^{l-1} \sqrt{P_{l'}} x_{l't} + n_{1t}|^2 \leq l \left(\sum_{l'=1}^{l-1} |h|^2 P_{l'} + |n_{1t}|^2 \right) \quad (6.13)$$

with $|x_{l't}|^2 = 1$. Thereby,

$$\rho_l \geq \frac{\rho_{h,1t} P_l}{l(\rho_{h,1t} \sum_{l'=1}^{l-1} P_{l'} + 1)}, \quad (6.14)$$

On the other hand, since $P_l = |w_{ml}|^2$, given (6.7), we have

$$\sum_{l=1}^L P_l \leq \frac{P}{L}. \quad (6.15)$$

As a consequence, for figuring out the power allocation scheme, we need to solve an equation array of $L + 1$ equations

$$\begin{cases} \frac{\bar{\rho}_{h,1t} P_l}{l(\bar{\rho}_{h,1t} \sum_{l'=1}^{l-1} P_{l'} + 1)} = \bar{\rho}, & l = 1, \dots, L, \\ \sum_{l=1}^L P_l = \frac{P}{L}. \end{cases} \quad (6.16)$$

After solving (6.16) (see Appendix 6.A), we get the threshold of $\rho_{h,1t}$

$$\bar{\rho}_{h,1t} = \frac{L \sum_{l=1}^L l \bar{\rho} \prod_{l'=1}^{l-1} (l' \bar{\rho} + 1)}{P} \quad (6.17)$$

and the power allocation scheme

$$\begin{aligned} P_1 &= \frac{\bar{\rho}}{\bar{\rho}_{h,1t}}, \\ P_l &= \frac{l\bar{\rho} \prod_{l'=1}^{l-1} (l'\bar{\rho} + 1)}{\bar{\rho}_{h,1t}}, \quad 2 \leq l \leq L. \end{aligned} \quad (6.18)$$

Hence, the layer-multiplexing vector \mathbf{w}_1 is

$$\mathbf{w}_1 = (\sqrt{P_1} \quad \dots \quad \sqrt{P_L}) . \quad (6.19)$$

At the receiver, the received vector \mathbf{y}_1 is processed by SIC from the top layer \mathbf{s}_L to the bottom layer \mathbf{s}_1 . Once a layer is successfully decoded, SIC starts again from the top to the bottom until no more layer can be decoded, namely, *cyclic SIC*. The correctness of decoding can be checked by the error detection code inserted in channel coding, e.g. cyclic redundancy code [1, 125–127]. When no more layer could be successfully decoded, the receiver feeds back a HARQ signal HARQ₁ for the first block transmission to indicate which layers have not been successfully decoded yet and the transmitter is required to prepare retransmission accordingly.

Note that HARQ₁ can be a byte or several bytes composed of binary bits representing success signals for respective layers, e.g., 0 is success and 1 is failure. In this chapter, for simplicity of presenting by expressions, HARQ_{*m*} is denoted by a binary row vector \mathbf{q}_m where 0 represents success and 1 represents failure.

In our scheme, the information of the current transmission to be stored in C1 is a $L \times T$ matrix \mathbf{Y}'_m . Each row of \mathbf{Y}'_m is a variation of the the received vector after canceling all-known inter-layer interference, which serves for subsequent processing on the corresponding layer. For \mathbf{Y}'_1 , all rows are the same,

$$\mathbf{y}'_{1,l} = \mathbf{y}_1 - \mathbf{q}_1 \mathbf{X}, \quad , 1 \leq l \leq L. \quad (6.20)$$

Note that only rows corresponding to undecoded layers are valid.

6.3.3 In the m^{th} transmission when $2 \leq m \leq L_w$

If the transmitter learns from \mathbf{q}_{m-1} that there are still L_m layers undecoded, it starts retransmission. Let $L_1 = L$.

The powers of the rest undecoded layers are amplified and the power scaling factor a_m for the m^{th} transmission,

$$a_m = \sqrt{\frac{P}{L_m \|(\mathbf{1} - \mathbf{q}_{m-1}) \cdot \mathbf{w}_1\|^2}} \quad (6.21)$$

where \cdot denotes the Hadamard product.

In the second block transmission, the rest undecoded layers are renumbered as $\mathbf{x}_1, \dots, \mathbf{x}_{L_2}$, i.e. \mathbf{X} is permuted, and a Walsh matrix \mathbf{W}_a of size $L_w = 2^{\lceil \log_2 L_2 \rceil}$ is set for layer-time coding. \mathbf{w}_1 and \mathbf{q}_1 are also permuted correspondingly. Then, the layer-multiplexing vector for the m^{th} block transmission is

$$\mathbf{w}_m = a_m \cdot \text{TZP}\{\mathbf{w}_{a,m}, L\} \cdot \mathbf{w}_1 \cdot (\mathbf{1} - \mathbf{q}_{m-1}), \quad 2 \leq m \leq L_w \quad (6.22)$$

where $\text{TZP}\{\mathbf{w}_{a,m}, L\}$ is the function to truncate or zero-pad the m^{th} row of \mathbf{W}_a , i.e. $\mathbf{w}_{a,m}$, to length L .

At the receiver, after cyclic SIC, for each retransmitted layer, we have

$$\mathbf{y}'_{m,l} = \frac{1}{a_m} w_{a,ml} \mathbf{y}_m + \mathbf{y}'_{m-1,l} - \mathbf{i}_{m,l}, \quad 1 < m \leq L_w \quad (6.23)$$

where $\mathbf{i}_{m,l}$ is the known inter-layer interference on the l^{th} layer. Subsequently, demodulation and decoding are done on the output of the matched filter $h^* \mathbf{y}'_{m,l}$. If \mathbf{x}_l cannot be successfully decoded, $\mathbf{y}'_{m,l}$ is sent to Cache 1 as the l^{th} row of the matrix \mathbf{Y}'_m for processing in the next block transmission.

When no more layer block can be successfully decoded, the HARQ vector \mathbf{q}_m is sent back to the transmitter for preparing the next block transmission.

In the L_w^{th} transmission, no matter how many layers have been decoded in previous transmissions, for the l^{th} layer, if it has not been successfully decoded yet, its received signal after processing

$$\mathbf{y}'_{L_w,l} = L_w h \sqrt{P_l} \mathbf{x}_l + \mathbf{n}'_{L_w,l} \quad (6.24)$$

where $\mathbf{n}'_{L_w,l}$ is the noise vector in $\mathbf{y}'_{L_w,l}$

$$\mathbf{n}'_{L_w,l} = \sum_{m=1}^{L_w} \frac{w_{a,ml} \mathbf{n}_m}{a_m}. \quad (6.25)$$

Obviously, there is no interference in $\mathbf{y}'_{L_w,l}$. In other words, after L_w block transmissions, the layer-multiplexing transmission is equivalent to single-layer sequential transmission.

6.3.4 When $L_w < m \leq M$

Recall that MT channel uses is the delay constraint given by the system. Generally, $M > L_w$.

Given by (6.24) and (6.25), the SNR in $\mathbf{y}'_{L_w,lt}$

$$\rho_{L_w,lt} = \frac{L_w^2 |h|^2 P_l}{|n'_{L_w,lt}|^2}, \quad (6.26)$$

which implies that, if a layer \mathbf{x}_l cannot be successfully decoded after L_w transmissions, the reason is probably because its initial power P_l is small relative to other undecoded layers and noises. For solving this problem, single-layer sequential ARQ transmission is employed to transmit each undecoded layer block alone at full peak power until this layer is successfully decoded. Thereby, if the l^{th} layer needs to be retransmitted alone, the layer-multiplexing vector is a row vector whose l^{th} element is \sqrt{P} and rest elements are zeros. This strategy is a compensation for the drawback of Walsh time-layer coding.

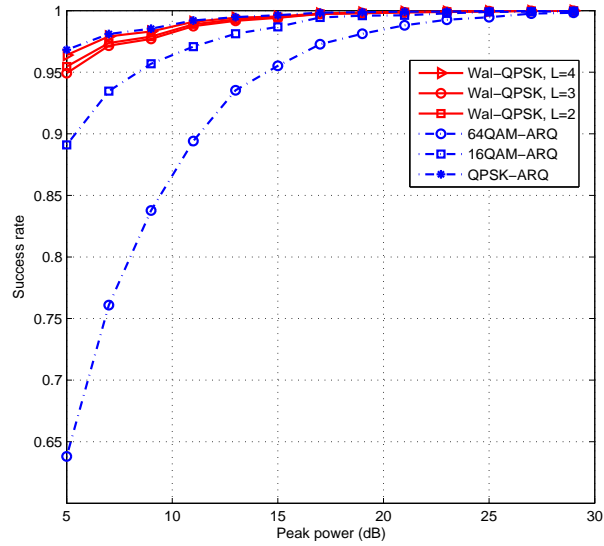
If there is still one or several layers undecoded after M block transmissions, as M is the allowable maximum number of block transmissions, the transmitter will stop retransmission and start to process another source packet.

Note that, although more layers can obtain a higher multiplexing gain (less latency) at relatively high SNR, it suffers inter-layer interference at relatively low SNR. Therefore, the number of layers is important to be decided, which might be empirical.

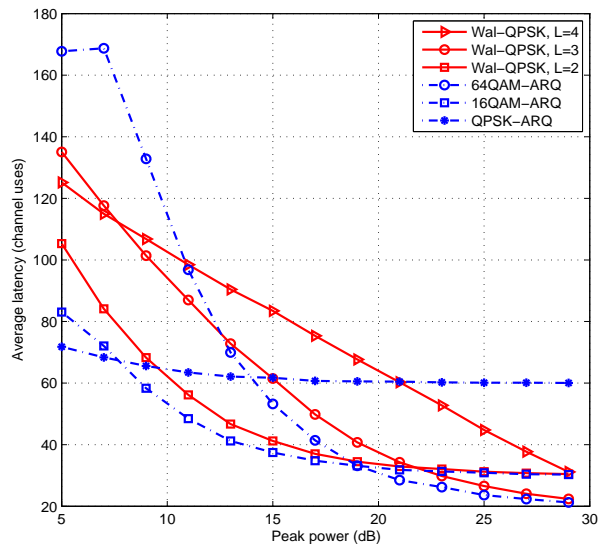
6.4 An example with simulation results

In this section, an example of transmitting a binary packet over a slow-fading AWGN channel is given. For clearness and simplicity, we assume that there is no channel coding and the correctness of demodulation and decoding can be told by the aid of a genie. The overheads of HARQ/ARQ feedback are neglected in our evaluation as it is small relative to data block length.

Suppose the source packet is composed of 120 bits which are independently identically uniformly binary distributed and the constraint of maximum latency is 300 channel uses. Three QPSK-modulated layer-multiplexing schemes with HARQ feedback ($L = 2, 3, 4$) are compared with three modulation schemes with ARQ feedback (QPSK, 16QAM, 64QAM). Herein, QPSK, 16QAM and 64QAM modulation schemes are chosen to be the reference as they are currently widely-used and combined together as an adaptive mod-



(a) Success rate



(b) Average latency of successful transmissions

Figure 6.2: Simulation results of the example

ulation scheme [128–131] with channel quality indicator (CQI) feedback in 3GPP LTE specifications [125, 132–138].

The six transmission schemes are evaluated by 10 000 Monte Carlo trials. In each trial, the source packet, channel gain and noise are generated independently and randomly. Both the channel gain h and the noise n_{mt} are supposed to be i.i.d. $\mathcal{CN}(0, 1)$. The success rate and average latency for successful transmission of the whole packet are investigated.

Fig.6.2(a) shows that, with respect to success rate, the three layer-multiplexing schemes performs very close to the QPSK modulation ARQ scheme. Especially at low SNR, the curves of success rate of these four are far above the ones of 64QAM and 16QAM ARQ schemes. Let us suppose 0.95 is the success rate threshold, i.e., only schemes with success rate higher than 0.95 are acceptable. Then, the three layer-multiplexing schemes and the QPSK modulation scheme with ARQ are acceptable when the peak power is above 5 dB, the 16QAM modulation scheme with ARQ is acceptable when the peak power is above 9 dB, and the 64QAM modulation scheme with ARQ is acceptable when the peak power is above 15 dB.

From Fig.6.2(b), we can see that, in the regime of high SNR, the average latency of the QPSK-modulated layer-multiplexing scheme with $L = 3$ is the same as the 64QAM-modulated ARQ scheme; so does the QPSK-modulated layer-multiplexing scheme with $L = 2$ with the 16QAM-modulated ARQ scheme. Thereby, corresponding to our intuition, with respect to the minimum latency in the regime of high SNR, a K -PSK-modulated L -layer-multiplexing scheme is equivalent to an Q -QAM modulation ARQ scheme when $L \log_2 K = \log_2 Q$.

Additionally, Fig.6.2(b) shows that, with respect to average latency (only successful transmission counted), for acceptable schemes, when peak power is in the range of 5 dB to 9 dB, the QPSK ARQ scheme achieves the smallest latency; from 9 dB to 19 dB, the 16QAM ARQ scheme achieves the smallest latency whereas the layer-multiplexing scheme with $L = 2$ is very close; from 19 dB to 30 dB, the 64QAM ARQ scheme the smallest latency whereas either the layer-multiplexing scheme with $L = 2$ or the layer-multiplexing scheme with $L = 3$ is very close.

Now, let us take a look at the processing complexity. Denote the processing complexity of ML decoder of n parameters by $\text{ML}(n)$. From Fig.6.2(b), in the peak power range of 9 dB to 19 dB, for the 16QAM ARQ scheme, the processing complexity for demodulating a symbol is $\text{ML}(16)$; whereas, for the QPSK-modulated layer-multiplexing scheme with $L = 2$, considering the worst case with cyclic SIC, the processing complexity is $2 \text{ML}(4) \sim 3 \text{ML}(4)$. In the peak power the range of 19 dB to 30 dB, for the 64QAM ARQ

scheme, the processing complexity per symbol is $ML(64)$; whereas, for the layer-multiplexing scheme with $L = 2$, it is $2 ML(4) \sim 3 ML(4)$, and for layer-multiplexing scheme with $L = 3$, it is $3 ML(4) \sim 6 ML(4)$. Therefore, we can see the advantage of the layer-multiplexing schemes with respect to processing complexity.

As a conclusion of this example, under the comprehensive consideration of success rate, average latency and complexity, rather than the adaptive modulation system, a QPSK-modulated adaptive layer-multiplexing system with $L = 1 \sim 3$ is recommended to achieve multiplexing gain at high SNR without losing reliability at low SNR.

6.5 Conclusion and future works

In this chapter, concerning the uncertainty of a channel and the peak power constraint, we have proposed a simple but practical layer-multiplexing transmission scheme with HARQ feedback for short-block cases. Walsh matrices are introduced to do layer-time coding. We have given an example to show the performance of our layer-multiplexing scheme in terms of success rate and average latency. It is compared with sequential ARQ schemes with denser constellations. By the figure of simulation results and our analysis, we have seen that, thanks to its good performance and relatively low processing complexity, an adaptive layer-multiplexing scheme could be an option to replace current widely-used adaptive modulation scheme.

6.A Solving the equation array (6.16)

Given (6.16), we have

$$\bar{\rho}_{h,1t}P_l = l\bar{\rho}(\bar{\rho}_{h,1t} \sum_{l'=1}^{l-1} P_{l'} + 1). \quad (6.27)$$

Namely,

$$\bar{\rho}_{h,1t}P_1 = \bar{\rho}, \quad (6.28)$$

$$\bar{\rho}_{h,1t}P_2 = 2\bar{\rho}(\bar{\rho} + 1), \quad (6.29)$$

$$\bar{\rho}_{h,1t}P_3 = 3\bar{\rho}(2\bar{\rho} + 1)(\bar{\rho} + 1), \quad (6.30)$$

and so on. Hence, we can hypothesize that $\bar{\rho}_{h,1t}P_l (l > 1)$ is in the form

$$\bar{\rho}_{h,1t}P_l = l\bar{\rho} \prod_{l'=1}^{l-1} (l'\bar{\rho} + 1). \quad (6.31)$$

On the other hand, for $l > 1$, (6.27) can also be written as

$$\begin{aligned} \bar{\rho}_{h,1t}P_l &= l\bar{\rho} \left(\bar{\rho}_{h,1t}P_{l-1} + \frac{\bar{\rho}_{h,1t}P_{l-1}}{(l-1)\bar{\rho}} \right), \quad l > 1 \\ &= l\bar{\rho}\bar{\rho}_{h,1t}P_{l-1} \frac{(l-1)\bar{\rho} + 1}{(l-1)\bar{\rho}}, \quad l > 1. \end{aligned} \quad (6.32)$$

Combining (6.32) and (6.31), we have

$$\begin{aligned} \bar{\rho}_{h,1t}P_{l+1} &= (l+1)\bar{\rho}\bar{\rho}_{h,1t}P_l \frac{l\bar{\rho} + 1}{l\bar{\rho}} \\ &= (l+1)\bar{\rho} \prod_{l'=1}^l (l'\bar{\rho} + 1) \end{aligned} \quad (6.33)$$

which exactly corresponds to our hypothesis (6.31). As a consequence,

$$\sum_{l=1}^L \bar{\rho}_{h,1t}P_l = \sum_{l=1}^L l\bar{\rho} \prod_{l'=1}^{l-1} (l'\bar{\rho} + 1). \quad (6.34)$$

Since under the peak power constraint, we have

$$\sum_{l=1}^L P_l = \frac{P}{L}, \quad (6.35)$$

the equation (6.34) yields

$$\bar{\rho}_{h,1t} = \frac{L \sum_{l=1}^L l \bar{\rho} \prod_{l'=1}^{l-1} (l' \bar{\rho} + 1)}{P}. \quad (6.36)$$

Therefore, straightforwardly, the layer power

$$P_l = \frac{l \bar{\rho} \prod_{l'=1}^{l-1} (l' \bar{\rho} + 1)}{\bar{\rho}_{h,1t}}, \quad 2 \leq l \leq L. \quad (6.37)$$

Chapter 7

Conclusion and Future Work

In this thesis, three topics on MIMO systems with limited feedback are investigated. They are optimum end-to-end distortion, analog channel feedback and layered multiplexing approach with hybrid automatic repeat request (HARQ). If the problems on MIMO systems with limited feedback are categorized into *what to feed back*, *how to feedback* and *where to use the feedback*, we see that the analysis on the optimum end-to-end distortion is relevant to what to feed back (instantaneous channel capacity) and where to use (outage-free transmission), the proposal of using orthogonal space-time coding on analog channel feedback is relevant to how to feed back (analog transmission other than digital), and the proposal of the layered multiplexing approach with HARQ is relevant to what to feed back (the HARQ signals) and where to use (layered multiplexing).

In Chapter 2, 3 and 4, assuming a continuous white Gaussian source is transmitted over a MIMO channel and the transmitter knows the instantaneous channel capacity, we analyze the joint impact of the source-to-channel bandwidth ratio (SCBR), spatial diversity, spatial correlation and time diversity on the optimum expected end-to-end distortion. The basis of our analysis is discrete MIMO channel capacity [42] and Shannon's inequality [22, 23] for continuous sources and continuous channels, which are connected by the channel sampling theorem [16, 10.3]. With Chiani et al.'s work on the moment generating function of capacity [94] and Bateman's

investigation on hypergeometric confluent functions [93], we provide the analytical expressions of the optimum expected end-to-end distortion for any SNR in different scenarios and the corresponding asymptotic expressions consisting of optimum distortion exponent and optimum distortion factor for high SNR. Before our work, the optimum distortion exponent has been figured out [38–41]. Our results on the optimum distortion factor can provide further insight into the behavior of the end-to-end distortion in MIMO systems.

In Chapter 2, the channel is assumed to be spatially uncorrelated and slow fading. By the results, it is illustrated that increasing antenna number, no matter on which side, always benefit on the optimum end-to-end distortion either via increasing the optimum distortion exponent or via decreasing the optimum distortion factor, and the commutation of the transmit antenna number and the receive antenna number affects the optimum end-to-end distortion due to its impact on the distortion factor.

In Chapter 3, the discussion is extended to the case of spatially correlated channel. We see that spatial correlation has no impact on the optimum distortion exponent but on the optimum distortion factor. It is proved that when the correlation matrix approaches an identity matrix, the asymptotic optimum end-to-end distortion for the case of spatially correlated channel converge to that for the case of uncorrelated channel. It is illustrated that the spatial correlation deteriorates the optimum end-to-end distortion as well as the asymptotic optimum end-to-end distortion. The results correspond to intuition.

In Chapter 4, the time diversity is involved into our analysis. It is proved that the time diversity always benefits the optimum end-to-end distortion, either by increasing the optimum distortion exponent or by decreasing the optimum distortion factor. Increasing time diversity branches can make a system in the low SCBR regime migrate into the high SCBR regime. When the system is in the high SCBR regime, increasing time diversity branches only impacts the optimum distortion factor and thus the impact is relatively not obvious, as shown by simulation results. Therefore, considering the extra processing complexity and delay for lengthening frames, we do not suggest lengthen frames to achieve the relatively trivial performance improvement when the time diversity branches is more than the given transit point where the system migrate into the high SCBR regime from the moderate SCBR regime. Analogous to our analysis in this chapter, the results for the case of correlated channel are straightforward and the results on frequency diversity would be similar.

Straightforwardly, our results on outage-free systems are upper bounds

for the scenarios where the transmitter has no knowledge about the channel and suffers to outage accidents happening at a certain probability.

Future work: The asymptotic optimum expected end-to-end distortion was derived from the polynomial form of the optimum expected end-to-end distortion and it is only effective at relative high SNR. When the SNR is not so high, there is gap between the asymptotic optimum expected distortion and the optimum expected distortion. In this case, if more terms in the polynomial of the optimum expected end-to-end distortion could involve, the analysis on the behavior of the optimum expected end-to-end distortion would be more precise.

Let us take an insight into the optimum distortion exponent. Define a non-negative integer m as

$$m = \begin{cases} N_{\min}, & 0 < \frac{2}{\eta} < |N_t - N_r| + 1; \\ N_{\min} - \left\lfloor \frac{\frac{2}{\eta} + 1 - |N_t - N_r|}{2} \right\rfloor, & |N_t - N_r| + 1 \leq \frac{2}{\eta} \leq N_t + N_r - 1; \\ 0, & \frac{2}{\eta} > N_t + N_r - 1. \end{cases} \quad (7.1)$$

Then, the optimum distortion exponent can be written in the form

$$\Delta^*(\eta) = (N_t - m)(N_r - m) + \frac{2m}{\eta}, \quad (7.2)$$

which looks quite similar to the formula of diversity multiplexing tradeoff [25] and the expression of the distortion exponent in tandem source-channel coding systems [35]. Note that (7.2) has nothing to do with outage since the instantaneous channel capacities is assumed to be known at the transmitter. This intriguing similarity induces us to conjecture that there may be a hidden connection to be explored here.

In chapter 5, considering the low complexity and reliability of linear analog transmission, we introduce the orthogonal space-time block coding (OSTBC) to linear analog channel feedback to exploit the spatial diversity in MIMO channels. It is proved that the linear analog approach with OSTBC can achieve the matched filter bound (MFB) on received SNR. The performance of the linear analog approach with OSTBC is compared with the random vector quantization (RVQ) approach with respect to average MSE and average direction error. Circulant space-time block coding (CSTBC) is another possible space-time coding for analog transmission. The performances of an analog feedback scheme with OSTBC and an analog feedback

scheme with CSTBC are compared and it is proved that the one with OSTBC performs better. For investigating the performance of linear analog channel feedback with OSTBC, assuming multiuser MIMO downlink zero-forcing beamforming (ZFBF) is employed at the base station, for a two-user case, SIR's for OSTBC linear analog channel feedback schemes with different latencies are simulated and compared to the upper bound. The simulation results show that within a short delay, the performance of the MU-MIMO ZFBF system using linear analog channel feedback OSTBC is quite close to the upper bound.

Future work: In our future work, more theoretical analysis on the performance of OSTBC linear analog channel feedback method in a multi-user multi-antenna ZFBF scheme is to be done. In the case that the complete CSI is required to be known at the transmitter, a nonlinear method of how to feedback the scaling factor is to be proposed and the performance of the hybrid feedback scheme is to be analyzed.

In Chapter 6, concerning the uncertainty of a channel and the peak power constraint, a simple but practical layer-multiplexing transmission method with HARQ feedback is proposed for short-block cases. Walsh matrices are used to do layer-time coding for inter-layer interference cancellation. This method is compared to comparable sequential ARQ schemes with denser constellations. By simulation results, we see that thanks to its good performance and relatively low processing complexity, an adaptive layer-multiplexing scheme could be an option to replace current widely-used adaptive modulation scheme.

Future work: Although we did not involve channel coding and decoding in our simulation, it is necessary in practice and the effect along could be seen by further simulation or demonstration.

This layer-multiplexing scheme could also be implemented for the case of the fast-fading channel with time-interleaving in channel coding, not only limited to the slow-fading channel. Such implementation is to be analyzed in future.

An alternative adaptive method to adaptive layer-multiplexing or modulation transmission is the adaptive error protection coding [139, 140]. In 3GPP LTE standards [125, 132–138], it is combined with adaptive modulation scheme. Straightforwardly, it can also be combined with our adaptive layer-multiplexing scheme. This combination and its optimization is to be studied in future.

MIMO system with limited feedback is a rich subject and its study spans

over many topics. Those have been studied in this thesis are only several fragments.

Bibliography

- [1] J. G. Proakis, *Digital Communications, Fourth Edition*. USA: The McGraw - Hill Companies, 2000.
- [2] D. Tse and P. Viswanath, *Fundamentals of Wireless Communication*. Cambridge University Press, 2004.
- [3] A. Goldsmith, *Wireless Communications*. Cambridge University Press, 2005.
- [4] R. B. Ertel, P. Cardieri, K. W. Sowerby, T. S. Rappaport, and J. H. Reed, "Overview of spatial channel models for antenna array communication systems," *IEEE Pers. Commun. Mag.*, pp. 10–22, Feb. 1998.
- [5] D. Gesbert, H. Bölcskei, D. A. Gore, and A. J. Paulraj, "Outdoor MIMO wireless channels: models and performance prediction," *IEEE Trans. Commun.*, vol. 50, pp. 1926–1934, 2002.
- [6] M. Debbah and R. R. Müller, "MIMO channel modeling and the principle of maximum entropy," *IEEE Trans. Inf. Theory*, vol. 51, pp. 1667–1690, 2005.
- [7] S. A. Jafar and A. Goldsmith, "Transmit optimization and optimality of beamforming for multiple antenna systems," *IEEE Trans. Wireless Commun.*, vol. 3, pp. 1165 – 1175, 2004.
- [8] A. Narula, M. J. Lopez, M. D. Trott, and G. W. Wornell, "Efficient use of side information in multiple-antenna data transmission over fading channels," *IEEE J. Sel. Areas Commun.*, vol. 16, pp. 1423–1436, 1998.
- [9] E. Visotsky and U. Madhow, "Space-time transmit precoding with imperfect feedback," *IEEE Trans. Inf. Theory*, vol. 47, pp. 2632–2639, 2001.

- [10] C.-C. J. Kuo, S.-H. Tsai, L. Tadjpour, and Y.-H. Chang, *Precoding techniques for digital communication systems*. Springer, 2008.
- [11] E. Biglieri, J. Proakis, and S. Shamai (Shitz), “Fading channels: information-theoretic and communications aspects,” *IEEE Trans. Inf. Theory*, vol. 44, pp. 2619–2692, Oct. 1998.
- [12] K. S. Zigangirov, “Upper bounds on the error probability for channels with feedback,” *Probl. Inform. Transm.*, vol. 6, pp. 87–92, 1979.
- [13] A. Goldsmith and P. Varaiya, “Capacity of fading channels with channel side information,” *IEEE Trans. Inf. Theory*, vol. 43, pp. 1986–1992, 1997.
- [14] G. Caire, G. Taricco, and E. Biglieri, “Optimum power control over fading channels,” *IEEE Trans. Inf. Theory*, vol. 45, pp. 1468–1489, 1999.
- [15] S. Verdú, “Fifty years of Shannon theory,” *IEEE Trans. Inf. Theory*, vol. 44, pp. 2057–2078, 1998.
- [16] T. M. Cover and J. A. Thomas, *Elements of Information Theory*. United States: John Wiley & Sons, 1991.
- [17] C.-N. Chuah, D. N. C. Tse, J. M. Kahn, and R. A. Valenzuela, “Capacity scaling in MIMO wireless systems under correlated fading,” *IEEE Trans. Inf. Theory*, vol. 48, pp. 637–650, 2002.
- [18] R. Knopp and P. A. Humblet, “Information capacity and power control in single-cell multiuser communications,” in *Proc. IEEE Int. Conf. on Communication*, Jun. 1995.
- [19] G. Caire and S. Shamai (Shitz), “On the achievable throughput of a multiantenna gaussian broadcast channel,” *IEEE Trans. Inf. Theory*, vol. 49, pp. 1691–1706, 2003.
- [20] M. Guillaud, D. T. M. Slock, and R. Knopp, “A practical method for wireless channel reciprocity exploitation through relative calibration,” in *Proc. Int. Symp. on Signal Processing and its Applications*, Sep. 2005.
- [21] T. J. Goblick, “Theoretical limitations on the transmission of data from analog sources,” *IEEE Trans. Inf. Theory*, vol. IT-11, pp. 558–567, Oct. 1965.

-
- [22] C. E. Shannon, "A mathematical theory of communication," *Bell Syst. Tech. J.*, vol. 27, pp. 379–423, 623–625, 1948.
- [23] —, "Communication in the presence of noise," *Proc. IRE.*, 1949.
- [24] R. G. Gallager, *Information theory and reliable communication*. John Wiley & Sons, 1968.
- [25] L. Zheng and D. N. C. Tse, "Diversity and multiplexing: A fundamental tradeoff in multiple-antenna channels," *IEEE Trans. Inf. Theory*, vol. 49, pp. 1073–1096, May. 2003.
- [26] J. Ziv and M. Zakai, "Some lower bounds on signal parameter estimation," *IEEE Trans. Inf. Theory*, vol. IT-15, pp. 386–391, May. 1969.
- [27] J. Ziv, "The behavior of analog communication systems," *IEEE Trans. Inf. Theory*, vol. IT-16, pp. 587–594, Sep. 1970.
- [28] J. N. Laneman, E. Martinian, G. W. Wornell, and J. G. Apostolopoulos, "Source-channel diversity approaches for multimedia communication," in *Proc. IEEE Int. Symp. on Information Theory*, Jul. 2004.
- [29] —, "Source-channel diversity for parallel channels," *IEEE Trans. Inf. Theory*, vol. 51, pp. 3518–3539, Oct. 2005.
- [30] S. Choudhury and J. D. Gibson, "Ergodic capacity, outage capacity, and information transmission over rayleigh fading channels," in *Proc. Information Theory and Applications Workshop*, Jan. 2007.
- [31] M. Zoffoli, J. D. Gibson, and M. Chiani, "On strategies for source information transmission over MIMO systems," in *Proc. IEEE Global Telecomm. Conf.*, New Orleans, USA, Dec. 2008.
- [32] —, "Source information transmission over MIMO systems with transmitter side information," in *Proc. 46th Annu. Allerton Conf.*, IL, USA, Sep. 2008.
- [33] T. Holliday and A. Goldsmith, "Joint source and channel coding for MIMO systems," in *Proc. 42nd Annu. Allerton Conf. Communications, Control, and Computing*, IL, United States, Oct. 2004.
- [34] —, "Optimizing end-to-end distortion in MIMO system," in *Proc. IEEE Int. Symp. on Information Theory*, Adelaide, Australia, Sep. 2005.

- [35] T. Holliday, A. J. Goldsmith, and H. V. Poor, "Joint source and channel coding for MIMO systems: is it better to be robust or quick?" *IEEE Trans. Inf. Theory*, vol. 54, pp. 1393 – 1405, 2008.
- [36] A. Gersho, "Asymptotically optimal block quantization," *IEEE Trans. Inf. Theory*, vol. 25, pp. 373 – 380, 1979.
- [37] B. Hochwald and K. Zeger, "Tradeoff between source and channel coding," *IEEE Trans. Inf. Theory*, vol. 43, pp. 1412 – 1424, 1997.
- [38] G. Caire and K. R. Narayanan, "On the distortion SNR exponent of hybrid digital-analog space-time coding," *IEEE Trans. Inf. Theory*, vol. 53, pp. 2867–2878, Aug. 2007.
- [39] —, "On the snr exponent of hybrid digital analog space time codes," in *Proc. 43rd Annu. Allerton Conf. Communications, Control and Computng*, IL, United States, Oct. 2005.
- [40] D. Gunduz and E. Erkip, "Distortion exponent of MIMO fading channels," in *Proc. IEEE Information Theory Workshop*, Punta del Este, Uruguay, Mar. 2006.
- [41] —, "Joint source-channel codes for MIMO block-fading channels," *IEEE Trans. Inf. Theory*, vol. 10, pp. 116–134, Jan. 2008.
- [42] I. E. Telatar, "Capacity of multi-antenna gaussian channels," *Europ. Trans. Telecomm.*, vol. 10, pp. 585–596, Nov. 1999.
- [43] K. R. Narayanan and G. Caire, "Further results on the SNR exponent of hybrid digital analog space time codes," in *USCD Workshop on Info. Theory and Its Applications*, San Diego CA, USA, Feb. 2006.
- [44] U. Mittal and N. Phamdo, "Hybrid digital-analog (HDA) joint source-channel codes for broadcasting and robust communications," *IEEE Trans. Inf. Theory*, vol. IT-48, pp. 1082–1103, May 2002.
- [45] K. Bhattad, K. R. Narayanan, and G. Caire, "On the distortion exponent of some layered transmission schemes," in *40th Aislomar Conf. on Sig., Syst. and Comp.*, Monterey CA, USA, Nov. 2006.
- [46] K. Bhattad, K. Narayanan, and G. Caire, "On the distortion SNR exponent of some layered transmission schemes," submitted to *IEEE Trans. Information Theory*, Mar. 2007, arXiv:cs/0703035.

- [47] D. Gunduz and E. Erkip, "Distortion exponent of parallel fading channels," in *Proc. IEEE Int. Symp. on Information Theory*, Seattle WA, USA, Jul. 2006.
- [48] H. Miyakawa and H. Harashima, "Matched-transmission technique for channels with intersymbol interference," *IEEE Trans. Commun.*, vol. 20, pp. 774–780, 1972.
- [49] M. Tomlinson, "New automic equalizer employing modulo arithmetic," *Electronic Letters*, vol. 7, pp. 138–139, 1971.
- [50] C. Windpassinger, R. F. H. Fischer, T. Vencel, and J. B. Huber, "Precoding in multiantenna and multiuser communications," *IEEE Trans. Wireless Commun.*, vol. 3, pp. 1305–1316, 2004.
- [51] M. V. Eyuboglu and G. D. Forney, Jr, "Trellis precoding: combined coding, precoding and shaping for intersymbol interference channels," *IEEE Trans. Inf. Theory*, vol. 38, pp. 301–314, 1992.
- [52] R. Esmailzadeh, E. Sourour, and M. Nakagawa, "Prerake diversity combining in time-division duplex cdma mobile communications," *IEEE Trans. Vehicular Techonology*, vol. 48, pp. 795–801, 1999.
- [53] R. L.-U. Choi, K. B. Letaief, and R. D. Murch, "MISO CDMA transmission with simplified receiver for wireless communication handsets," *IEEE Trans. Commun.*, vol. 49, pp. 888–898, 2001.
- [54] M. Brandt-Pearce and A. Dharap, "Transmitted-based multiuser interference rejection for the down-link of a wireless CDMA system in a multipath environment," *IEEE J. Sel. Areas Commun.*, vol. 18, pp. 407–417, 2000.
- [55] B. R. Vojcic and W. M. Jang, "Transmitter precoding in synchronous multiuser communications," *IEEE Trans. Commun.*, vol. 46, pp. 1346–1355, 1998.
- [56] M. Joham, W. Utschick, and J. A. Nossek, "Linear transmit processing in MIMO communication systems," *IEEE Trans. Signal Processing*, vol. 53, pp. 2700–2712, 2005.
- [57] H. Sampath, P. Stoica, and A. Paulraj, "Generalized linear precoder and decoder design for MIMO channels using the weighted MMSE criterion," *IEEE Trans. Commun.*, vol. 49, pp. 2198–2206, 2001.

- [58] A. Scaglione, P. Stoica, S. Barbarossa, G. B. Giannakis, and H. Sampath, "Optimal design for space-time linear precoders and decoders," *IEEE Trans. Signal Processing*, vol. 50, pp. 1051–1064, 2002.
- [59] G. Caire and S. Shamai (Shitz), "On the capacity of some channels with channel state information," *IEEE Trans. Inf. Theory*, vol. 45, pp. 2007–2019, 1999.
- [60] M. Gastpar, B. Rimoldi, and M. Vetterli, "To code, or not to code: lossy source-channel communication revisited," *IEEE Trans. Inf. Theory*, vol. 49, pp. 1147–1158, May. 2003.
- [61] D. J. Love, R. W. Heath Jr, V. K. N. Lau, D. Gesbert, B. D. Rao, and M. Andrews, "An overview of limited feedback in wireless communication systems," *IEEE J. Sel. Areas Commun.*, vol. 26, pp. 1341–1365, 2008.
- [62] J. C. Roh and B. D. Rao, "Transmit beamforming in multiple-antenna systems with finite rate feedback: a vq-based approach," *IEEE Trans. Inf. Theory*, vol. 52, pp. 1101–1112, 2006.
- [63] A. Gersho and R. M. Gray, *Vector Quantization and Signal Compression*. Norwell, MA: Kluwer Academics, 1992.
- [64] Y. Linde, A. Buzo, and R. M. Gray, "An algorithm for vector quantizer design," *IEEE Trans. Commun.*, vol. 28, pp. 84–95, 1980.
- [65] S. P. Lloyd, "Least squares quantization in PCM's," *Bell Telephone Laboratories Paper*, 1957.
- [66] D. J. Love, R. W. Heath Jr., and T. Strohmer, "Grassmannian beamforming for multiple-input multiple-output wireless systems," *IEEE Trans. Inf. Theory*, vol. 49, pp. 2735–2747, 2003.
- [67] W. Santipach and M. L. Honig, "Asymptotic capacity of beamforming with limited feedback," in *Proc. IEEE Int. Symp. on Information Theory*, Jun. 2004.
- [68] W. Santipach and M. Honig, "Signature optimization for CDMA with limited feedback," *IEEE Trans. Inf. Theory*, vol. 51, pp. 3475–3492, Oct. 2005.
- [69] T. Berger, *Rate Distortion Theory*. Engelwood Cliffs: Prentice-Hall, 1971.

- [70] H. L. V. Trees, *Detection, Estimation and Modulation Theory, Pt-II: Nonlinear Modulation Theory*. New York: Wiley, 1971.
- [71] J. Xiao, Z. Luo, and N. Jindal, "Linear joint source-channel coding for Gaussian sources through fading channels," in *Proc. IEEE Global Telecomm. Conf.*, San Francisco, USA, Nov. 2006.
- [72] D. Samardzija and N. Mandayam, "Unquantized and uncoded channel state information feedback in multiple-antenna multiuser systems," *IEEE Trans. Commun.*, vol. 54, pp. 1335–1345, Jul. 2006.
- [73] E. Visotsky and U. Madhow, "Space-time transmit strategies and channel feedback generation for wireless fading channels," in *Thirty-Fourth Asilomar Conference*, 2001.
- [74] T. A. Thomas, K. L. Baum, and P. Sartori, "Obtaining channel knowledge for closed-loop multi-stream broadband MIMO-OFDM communications using direct channel feedback," in *Proc. IEEE Global Telecomm. Conf.*, St.Louis, USA, Nov. 2005.
- [75] T. L. Marzetta and B. M. Hochwald, "Fast transfer of channel state information in wireless systems," *IEEE Trans. Signal Processing*, vol. 54, pp. 1268–1278, Apr. 2006.
- [76] G. Caire, N. Jindal, M. Kobayashi, and N. Ravindran, "Quantized vs. analog feedback for the MIMO downlink: a comparison between zero-forcing based achievable rates," in *Proc. IEEE Int. Symp. on Information Theory*, Nice, France, Jun. 2007.
- [77] —, "Multiuser MIMO downlink made practical: achievable rates with simple channel state estimation and feedback schemes," submitted to *IEEE Trans. Information Theory*, Nov. 2007, arXiv:0711.2642.
- [78] S. Shamai (Shitz) and A. Steiner, "A broadcast approach for a single-user slowly fading MIMO channel," *IEEE Trans. Inf. Theory*, vol. 49, pp. 2617–2635, 2003.
- [79] F. Etemadi and H. Jafarkhani, "Optimal layered transmission over quasi-static fading channels," in *Proc. IEEE Int. Symp. on Information Theory*, Jul. 2006.
- [80] C. T. K. Ng, D. Gunduz, A. J. Goldsmith, and E. Erkip, "Minimum expected distortion in Gaussian layered broadcast coding with succe-

- sive refinement,” in *Proc. IEEE Int. Symp. on Information Theory*, Jun. 2007.
- [81] C. Tian, A. Steiner, S. Shamai (Shitz), and S. N. Diggavi, “Successive refinement via broadcast: optimizing expected distortion of a Gaussian source over a Gaussian fading channel,” *IEEE Trans. Inf. Theory*, vol. 54, pp. 2903–2918, 2008.
- [82] W. H. R. Equitz and T. M. Cover, “Successive refinement of information,” *IEEE Trans. Inf. Theory*, vol. 37, pp. 269–275, 1991.
- [83] B. Rimoldi, “Successive refinement of informatino: characterization of achievable rates,” *IEEE Trans. Inf. Theory*, vol. 40, pp. 253–259, 1994.
- [84] D. J. C. MacKay, *Information theory, inference, and learning algorithms*. Cambridge University Press, 2003.
- [85] —, “Fountain codes,” in *The IEE Seminar on Sparse-Graph Codes*. London: IEE, 2004, pp. 1–8.
- [86] M. Luby, “LT codes,” in *Proc. 43rd Annual IEEE Symposium on the Foundations of Computer Science*, 2002.
- [87] A. Shokrollahi, “Raptor codes,” in *Technical report, Laboratoire d’algorithmique, École Polytechnique Fédérale de Lausanne, Lausanne, Switzerland*.
- [88] U. Erez, G. W. Wornell, and M. D. Trott, “Faster-than-nyquist coding: the merits of a regime change,” in *Proc. 42rd Annu. Allerton Conf. Communications, Control and Computng*, IL, United States, Sep. 2004.
- [89] U. Erez, M. D. Trott, and G. W. Wornell, “Rateless coding for Gaussian channels,” *IEEE Trans. Inf. Theory*, submitted for publication.
- [90] J. M. Shapiro, R. J. Barron, and G. W. Wornell, “Practical layered rateless codes for the gaussian channel: power allocation and implementation,” in *Proc. IEEE Workshop on Signal Processing Advances in Wireless Communications*, Helsinki, Finland, Jun. 2007.
- [91] G. J. Foschini, G. D. Golden, R. A. Valenzuela, and P. W. Wolniansky, “Simplified processing for high spectral efficiency wireless communication employing multi-element arrays,” *IEEE J. Sel. Areas Commun.*, vol. 17, pp. 1841–1852, 1999.

- [92] L. S. Gradshteyn and I. M. Ryzhik, *Tables of Integrals, Series, and Products*. San Diego, United States: Academic Press, 1994.
- [93] H. Bateman, *Higher Transcendental Functions*. United States: Robert E. Krieger Publishing Company, 1953.
- [94] M. Chiani, M. Z. Win, and A. Zanella, "On the capacity of spatially correlated MIMO Rayleigh-fading channels," *IEEE Trans. Inf. Theory*, vol. 49, pp. 2363–2371, Oct. 2003.
- [95] R. A. Horn and C. R. Johnson, *Matrix Analysis*. Cambridge, United Kingdom: Cambridge University Press, 1985.
- [96] R. O. Hill, *Elementary Linear Algebra with Applications*, 3rd ed. United States: Harcourt College Publishers, 1996.
- [97] W. Rudin, *Principles of Mathematical Analysis*, 3rd ed. United States: McGraw-Hill, 1976.
- [98] V. A. Aalo, "Performance of maximal-ratio diversity systems in a correlated nakagami-fading environment," *IEEE Trans. Commun.*, vol. 43, pp. 2360–2369, Aug. 1995.
- [99] S. G. Wilson and Y. S. Leung, "Trellis-coded phase modulation on Rayleigh channels," in *Proc. IEEE Int. Conf. on Communication*, Jun. 1987.
- [100] D. Divsalar and M. K. Simon, "The design of trellis coded modulation for mpsk for fading channels: performance criteria," *IEEE Trans. Commun.*, vol. 36, pp. 1004–1012, Sep. 1988.
- [101] E. Zehavi, "8-psk trellis codes for a Rayleigh channel," *IEEE Trans. Commun.*, vol. 40, pp. 873–884, May 1992.
- [102] J. V-Traveset, G. Caire, E. Biglieri, and G. Taricco, "Impact of diversity reception on fading channels with coded modulation - partial coherent detection," *IEEE Trans. Commun.*, vol. 45, pp. 563–572, May 1997.
- [103] G. Caire, G. Taricco, and E. Biglieri, "Bit-interleaved coded modulation," *IEEE Trans. Inf. Theory*, vol. 44, pp. 927–946, May 1998.
- [104] N. Phamdo and U. Mittal, "A joint source-channel speech coder using hybrid digital-analog(HDA) modulation," *IEEE Trans. Inf. Theory*, vol. 10, pp. 222–231, May. 2002.

- [105] M. R. McKay and I. B. Collings, "Performance bounds for MIMO bit-interleaved coded modulation with zero-forcing receivers," in *Proc. IEEE Global Telecomm. Conf.*, Dec. 2004.
- [106] A. Martinez, A. Guillén, and G. Caire, "Error probability analysis of bit-interleaved coded modulation," *IEEE Trans. Inf. Theory*, vol. 52, pp. 262–271, Jan 2006.
- [107] S. M. Alamouti, "A simple transmit diversity technique for wireless communications," *IEEE J. Sel. Areas Commun.*, vol. 16, pp. 1451–1458, Oct. 1998.
- [108] V. Tarokh, H. Jafarkhani, and A. Calderbank, "Space-time block codes from orthogonal designs," *IEEE Trans. Inf. Theory*, vol. 45, pp. 1456–1467, Mar. 1999.
- [109] G. Ganesan and P. Stoica, "Space-time block codes: a maximum snr approach," *IEEE Trans. Inf. Theory*, vol. 47, pp. 1650–1656, 2001.
- [110] O. Tirkkonen and A. Hottinen, "Square-matrix embeddable space-time block codes for complex signal constellations," *IEEE Trans. Inf. Theory*, vol. 48, pp. 384–395, 2002.
- [111] X. Liang, "Orthogonal designs with maximal rates," *IEEE Trans. Inf. Theory*, vol. 49, pp. 2468–2503, 2003.
- [112] W. Su and X. Xia, "Two generalized complex orthogonal space-time block codes of rates $7/11$ and $3/5$ for 5 and 6 transmit antennas," *IEEE Trans. Inf. Theory*, vol. 51, pp. 313–316, 2003.
- [113] W. Su, X. Xia, and K. Liu, "A systematic design of high-rate complex orthogonal space-time block codes," *IEEE Commun. Lett.*, vol. 8, pp. 380–382, 2004.
- [114] K. Lu, S. Fu, and X. Xia, "Closed-form designs of complex orthogonal space-time block codes of rates $(k+1)/(2k)$ for $2k-1$ or $2k$ transmit antennas," *IEEE Trans. Inf. Theory*, vol. 51, pp. 4340–4347, 2005.
- [115] W. Su, S. N. Batalama, and D. A. Pados, "On orthogonal space-time block codes and transceiver signal linearization," *IEEE Commun. Lett.*, vol. 10, pp. 91–93, 2006.
- [116] P. Balaban and J. Salz, "Optimum diversity combining and equalization in digital data transmission with applications to cellular mobile

- radio - part I: theoretical considerations," *IEEE Trans. Commun.*, vol. 40, pp. 885–894, May. 1992.
- [117] Y. Shang and X. Xia, "Space-time block codes achieving full diversity with linear receivers," *IEEE Trans. Inf. Theory*, vol. 54, pp. 4528–4547, 2008.
- [118] A. Hurwitz, "Über die komposition der quadratischen formen," *Math. Ann.*, vol. 88, pp. 641–666, 1923.
- [119] J. Radon, "Lineare scharen orthogonaler matrizen," *Abhandlungen aus dem Mathematischen Seminar der Hamburgischen Universitat*, vol. I, pp. 1–14, 1922.
- [120] C. Au-Yeung and D. J. Love, "On the performance of random vector quantization limited feedback beamforming in a miso system," *IEEE Trans. Wireless Commun.*, vol. 6, pp. 458–462, 2007.
- [121] N. Jindal, "MIMO broadcast channels with finite-rate feedback," *IEEE Trans. Inf. Theory*, vol. 52, pp. 5045–5060, Nov. 2006.
- [122] J. P. Davis, "Leonhard euler's integral: A historical profile of the gamma function," *Amer. Math. Monthly*, vol. 66, pp. 849–869, 1959.
- [123] R. Gray, *Toeplitz and Circulant Matrices: A review*. Now Publishers Inc, 2006.
- [124] J. L. W. V. Jensen, "Sur les fonctions convexes et les inégalités entre les valeurs moyennes," *Acta Math*, vol. 30, pp. 175–193, 1906.
- [125] *Multiplexing and channel coding*, 3GPP Std. 36.212, Rev. 8.5.0, Feb. 2009.
- [126] P. Sweeney, *Error Control Coding*. England: Wiley, 2002.
- [127] R. D. Gitlin, J. F. Hayes, and S. B. Weinstein, *Data Communications Principles*. New York: Plenum Press, 1992.
- [128] H.-J. Lee, S. Komaki, and N. Morinaga, "Theoretical analysis of the capacity controlled digital mobile system in the presence of interference and thermal noise," *IEICE, Trans. Commu.*, vol. E75-B, 6, pp. 487–493, 1992.
- [129] W. T. Webb, "QAM; the modulation scheme for future mobile radio communications," *Elec. & Com. Eng.*, vol. 4, pp. 167–176, 1992.

-
- [130] Y. Kamio, S. Sampei, H. Sasaoka, and N. Morinaga, "Performance of modulation-level-controlled adaptive-modulation under limited transmission delay time for land mobile communications," in *Proc. 45th Vehicule Technology Conference*, IL, USA, Jul. 1995.
- [131] J. M. Torrance and L. Hanzo, "Upper bound performance of adaptive modulation in a slow rayleigh fading channel," *Electronics Letters*, vol. 8, pp. 718–719, 1996.
- [132] P. Lescuyer and T. Lucidarme, *Evolved Packet Systems (EPS)*. England: John Wiley & Sons, Ltd, 2008.
- [133] *Long Term Evolution physical layer: General description*, 3GPP Std. 36.201, Rev. 8.2.0, Feb. 2009.
- [134] *Physical channels and modulation*, 3GPP Std. 36.211, Rev. 8.5.0, Feb. 2009.
- [135] *Physical layer procedures*, 3GPP Std. 36.213, Rev. 8.5.0, Feb. 2009.
- [136] *E-UTRAN overall description: Stage 2*, 3GPP Std. 36.300, Rev. 8.7.0, Jan. 2009.
- [137] *E-UTRAN services provided by the physical layer*, 3GPP Std. 36.302, Rev. 8.0.0, Nov. 2008.
- [138] *Medium Access Control (MAC) protocol specification*, 3GPP Std. 36.321, Rev. 8.4.0, Jan. 2009.
- [139] J. Hagenauer, N. Seshadri, and C. E. W. Sundberg, "Rate compatible punctured convolutional codes (RCPC-codes and their application)," *IEEE Trans. Commun.*, vol. 36, pp. 389–400, 1988.
- [140] —, "The performance of rate-compatible punctured convolutional codes for digital mobile radio," *IEEE Trans. Commun.*, vol. 38, pp. 966–980, 1990.